



ELETTRA HIGHLIGHTS

1997

ELETTRA HIGHLIGHTS 1997
ELETTRA HIGHLIGHTS
HIGHLIGHTS





EDITORIAL COMMITTEE

Carlo J. Bocchetta

Gino D'Eliso

Stefano Fontana

Giorgio Margaritondo

...➤ <http://www.elettra.trieste.it>

PHOTOS

Mario Marin, Giovanni Montenero,

Neva Gasparo

GRAPHIC DESIGN

Sandra Zorzetti, Rado Jagodic

(Link, Trieste)

...➤ linkts@tin.it

*Printed and bound in Trieste
by Stella Arti Grafiche, 1998*

WELCOME TO ELETTRA

This first issue of the ELETTRA Highlights presents the major achievements of the ELETTRA synchrotron laboratory in its first period of full operation. We feel this is a good moment to illustrate to outside observers the present state, to attract their opinions and, we hope, their collaboration.

ELETTRA has been built to serve an international user community, in a range complementary to ESRF in Grenoble. Its location on the eastern border of Italy (few hundred meters from Slovenia) has been chosen to be open to the researchers of the neighbouring Countries, as well as to the Italian and European scientific communities at large.

The early goals to meet stringent quality parameters for the accelerator and to open the facility to international users have been met satisfactorily, as it can be seen from the “*Facts and Figures*” section, and are being continuously improved.

The first beam lines opened to experiments are also reaching increasingly good results and their numbers are evolving towards a full complement to be reached in the next three years. A full account of what is happening and several details of the technical developments, as well as improvements of the accelerator, are given in the three sections of these Highlights.

The staff of ELETTRA is steadily being complemented by the staff of the Collaborating Research Groups from Italian and foreign institutions and this is ensuring an increasingly mobile international and scientifically competitive environment.

Special thanks are due to the local staff and particularly to those who have worked hard to realize the laboratory and to those who have invested extra energy and effort to prepare this issue. Their enthusiasm and self-motivation deserve the full success of their efforts.

C. Rizzuto
Consigliere Delegato

CONTENTS

1997: A REMARKABLE YEAR FOR ELETTRA 9



EXPERIMENTAL PROGRAMS 11

CHEMICAL WAVES 12

OSCILLATORY SURFACE CORE LEVEL SHIFTS: BE (10 $\bar{1}$ 0) 15

HETERODEPITAXY OF GE ON SI(100)C 4x2 IN THE PRESENCE OF SB AS SURFACTANT ELEMENT STUDIED AT THE VUV BEAMLINE OF ELETTRA 18

RESONANT PHOTOELECTRON SPECTROSCOPY AND XANES FROM ENDOHEDRAL LA@CB2 20

SUB-NATURAL LINewidth ABSORPTION SPECTROSCOPY 22

GROWTH, ELECTRONIC AND STRUCTURAL CHARACTERISATION OF FE ON Ni(100) 25

EXTREMELY FAST CHARGE TRANSFER DYNAMICS OF ADSORBATES INVESTIGATED BY AUGER RESONANT RAMAN MEASUREMENTS 28

300 MPA JUMP-RELAXATION STUDIES OF PHASE TRANSITIONS INVESTIGATED BY TIME-RESOLVED SMALL-ANGLE X-RAY SCATTERING IN THE MS RANGE 31

INFRARED-LASER T-JUMPS WITH 10⁴ K/SEC AT THE SAXS BEAMLINE 33

STRUCTURE OF THE DNA-BINDING DOMAIN FROM THE SACCHAROMYCES CEREVISIAE CELL CYCLE TRANSCRIPTION FACTOR MBP-1 BY MAD 36

SUCCESSFUL DETERMINATION OF THE D(ACGTACG(5BRU))₂ STRUCTURE USING THE MAD METHOD AT ELETTRA 41

IN-SITU SYNCHROTRON X-RAY SCATTERING STUDY OF THE TENSILE PROPERTIES OF COLLAGEN 44

LOW DOSE PHASE CONTRAST X-RAY MEDICAL IMAGING AT ELETTRA 48



TECHNICAL PROGRAMS 51

FIRST IMAGE FROM THE SPECTROMICROSCOPE SUPERMAXIMUM 52

THE SPELEEM MICROSCOPE 54

PROGRESS ON THE GAS PHASE PHOTOEMISSION BEAMLINE 55

THE NEW OPTICAL CONFIGURATION FOR A MONOCHROMATOR APPLIED TO THE ALDISA BEAMLINE 58

THE MULTILAYER TECHNOLOGY LABORATORY AT ELETTRA PRODUCES STATE-OF-THE-ART MULTILAYER COATINGS 61

A COMPLETE DATA ACQUISITION SYSTEM
FOR VERY LOW CURRENT MEASUREMENTS 64

HIGHLY RESOLVING (<10 MILLIK)
TEMPERATURE-GRADIENT-CELL FOR X-RAY
SCATTERING STUDIES ON SOLUTIONS 67



ELETTRA BEAMLINE STATUS
(DECEMBER 1997) 69



THE MACHINE 73

THE ACCELERATORS 74

MACHINE OPERATION 80

MACHINE PERFORMANCE ISSUES 83

MACHINE DEVELOPMENTS IN 1997 87



ELETTRA SR PARAMETERS
(1997) 91



FACTS AND FIGURES 95

1997: A REMARKABLE YEAR

FOR ELETTRA

This was the second full year of official operation of ELETTRA; it was a good year: the machine produced a remarkable wealth of experimental results. Most importantly, most of the experiments fully exploited the unique source capabilities.

It is quite difficult to single out specific examples without unjustly neglecting other important contributions. One point, however, must be stressed: the increasing role of coherence. ELETTRA is fully spatially coherent up to at least 10 eV, and remains highly coherent at higher energies. Images speak more than words: the coherence-based “phase contrast” radiographs obtained by the SYRMEP cooperation (at dose levels compatible with medical radiology) are quite striking. The diffraction fringes observed on two spectromicroscopy beamlines also promise exciting future developments, such as microscopic-scale interferometry.

ELETTRA is quite active in photoelectron spectroscopy and spectromicroscopy. We note the many results of the Escamicroscopy beamline, using the microchemical analysis of chemical waves. In imaging spectromicroscopy, the Spe-Leem beamline pushed the world record of spatial resolution to 200-300 Å. As to spectroscopy, we note the detection of the Si2p core levels with an unprecedentedly narrow linewidth on the VUV photoemission beamline.

The Gas Phase Photoemission (GAPH) and Aloisa (surface diffraction) beamlines were recently commissioned, both reaching high energy resolution. The SuperEsca beamline continued to exploit the source brightness for time resolved photoemission analysis. We note among its results the work on Auger Raman measurements by the group of Professor Menzel.

ELETTRA was also quite active at shorter wavelengths, with the crystallography and the small-angle X-ray scattering beamlines. Quite remarkable were the several examples of MAD crystallography. The Small-angle scattering facility initiated structural experiments as a function of time, studying the transient effects of ultrarapid temperature changes.

These and many other results were made possible by the reliable operation of the source. In addition to eliminate the problems affecting reliability, the accelerator team achieved several significant

improvements: the initial commissioning of the elliptical wiggler for the Circular Polarization beamline; the upgrade of the ELETTRA vacuum system that opened the way to increased current levels; the start of construction of a feedback system to control multibunch instabilities; the implementation of a new high brilliance mode, already exploited by several users.

We also wish to gratefully acknowledge here the work of many other people in the ELETTRA staff who are not as visible as the research scientists. A key factor for success was the effort of the ELETTRA users, a very large fraction of which comes from abroad.

The performance of ELETTRA indeed attracts scientists beyond national borders, and the laboratory is open to foreign users through an unbiased competition based on merit.

In 1997, the European Commission entrusted to ELETTRA the coordination of the European Round Table on synchrotron radiation and free electron lasers. This is an important task, since European Commission contracts play a central role in the internationalisation of ELETTRA and of other facilities throughout Europe.

What lays ahead? First of all, new beamlines, which are urgently needed. The beamtime shortage is acute and growing, due to a growing national and international demand. The INFN, the CNR, the Czech Academy of Science, the republic of Slovenia and the European Commission are all endeavouring to provide new resources for new beamlines. The construction of four new INFN-supported beamlines is already started.

In short, 1997 was a bright and productive year. Best wishes to everybody for an even better 1998!

*S. Fontana
G. Margaritondo*



EXPERIMENTAL PROGRAMS

CHEMICAL WAVES

M. KISKINOVA

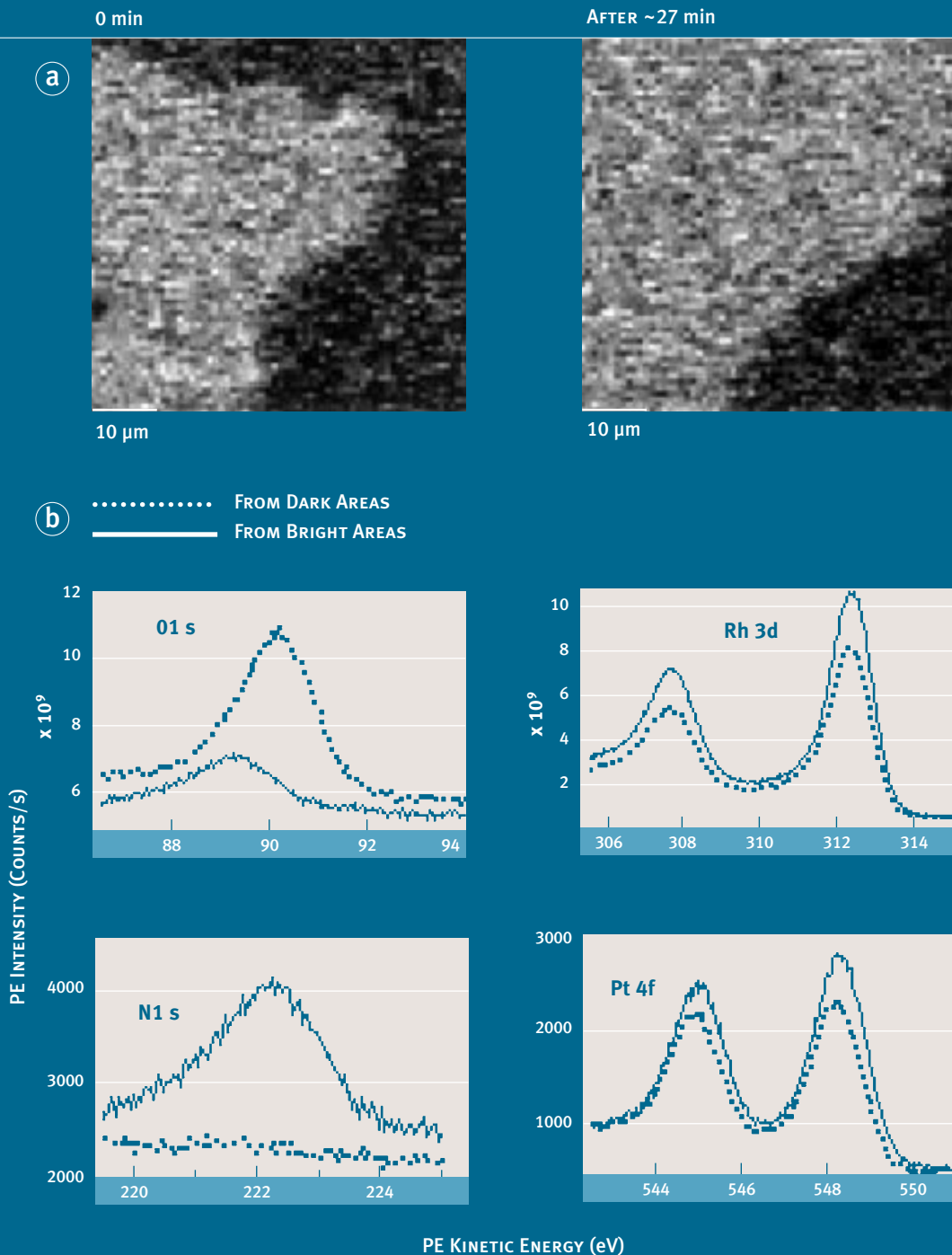
(Sincrotrone Trieste, Italy)

✉ kiskinova@elettra.trieste.it

The formation and propagation of chemical waves during reactions taking place on metal catalysts are observed and studied by spatially resolved photoemission electron microscopy, imaging the changes of the work function induced by the adlayer [1]. The different grey scales of the work function patterns formed during the surface reactions have recently obtained their actual composition assignment at the ESCA microscopy beamline on ELETTRA. In 1997 Prof. Imbihl and collaborators from the University of Hannover together with ELETTRA staff obtained the first spatially resolved XPS maps following the spatiotemporal pattern formation in the H_2+NO and H_2+O_2 reactions on a microstructured Rh/Pt(100) surface.

The exact nature of the local transformations, i.e. the type and chemical state of the adsorbate and the metal catalyst, the adsorbate coverage and adsorbate induced segregation processes and the structure of the Pt/Rh interface, were probed on minutes time scales, both in imaging and microspectroscopy mode. Figure 1(a) illustrates N1s chemical maps taken at different

Fig. 1: (a) Two dimensional 64x64 μm^2 N1s maps taken at different moments during the NO+H₂ reaction. Partial pressure: 3×10^{-7} mbar, reaction temperature: 450 K; (b) Core level spectra taken on the dark and bright areas of the N1s maps.



moments after the onset of the H_2+NO reaction.

The selected maps show the propagation of the chemical wave with reaction time. The contrast corresponds to the variation in the nitrogen coverage on the different sides of the propagating front. The high spatial resolution and the sufficient signal obtained for low PE cross section elements like O and N allowed monitoring the composition of the adlayer on both sides of the reaction front and the variation in the composition across the waves boundaries.

Figure 1(b) presents selected micro-spectroscopy data: the intensity and the shape of the measured core levels carry detailed information about the complex local composition of the adalayer and the status of the Rh/Pt interface.

REFERENCE

- [1] R. Imbibi and G. Ertl, *Chem. Rev.* 95 (1995) 697 and references therein.



OSCILLATORY SURFACE CORE

LEVEL SHIFTS: BE ($10\bar{1}0$)

Beryllium is a simple metal with most unusual properties. It has the smallest c/a ratio among hcp metals and the bulk electronic density of states shows a minimum at the Fermi-level indicating large deviations from free-electron like bonding. On some Be surfaces electronic surface states exist in the wide gaps of the projected bulk band structure around the Fermi level and lead to electronic, vibrational and structural properties very different from the bulk [1,2]. In particular, high-resolution XPS studies of the Be 1s core level have attracted considerable attention. Johansson and co-workers have found that the Be 1s XPS line consists of n peaks (Be(0001): $n=4$, Be($11\bar{2}0$): $n=2$, Be($10\bar{1}0$): $n=4$) which are assigned to a component from the bulk and $n-1$ components from the $n-1$ topmost layers, the component from the first layer having the largest shift [3-5]. For Be($10\bar{1}0$) the binding energy shift ΔE of the first (S1), second (S2) and third layer with respect to the bulk was found to be -700, -500, -220 meV respectively. Further, Johansson et al. have used

PH. HOFMANN

(Fritz-Haber-Inst. der Max-Planck-Gesellschaft, Berlin, Germany)

K. POHL, E.W. PLUMMER

(Dep. of Physics and Astronomy, Univ. of Tennessee, Knoxville; Oak Ridge National Lab., TN, USA)

S. LIZZIT, A. BARALDI, G. COMELLI*

*(Sincrotrone Trieste, Italy; *Dip. di Fisica, Lab. TASC - INFN e Univ. di Trieste, Italy)*

V. FRITZSCHE

(Inst. für Theoretische Physik, Technische Univ. Dresden, Germany)

R. STUMPF

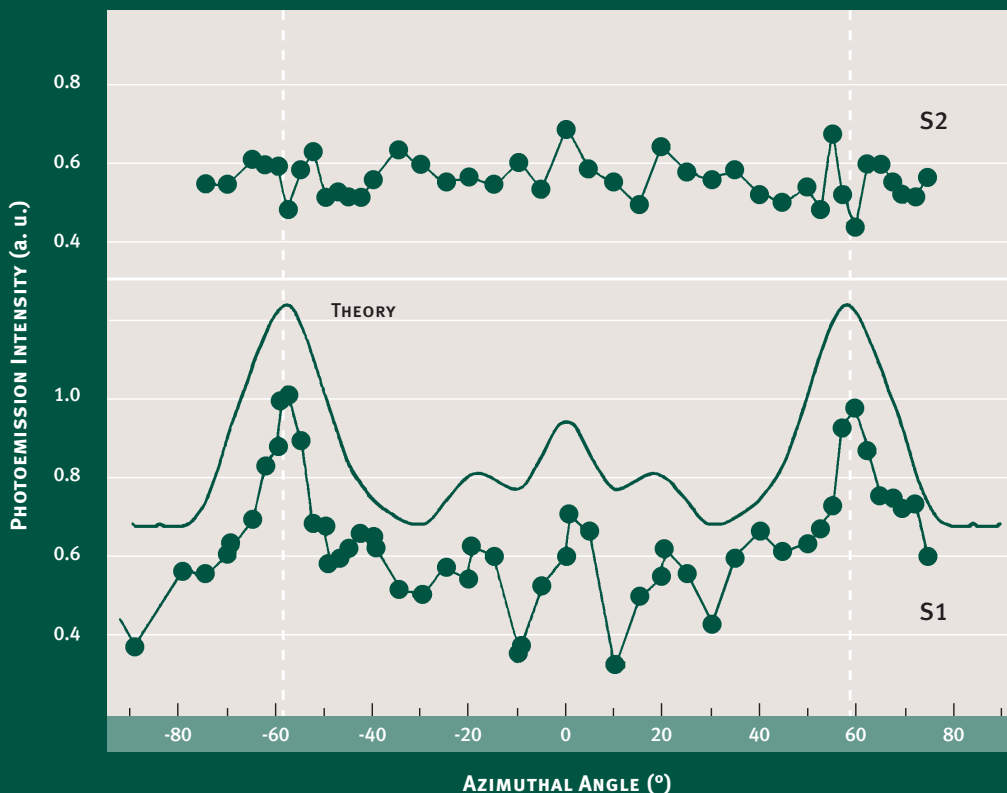
(Sandia National Labs, Albuquerque, NM, USA)

the energy-dependent intensity ratio of the surface to bulk components of Be(0001) and Be(10 $\bar{1}0$) to determine the electronic mean free path in Be [6].

While for the close-packed (0001) surface the position of the peaks as well as their assignment has been confirmed by several first-principles calculations [7-10], the first-principles calculation for Be(10 $\bar{1}0$) can only be reconciled with the experimental results assuming that the SCLS is not a monotonic function of depth of the plane, in other words that the second layer gives the largest shift and the first one gives the second

largest shift. Very recently, we have tested this unusual assignment by a photoelectron diffraction experiment which makes use of the high atomic forward scattering factor and small scattering phase shift for kinetic energies greater than 400 eV. In a forward scattering geometry where an atom of the first layer lies on a straight line between a second layer atom and the detector, the strong forward scattering ensures an enhancement of the core level component from the second layer while the intensity from the first layer is more or less constant. An inspection of the spectra taken in an

Fig. 2: Be 1s photoemission intensity vs azimuthal angle at 70 degrees off-normal emission. S1 is the component with the largest shift ($\Delta E = -0.7$ eV) and S2 that with the second largest shift ($\Delta E = -0.5$ eV). The azimuthal angle is taken with respect to the [0100] direction. The "theory" curve is the calculated modulation function for the second layer. The dashed lines represent the forward scattering direction.



angular scan around this forward scattering geometry reveals the identity of the second layer peak. In figure 2 it is possible to see that the experimental results clearly confirm the assignment suggested by the calculation.

The present work illustrates both the capabilities of high resolution XPS as well as the possible limitations and pitfalls. Beryllium is an ideal model system for such tests because it can be treated very precisely within state-of-the-art first-principles calculations. Our results show that a quite obvious assignment of the peak's origin like Johansson's may fail even for very simple systems like a clean metal surface. On the other hand we demonstrate that it is possible to find the right assignment experimentally using high-resolution photoelectron diffraction at a third generation synchrotron radiation source. Our example also provides yet another illustration of the fact that a quantitative interpretation of the peaks intensity is not straightforward unless photoelectron diffraction or, in other words, the effect of the unoccupied band structure is taken into account correctly.

REFERENCE

- [1] E.W. Plummer and J.B. Hannon, *Prog. Surf. Sci.* 46, 149 (1994).
- [2] R. Stumpf, J.B. Hannon, P.J. Feibelman and E.W. Plummer, *Heraeus Seminar (World Scientific, Bad Honnef, 1995)*, S.
- [3] L.I. Johansson, H.I.P. Johansson, J.N. Andersen, E. Lundgren and R. Nyholm, *Phys. Rev. Lett.* 71, 2453 (1993).
- [4] L.I. Johansson, H.I.P. Johansson, E. Lundgren, J.N. Andersen and R. Nyholm, *Surf. Sci.* 321, L219 (1994).
- [5] L.I. Johansson, H.I.P. Johansson, J.N. Andersen, E. Lundgren and R. Nyholm, *Phys. Rev. B* 49, 17460 (1994).
- [6] L.I. Johansson and B.O. Sernelius, *Phys. Rev. B* 50, 16817 (1994).

- [7] M. Alden, H.L. Skriver and B. Johansson, *Phys. Rev. Lett.* 71, 2457 (1993).
- [8] P.J. Feibelman, *Phys. Rev. B* 49, 13809 (1994).
- [9] P.J. Feibelman and R. Stumpf, *Phys. Rev. B* 50, 17480 (1994).
- [10] R. Stumpf and P.J. Feibelman, *Phys. Rev. B* 51, 13748 (1995).

HETEROEPITAXY OF GE ON Si(100)c 4x2 IN THE PRESENCE OF SB AS SURFACTANT ELEMENT STUDIED AT THE VUV BEAMLINE OF ELETTRA

P. DE PADOVA, C. OTTAVIANI,
C. QUARESIMA, C. COMICIOLI,
C. HÅKANSSON, M. PELAI, B. RESSEL

*(Ist. di Struttura della
Materia del CNR)*

R. LARCIPRETE

(ENEA, Dip. INN/FIS)

✉ depadova@dns.ism.rm.cnr.it

Heteroepitaxy of Ge on Si(100)c 4x2 in the presence of Sb as a surfactant element was studied by high resolution photoemission spectroscopy with synchrotron radiation at the VUV beamline of ELETTRA.

One ML of Sb was evaporated first on the clean Si surface at 450 °C. Subsequently, an increasing Ge amount, up to 2,5 MLs was deposited while the sample was kept at 350 °C. In both cases the system exhibited a 2x1 surface reconstruction. Si 2p, Ge 3d and Sb 4d core level peaks were measured as a function of the adsorbate coverage with the sample held at liquid nitrogen temperature. Spectra were taken at normal and grazing emission angles obtaining a bulk- and a surface-sensitive configuration, respectively.

The deconvolution of the Si 2p peak allowed to monitor the evolution of the atoms localised at the different layers of the reconstructed surface. When 1 ML of Sb was deposited on the clean Si surface, a new component (S*) was clearly identified in the

Si 2p spectrum, at a binding energy 200 meV higher than the bulk position, which was attributed to second layer Si atoms in contact with Sb dimers.

After Ge deposition, the comparison between the Sb 4d and Ge 3d spectra, measured in the bulk- and surface-sensitive configurations, revealed the predominant localisation of Ge below Sb after a site-exchange process. Simultaneously, with increasing Ge coverage, the S^* peak in the Si 2p spectrum decreased, since the Ge intralayer progressively decoupled the Si top-layer atoms from the Sb dimers.

A perfect bulk-like termination of the Si crystal was obtained after the evaporation

of 2,5 MLs of Ge, as indicated by the Si 2p spectrum shown in figure 3. This spectrum was taken at a photon energy of 135 eV. The best fit of the spectrum shows a dominating bulk component having a Voigt line shape with a Lorentzian FWHM of 20 ± 5 meV.

Since in the Lorentzian width we cannot exclude the presence of possible contributions from local disorder and strain propagating to the Si side, we claim that the interface between Si and Ge we obtained is a nearly perfect epitaxial interface and the 20 meV Lorentzian lifetime is the nearest value to the lifetime broadening ever found for Si 2p.

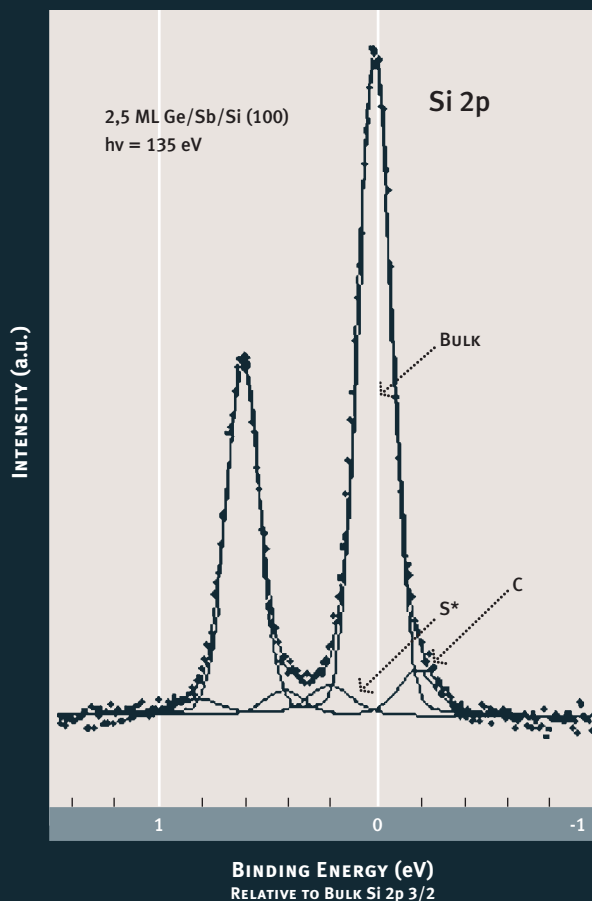


Fig. 3

RESONANT PHOTOELECTRON SPECTROSCOPY AND XANES FROM ENDOHEDRAL LA@C82

B. KESSLER, S. CRAMM,

C. SCHLEBUSCH, W. EBERHARDT

(Forschungszentrum Jülich,

IFF, Germany)

S. SUZUKI, Y. ACHIBA

(Department of Chemistry, Tokyo

Metropolitan University, Japan)

F. ESCH, M. BARNABA, D. COCCO

(Sincrotrone Trieste, Italy)

Photoelectron and X-ray absorption near edge spectra (XANES) from sublimated layers of chromatographically purified La@C82 are presented. The La-3d and -4d core-level data are in accordance with a transfer of 3 electrons from the La to the fullerene cage. With photon energies corresponding to the La-3d to -4f transition a resonant enhancement of the La-derived states is observed that clearly demonstrates that the valence bands contain a nonzero occupation of localized La-derived states. These data shed new light on the charge state of the La inside the fullerene cage.

(The work was supported by the European community under contract #ERBFM GECT950022. B.K. acknowledges the financial support by the Ministerium für Wissenschaft und Forschung des Landes Nordrhein-Westfalen.)

Fig. 4: Valence-band spectra of a thick layer of La@C₈₂ at different photon energies. The bottommost spectrum has been recorded using a He-lamp, the other spectra are taken with synchrotron radiation. The binding-energy scale is referenced to the Fermi level of the Au substrate. The intensity scale of the spectra at $h\nu=848\text{eV}$ (topmost curve) and 840eV (dotted line) has been normalized to each other in a binding energy region of about 12 to 18eV. The inset shows an X-ray absorption spectrum (XANES) in the region of the La-3d excitation into unoccupied states as a function of the photon energy.





SUB-NATURAL LINEWIDTH ABSORPTION SPECTROSCOPY

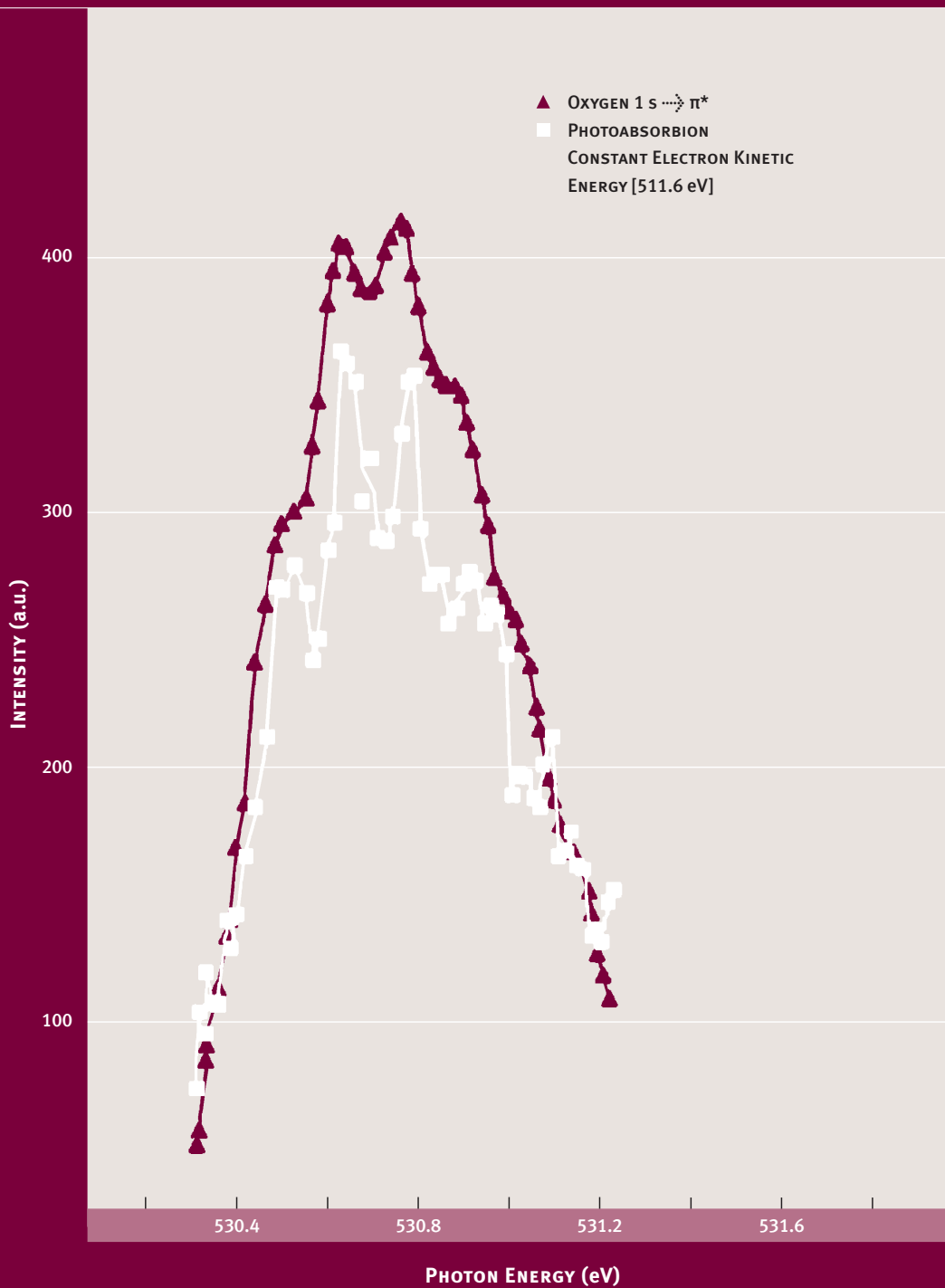
M.N. PIANCASTELLI

(Sincrotrone Trieste, Italy)

One of the problems at ELETTRA is that the energy resolution of some beam lines is so high that it is difficult to measure it! This is because photon bandwidth is typically measured by gas phase absorption spectroscopy, which works well for resolution comparable to natural line width. When the resolution is much higher, it is difficult to deconvolute the Gaussian line width which corresponds to the monochromator spectral function from the Lorentzian line width of a measured absorption peak.

Several very interesting experimental findings have been recently reported in the field of resonant photoemission following a core-to-bound excitation in isolated atoms or molecules with a photon bandwidth narrower than the natural line width of the primary excitation as measured in absorption, largely based on the resonant Auger Raman effect (1-4). However, at variance with resonant photoemission, the natural line width in absorption measurements cannot be overcome by the usual methods (photoabsorption or total electron yield or total ion yield).

Fig. 5



A new method has been recently developed (5) and now applied at ELETTRA on the Gas Phase Photoemission beamline by the author and the beamline research group (R. Camilloni, L. Avaldi, M. Coreno, G. Stefani, C. Furlani, M. de Simone, S. Stranges, K.C. Prince) which allows us to overcome the physical limit of the natural line width in absorption measurements. The basis of it is to measure absorption spectra by means of a constant final state technique: a constant kinetic energy scan is recorded in the photon energy region of a core-to-bound resonance. The chosen kinetic energy corresponds to electron emission leading to an ionic final state which apparently does not show dispersion as a function of photon energy. In our case, the system is molecular oxygen and the selected final state is $C^2\Phi_u$.

The upper curve of figure 5 shows the normal absorption spectrum of oxygen at the $1s \rightarrow \pi^*$ resonance, where the vibrational structure is partly resolved. The lower curve shows a constant electron kinetic energy spectrum. This was taken by fixing the kinetic energy of an analyser at 511.6 eV, corresponding to the $C^2\Phi_u$ state, and then scanning the photon energy. The vibrational structure is more clearly resolved and under these conditions the width is determined only by the resolution of the photons and analyser. The preliminary data confirm that the beamline has a resolution of about 10,000 or better. This promises to allow a more precise determination of resolution, but more importantly opens the way to new experiments in molecular physics.

REFERENCE

- [1] M.N. Piancastelli, M. Neeb, A. Kivimäki, B. Kempgens, H.M. Köppe, K. Maier and A.M. Bradshaw, *Phys. Rev. Lett.* 77 (1996) 4302.
- [2] R. Camilloni, M. Zitnik, C. Comicioli, K.C. Prince, M. Zacchigna, C. Crotti, C. Ottaviani, C. Quaresima, P. Perfetti and G. Stefani, *Phys. Rev. Lett.* 77 (1996) 2646.
- [3] A. Kivimäki, A. Naves de Brito, S. Aksela, H. Aksela, O.-P. Sairanen, A. Ausmees, S.J. Osborne, L.B. Dantas and S. Svensson, *Phys. Rev. Lett.* 71 (1993) 4307.
- [4] S. Aksela, E. Kukkk, H. Aksela and S. Svensson, *Phys. Rev. Lett.* 74 (1995) 2917.
- [5] A. Kivimäki, K. Maier, M.N. Piancastelli, B. Kempgens, A. Rudel, U. Hergenbahn and A.M. Bradshaw, *to be published.*



GROWTH, ELECTRONIC AND STRUCTURAL CHARACTERISATION OF Fe ON Ni(100)

Catalysis and low dimensional magnetism are the two main areas to which the study of the growth of Fe on Ni is addressed. Bimetallic catalysts are known to result in an increase in reactivity, greater selectivity and resistance to poisoning. Ni is known to be a good methanation catalyst and it has been shown that, in presence of Fe, the reactivity and selectivity toward higher hydrocarbons are increased. On the other side the magnetic behaviour of Fe is complex. α -Fe is a body centred cubic ferromagnetic crystal stable up to 770 °C while γ -Fe is a face centred cubic crystal stable at higher temperatures showing, depending on Wigner-Seitz radius, zero, low or high spin density phases. Consequently, seen from the angle of the interplay between structure and physical (mainly magnetic) properties, interesting physical situations might occur depositing Fe when conditions for epitaxial growth are satisfied. Fcc Fe can be obtained at room temperature on fcc substrates and, depending on substrate lattice parameter, different low dimensional phases (possibly magnetic) can

**F. BRUNO, L. FLOREANO, R. GOTTER,
A. MORGANTE, A. VERDINI, D. CVETKO***
(TASC-INFN; *Sincrotrone Trieste, Italy)

A. SANTANIELLO,
(Sicotronne Trieste, Italy)

**S. DADDATO, A. DI BONA, G.C. GAZZADI,
P. LUCHES, L. MARASSI, S. NANNARONE,
L. PASQUALI, S. VALERI**
(Univ. of Modena, Dip. di Fisica, Italy)

G. GRANOZZI, M. SAMBI
(Univ. of Padova, Dip. di Chimica Inorganica, Italy)

C. MANNORI
(Univ. of Genova, Dip. di Fisica, Italy)

M. PIRLITescu
(Univ. of Calabria, Dip. di Fisica, Italy)

be obtained. In addition magnetic substrates can polarise the growing film, or vice versa, giving size to a rich phenomenology.

Here we report on the experimental results obtained on the ALOISA beamline on the growth of Fe on Ni(100) specifically addressing the nature (crystal phase, dislocations density, strain and structure phase transition) and the electronic properties (density of states and band dispersion) of ultrathin layers. The lower lattice parameter of the (100) Ni surface should force the Fe layer into two nearly degenerate non-magnetic or antiferromagnetic phases. Data allow to get information on the chemisorption stage (first couple of monolayers) and on the first (10-15) atomic planes of the growing Fe crystal. In figure 6 the intensity variation of Fe 3p photoemission core level due to photoelectron diffraction (PED) effects is shown for different values of coverage. The analyser scan was along the [100] azimuth with a photon energy of 1400 eV. The lowest curve is the PED of Ni 3p and is reported for comparison. In the chemisorption region (1-2 ML) the zero angle emission peak is, if any, at the noise level. The zero angle emission clearly shows up at 3 ML. This strongly suggests that the Fe film has a tendency to grow layer-by-layer also at the chemisorption stage. However, some intermixing or island formation below 3 ML cannot be completely ruled out. In the 3-11 ML range the inspection of PED spectra indicates epitaxial growth of fcc Fe on Ni(100) characterised by a good asymmetry ratio and by a clear shift of the peak at about 45° towards the surface normal. Assuming that the Fe layer grows pseudomorphically with the Ni substrate one is induced to ascribe this effect to a vertical strain of the Fe film. Numerically it results to be of the order of 10% of the fcc Fe lattice parameter. A confirmation of the high degree of local order comes from the well evident fine structure

Fig. 6: Fe3p polar scans along the [100] azimuth as a function of coverage (blue line). The clean Ni3p signal (red line) is reported for comparison.

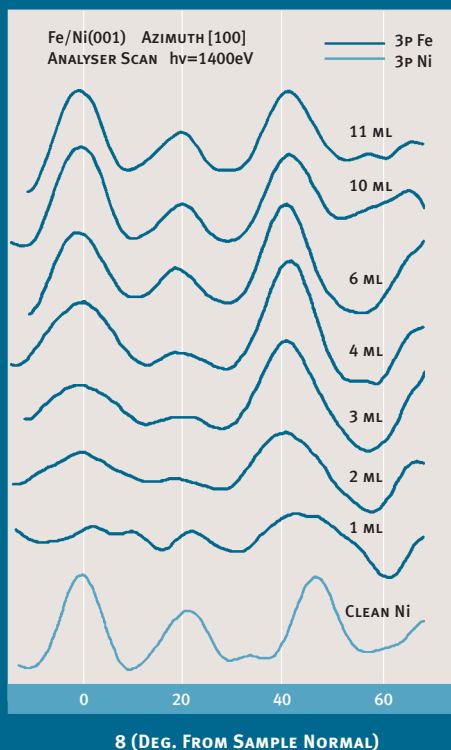


Fig. 7: Fe reflectivity across the K absorption edge.

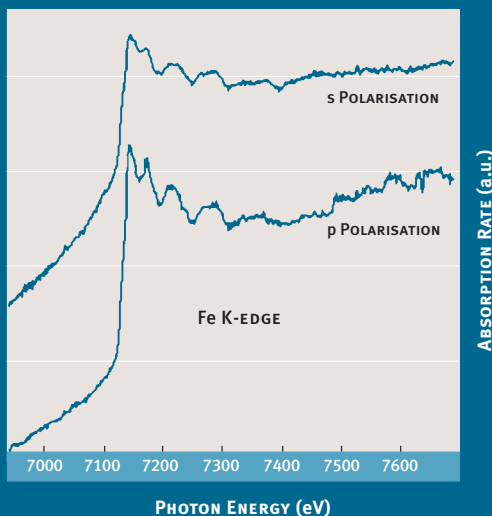
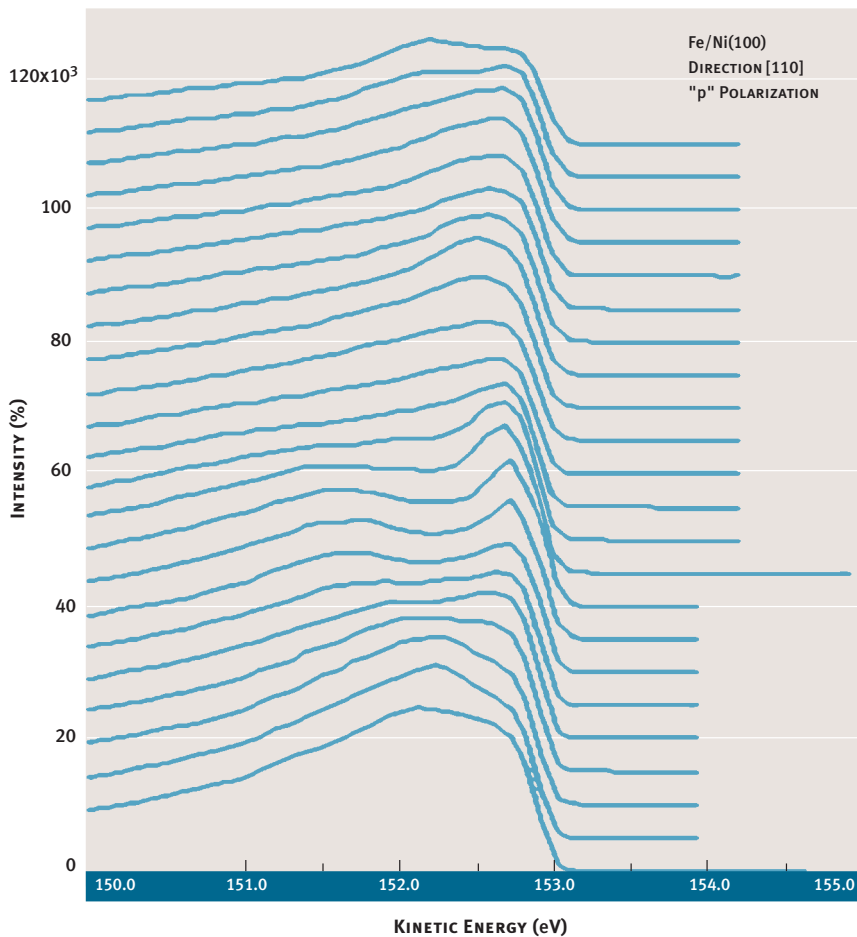


Fig. 8: Energy distribution curves of an ultrathin Fe layer along the [110] azimuth. The photon energy is 150 eV.



of the reflectivity spectra above the Fe K-edge shown in figure 7 for a Fe coverage in the layer-by-layer growth regime.

Bridging with electronic properties was obtained by angle resolved photoemission and optical reflectivity at the Ni $L_{2,3}$ and Fe $L_{2,3}$ edges (both not reported here). A typical stack of electron energy distribution curves taken along the [110] azimuth is reported in figure 8. Energy position and dispersion of features are different from the Ni ones (not shown) allowing to single out

the Fe states. Data analysis is under way. However, some hints about the electronic structure can be obtained by an inspection of figure 8. An emission close to E_F coming from d states (full for the high spin phase) seems to be absent for any angular position in the photoemission spectra, indicating a non magnetic phase. This might be related to the contraction of the Fe lattice parameter under epitaxial growth on Ni(100).

EXTREMELY FAST CHARGE TRANSFER DYNAMICS OF ADSORBATES INVESTIGATED BY AUGER RESONANT RAMAN MEASUREMENTS

W. WURTH, C. KELLER,

M. STICHLER, D. MENZEL

(Physik-Department E20, TU

München, Germany)

G. COMELLI, F. ESCH, S. LIZZIT

(Sincrotrone Trieste, Italy)

The basis of many important questions in Surface Chemical Physics is the coupling of adsorbates to the substrate. This coupling leads to the adsorbate bond, but manifests itself also in the lifetime of an excitation initially localized on an adsorbate - a decisive quantity for electronically induced desorption and surface photochemistry [1]. Indirect conclusions from the latter effects show that, e.g., the charge transfer (CT) time of an excited electron from a chemisorbate into a metal substrate must be of the order of or less than a fs; for more weakly bound species CT times should be longer, but still in the fs range. Times so short are at present not yet accessible to pump-probe laser experiments. A new approach to such timescales has become possible very recently using highly resolved core level excitation-decay spectroscopies. The main point here is to use the lifetime of a suitable core hole in an adsorbate, which for light atoms is in the range of some fs, as an internal time

O 1s - 2π AUTOIONISATION FOR CO ON Ru(001)

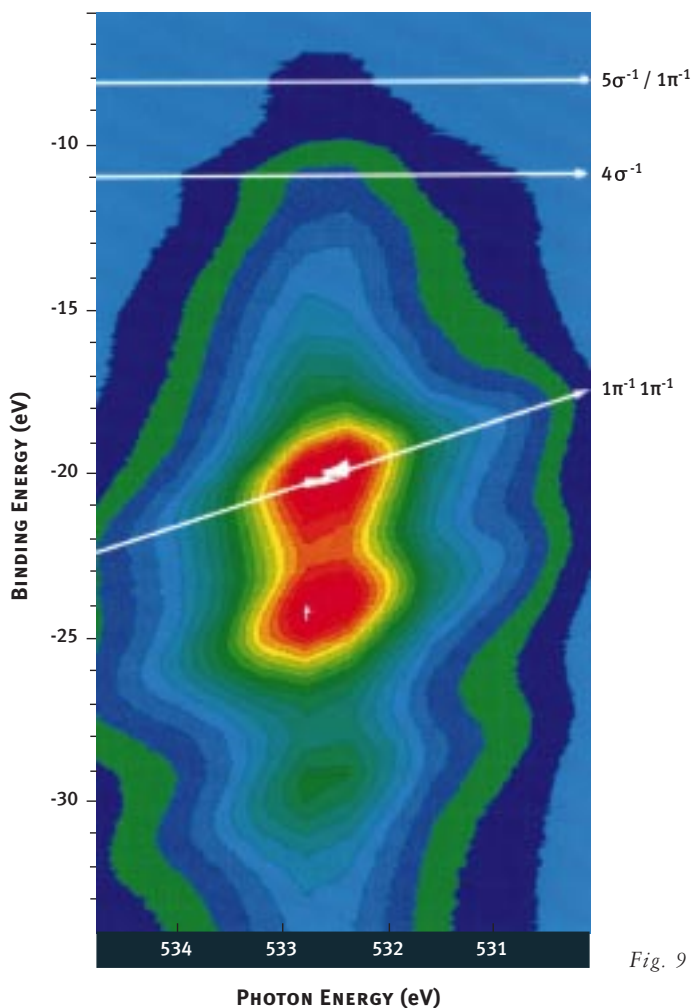


Fig. 9

standard against which the CT time can be measured.

Resonant photoexcitation of a core electron to an empty but bound state of a system leads to intermediate states which for light atoms decay by autoionization. The study of these excitation-decay processes becomes particularly interesting when band widths of the exciting soft X-radiation are used which are narrower than the lifetime width of the intermediate resonance. When the narrow band of exciting

radiation is tuned through the core resonance of an isolated atom or molecule the decay lines disperse linearly with photon energy, contrary to normal Auger decay. This is a consequence of energy conservation [2]. Further-more, the spectral widths of the lines become independent of the lifetime of the intermediate state and are given by the lifetimes of the final states and the experimental resolutions. All these characteristics of the so-called Auger resonant Raman effect can be understood in terms of

a coherent one-step excitation-decay mechanism [2].

The use of this effect to measure the CT time of an adsorbate resonance is straightforward. Very different decay spectra are expected for the cases that at the time of core hole decay the excited electron is still localized on the adsorbate, or has already hopped into the substrate. In the first case the behavior of the decay spectra will be like for the isolated system, i.e. the kinetic energies of the decay electrons will disperse with photon energy (or: plotted on a binding energy scale the energy stays constant). The overall process is then still coherent. In the second case the electron hopping into the substrate has taken the information about the exact primary energy with it, and the kinetic energy of the decay electrons stays constant with photon energy (or: the binding energy disperses); the coupling has made the process incoherent [3]. This different behavior with photon energy which makes the separation of the two sets of channels quite easy can be seen in the contour plot for the case of CO chemisorbed on Ru. In a simple rate approach, the ratio of the intensities of the two types of decay spectra is a direct measurement of the CT time compared to the core hole decay time. We stress that this is an experiment in the time domain. It can be regarded as a pump-probe experiment in which the probe delay is not variable.

We have carried out such experiments at the SuperESCA beamline at ELETTRA for adsorbed Ar atoms on Ru(001), and on this surface modified by preadsorbed species to vary the coupling strength; as well as on chemisorbed CO. For Ar, CT times between less than 2 and more than 50 fs result under these conditions [4]. For the chemisorbates, the CT times are clearly below 1 fs [5]. Furthermore, the CT time

for any one system varies across the resonance, i.e. with its distance from the Fermi level, which can be understood in terms of the variation of the density of states in the substrate, possibly with contributions from symmetry matching.

This new method of estimation of extremely short charge transfer times, which are not accessible so far by any other method, appears to be of general applicability. It will be more accurate the closer the two compared timescales are to each other, and can be extended even to much shorter times by suitable selection of the core level used.

This work has been supported by the Deutsche Forschungsgemeinschaft through project Me 266/22, and by the European Community through its Large Scale Installation program under ERBFMGET CT950022.

REFERENCE

- [1] See, e.g., P. Feulner and D. Menzel, in "Laser Spectroscopy and Photochemistry on Metal Surfaces", H.-L. Dai and W. Ho, eds., World Scientific, Singapore 1995, p. 627.
- [2] T. Aberg, *Physica Scripta* T41 (1992) 3271.
- [3] O. Karis et al., *Phys. Rev. Lett.* 76, 1380 (1996); W. Wurth, *Applied Physics* A65, 597 (1997).
- [4] C. Keller, M. Stichler, G. Comelli, F. Esch, S. Lizzit, D. Menzel, and W. Wurth, *Phys. Rev. Lett.* (subm.).
- [5] C. Keller, M. Stichler, G. Comelli, F. Esch, S. Lizzit, W. Wurth, and D. Menzel, *Phys. Rev. Lett.* (in press).

300 MPA JUMP-RELAXATION STUDIES OF PHASE
TRANSITIONS INVESTIGATED BY TIME-RESOLVED
SMALL-ANGLE X-RAY SCATTERING IN THE MS RANGE

Phospholipids, major constituents of all biological cell membranes, show a variety of mesomorphic phases and phase transitions as a function of temperature, pressure and hydration. These phases include one-dimensional lamellar, two-dimensional hexagonal and three-dimensional (bicontinuous) cubic structures with cell parameters usually in the range from 5 to 10 nm which is easily accessible by small-angle X-ray scattering.

We have studied the dynamics of these phase-transitions by jump-relaxation methods, i.e. by time-resolved X-ray diffraction in millisecond time resolution. For that purpose the thermotropic or barotropic phase transition is caused by a quick temperature or pressure jump, triggered either by an infrared laser or an p-jump apparatus applying jump amplitudes in the order of up to 10 °C within 2 ms or up to 3 kbar within 10 ms (pressurizing and depressurizing), respectively. The relaxation into the new equilibri-

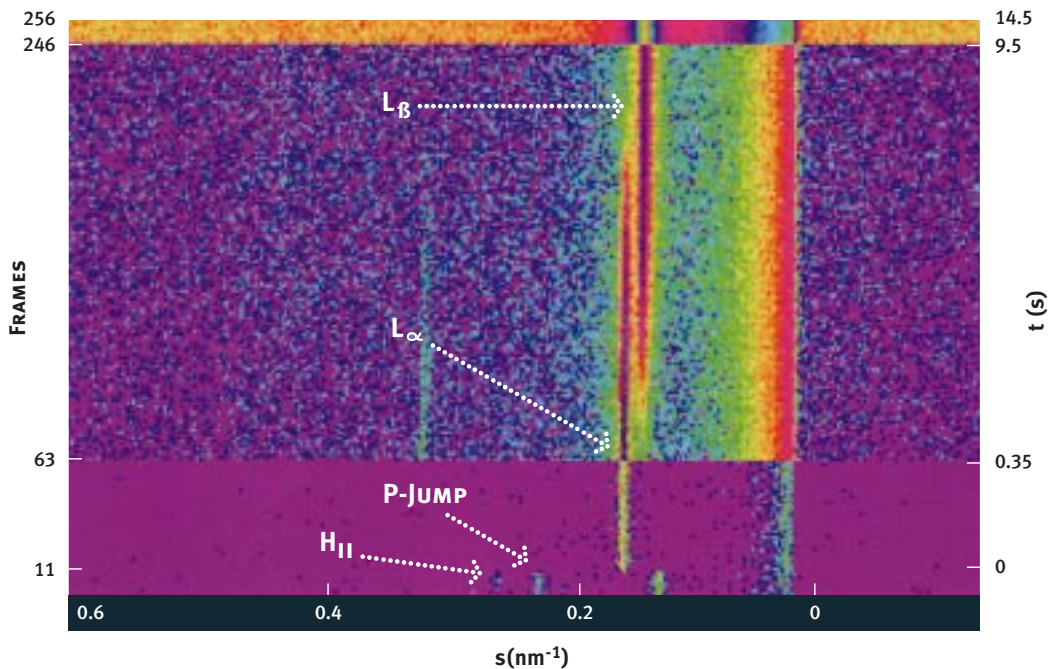
M. KRIECHBAUM, P. LAGGNER,
M. STEINHART, K. PRESSL,
C. KRENN, H. AMENITSCH,
M. RAPPOLT

*(Inst. of Biophysics and X-ray
Structure Research, Austrian
Academy of Science, Graz, Austria)*

S. BERNSTORFF

(Sincrotrone Trieste, Italy)

Fig. 10: p-jump of DOPE in water 20% from 250 to 2300 bar at frame 11 within 10 ms.



um phase was simultaneously recorded by time-sliced X-ray small-angle diffraction patterns with 5 ms (for p-jumps, see figure 10) and 100 ms (for T-jumps) frames.

This method allowed us to study the existence of short-lived intermediates appearing during the interconversion from one topological phase into the other, which are not detectable in slow-scan (near-equilibrium) phase-transitions, giving us a unique tool in the interpretations of the mechanistic and structural steps underlying the principle of these phase-transitions.



INFRARED-LASER T-JUMPS WITH 10^4 K/SEC AT THE SAXS BEAMLINE

The fastest temperature-jump (T-jump) facility presently world-wide available for time resolved X-ray diffraction studies on aqueous disperse systems, as e.g. liquid crystals or polymer solutions, has been installed recently at the SAXS beamline at ELETTRA. This system features as core element an Erbium glass infrared laser which is commercially available from Dr. Rapp Optoelektronik, Hamburg, Germany. This laser can be triggered to emit 1-2 kJ pulses for durations of about 1 ms. Using suitable crystal optics the laser pulse can be deposited onto a capillary sample holder for SAXS such that temperature jumps of 10-20 °C are made in 1 ms time, which corresponds to heating rates of 10^4 K/sec. For the investigation of liquid crystalline phase transitions which frequently span a transition range of 0.1 °C or less, this means that the transition can be triggered within tens of microseconds.

In a first experimental session, the formation of a short-lived intermediate, designated as $L\alpha^*$, during the pretransition of

G. PABST, H. AMENITSCH, C. KRENN,

M. RAPPOLT, P. LAGNER

*(Inst. of Biophysics and X-ray Structure
Research, Austrian Academy
of Sciences, Graz, Austria)*

S. BERNSTORFF

(Sincrotrone Trieste, Italy)

✦✦✦ Bernstorff@elettra.trieste.it

✦✦✦ Amenitsch@elettra.trieste.it

Tab. 1: Lifetime of the $L\alpha^*$ intermediate depending on the concentration of the NaCl in the solvent. T_0 is the temperature of the sample before the T-jump. The lifetime is given by the inflection-point of the mean d-spacing curves in the $L\alpha^*$ to $P\beta'$ transition.

NaCl-CONCENTRATION	T_0	LIFETIME [S]
0 M	27.4	11.63
0.5 M	26	11.23
1 M	26	10.22

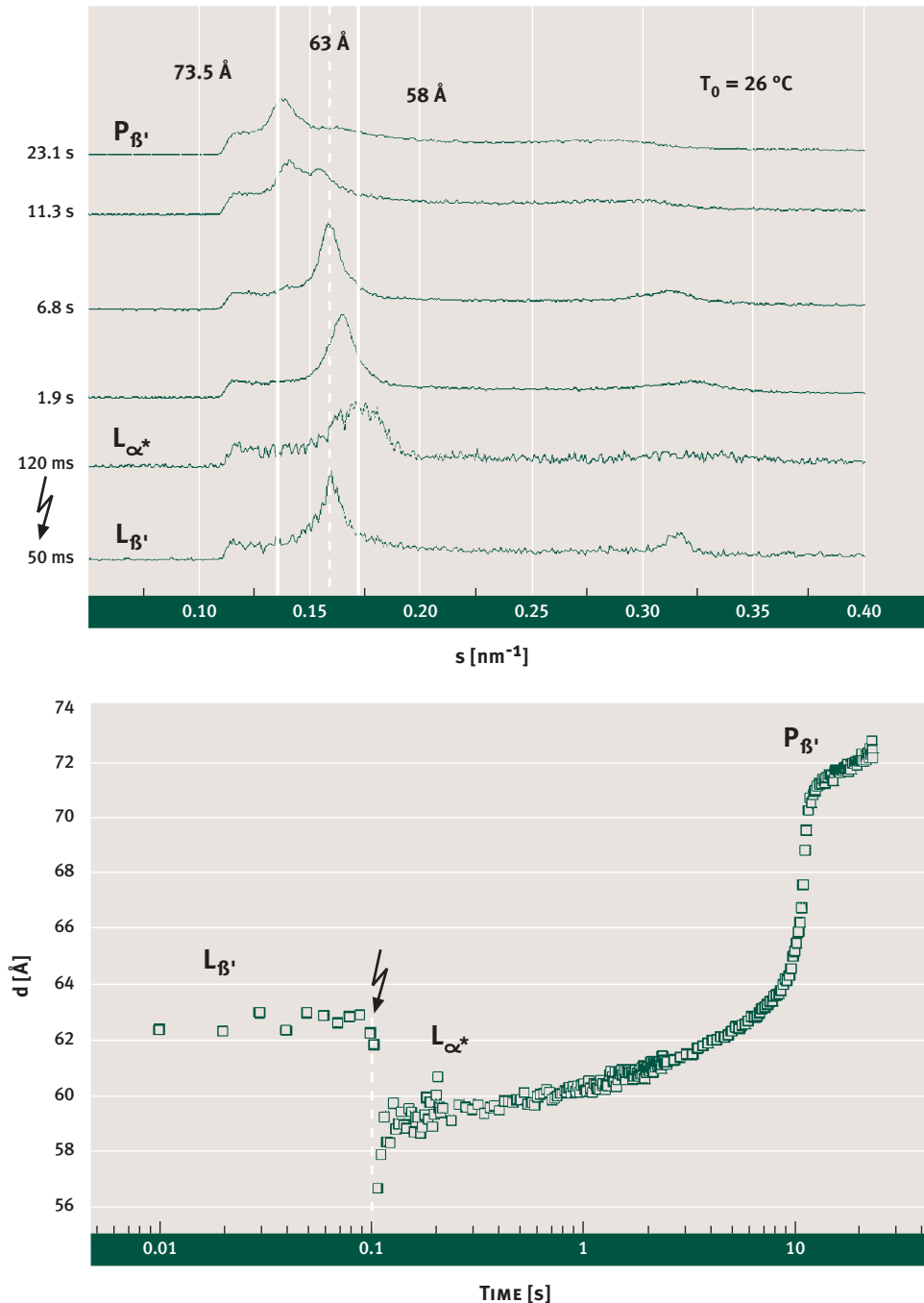
DPPC (Dipalmitoyl-lecithin) has been investigated by time-resolved X-ray small angle diffraction. The results show that the transition proceeds in at least two steps, if conducted in a strongly non-equilibrium fashion: In the first step, the appearance of a discrete reflection at $1/58 \text{ \AA}^{-1}$ (compared to the 63 \AA lamellar repeat distance of the initial $L\beta'$ gel phase) indicates the production of a thin liquid crystalline bilayer phase. This new phase which is not seen under equilibrium conditions is designated as $L\alpha^*$. The lifetime of this intermediate, which coexists with variable amounts of the initial gel phase structure, can be varied by changing the power of the laser beam, and the chemical composition of the system. In the second step, which has a characteristic time scale of seconds, the $L\alpha^*$ phase structure gradually relaxes into the stable ripple phase structure $P\beta'$ (see schematic model) [1, 2].

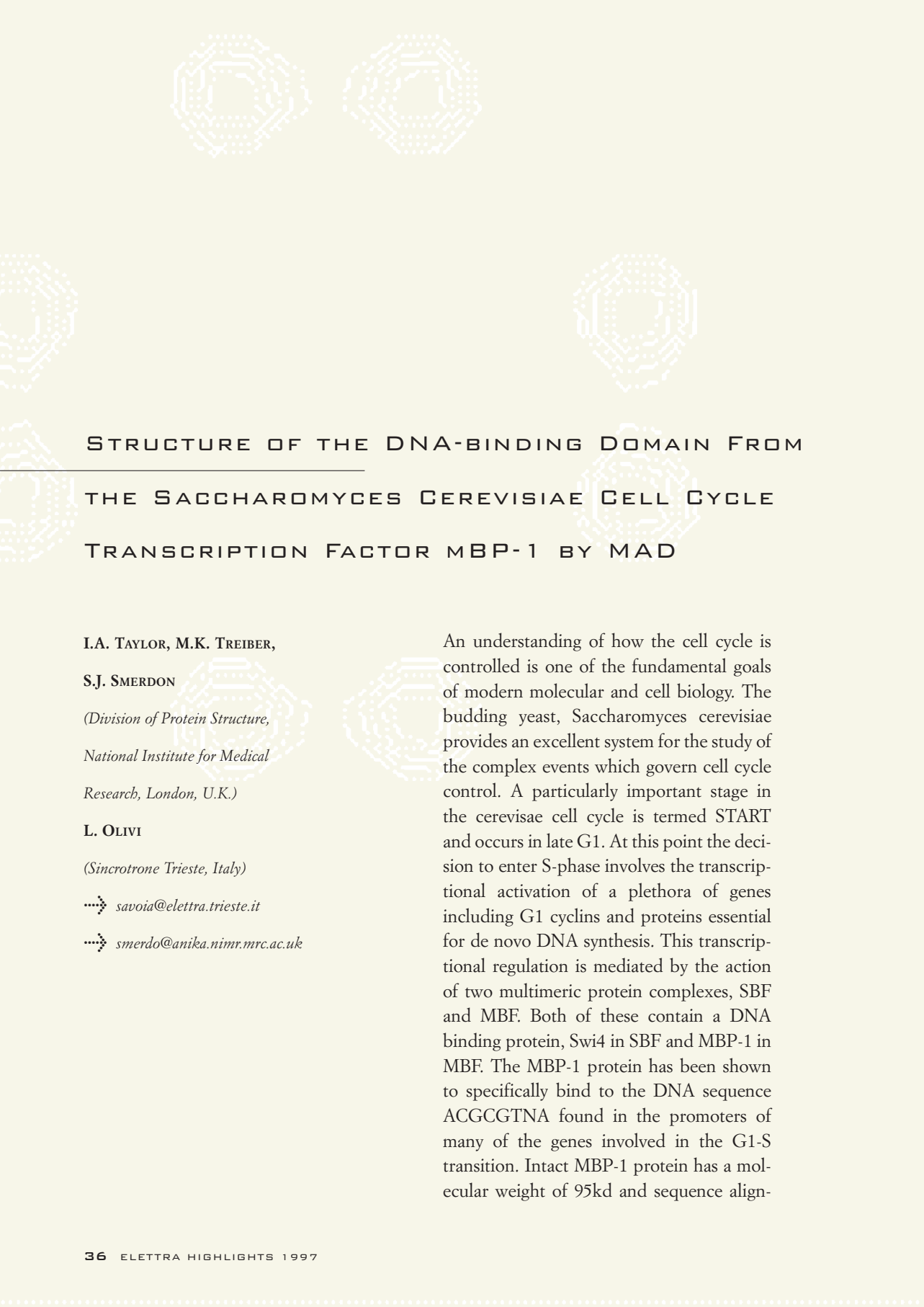
Research is now directed to the identification of factors which may prolong the lifetime of the intermediate structures. On the one hand, this will facilitate the detailed structural analysis of the intermediate and thereby provide a point of entry for a full understanding of the mechanism of this and other, related phospholipid phase transitions. On the other hand, this may lead to interesting nanostructures which are not accessible under equilibrium conditions.

REFERENCE

- [1] P. Laggner, M. Kriechbaum and G. Rapp. *Structural intermediates in phospholipid phase transitions*. J. Appl. Cryst. 24: 836-842, 1991.
- [2] M. Rappolt. *Zeitaufgelöste Röntgenbeugung zur Untersuchung von Phasenübergängen an Modellmembranen*. PhD thesis, Universität Hamburg, 1995.

Figure 11: The pretransition in the SAXS regime of an aqueous dispersion of dipalmitoylphosphatidylcholine (0.5 M NaCl), which had been induced by a T-jump.
 a) The stack-plot shows six characteristic diffraction patterns: one before the laser shot ($L_{\beta'}$), three during the lifetime of the intermediate (L_{α^*}), one in the mid of the L_{α^*} to $P_{\beta'}$ transition and one in the pure ripple phase ($P_{\beta'}$). The flash indicates the laser shot.
 b) Shows the mean d -spacing of the existing phases during the transition (versus elapsed time).





STRUCTURE OF THE DNA-BINDING DOMAIN FROM THE SACCHAROMYCES CEREVISIAE CELL CYCLE TRANSCRIPTION FACTOR MBP-1 BY MAD

I.A. TAYLOR, M.K. TREIBER,

S.J. SMERDON

*(Division of Protein Structure,
National Institute for Medical
Research, London, U.K.)*

L. OLIVI

(Sincrotrone Trieste, Italy)

✦ savoia@elettra.trieste.it

✦ smerdo@anika.nimr.mrc.ac.uk

An understanding of how the cell cycle is controlled is one of the fundamental goals of modern molecular and cell biology. The budding yeast, *Saccharomyces cerevisiae* provides an excellent system for the study of the complex events which govern cell cycle control. A particularly important stage in the *cerevisiae* cell cycle is termed START and occurs in late G1. At this point the decision to enter S-phase involves the transcriptional activation of a plethora of genes including G1 cyclins and proteins essential for de novo DNA synthesis. This transcriptional regulation is mediated by the action of two multimeric protein complexes, SBF and MBF. Both of these contain a DNA binding protein, Swi4 in SBF and MBP-1 in MBF. The MBP-1 protein has been shown to specifically bind to the DNA sequence ACGCGTNA found in the promoters of many of the genes involved in the G1-S transition. Intact MBP-1 protein has a molecular weight of 95kd and sequence align-

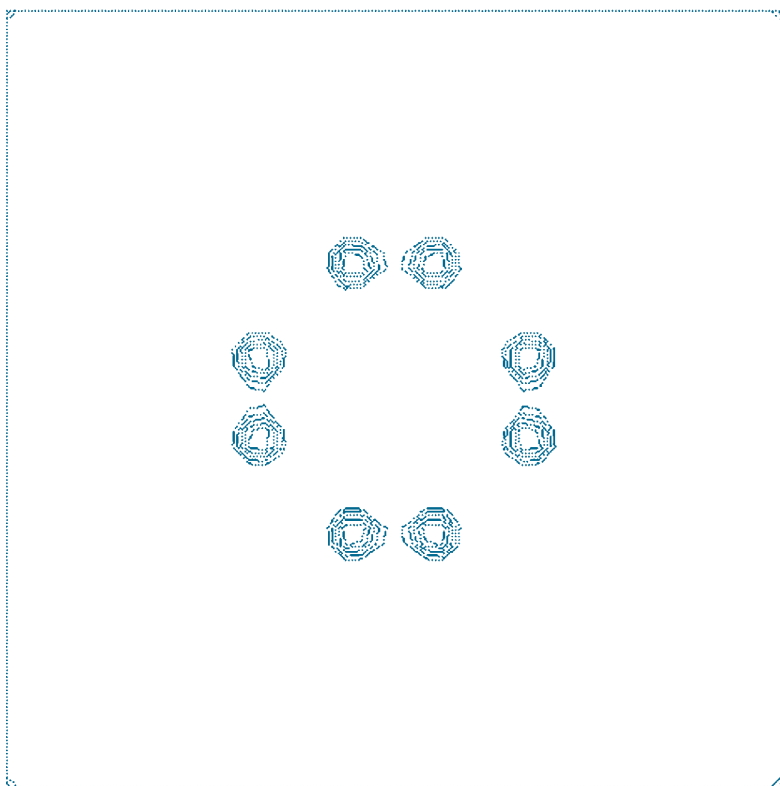


Fig. 12

ments show it to be made up of a number of distinct functional regions. The N-terminal region contains the DNA binding domain of the protein from which we have produced and crystallised a 124 amino acid fragment which specifically binds to the MBP-1 recognition sequence.

EXPERIMENTAL

The protein was produced as a histidine tagged fusion protein (Mr 15400) from an *E. coli* T7 expression system. Crystals were

grown by the method of vapour diffusion in hanging drops over two weeks, finally reaching maximum dimensions of 0.6 x 0.2 x 0.2 mm. They belong to space group P41212, with cell dimensions $a=b=42.5\text{\AA}$ $c=123.5\text{\AA}$ containing a single protein molecule in the asymmetric unit (with a notably low solvent content of 25%). Crystals were also prepared from seleno-methionine containing protein.

Datasets were collected at ELETTRA at various wavelengths around the Se absorption edge. Anomalous and dispersive difference Pattersons both clearly revealed the single Se site (figure 12).

Fig. 13



Fig. 14



Phases to 3\AA were calculated using MLPHARE, enabling the real and anomalous occupancies to be refined. A plot of each is shown in figure 15. These plots were used during the data collection experiment to select the optimal wavelengths for f' and f'' collection. The resulting phases were of high quality with an overall FOM of 0.81. The electron density map was readily interpretable after phase extension with DM.

DESCRIPTION OF STRUCTURE

The structure is shown in a ribbons representation in figure 13 (previous page).

Topologically, it may be described as β 1- β 2- β 3- β 4- α 1- α 2- β 5- β 6- α 3- α 4.

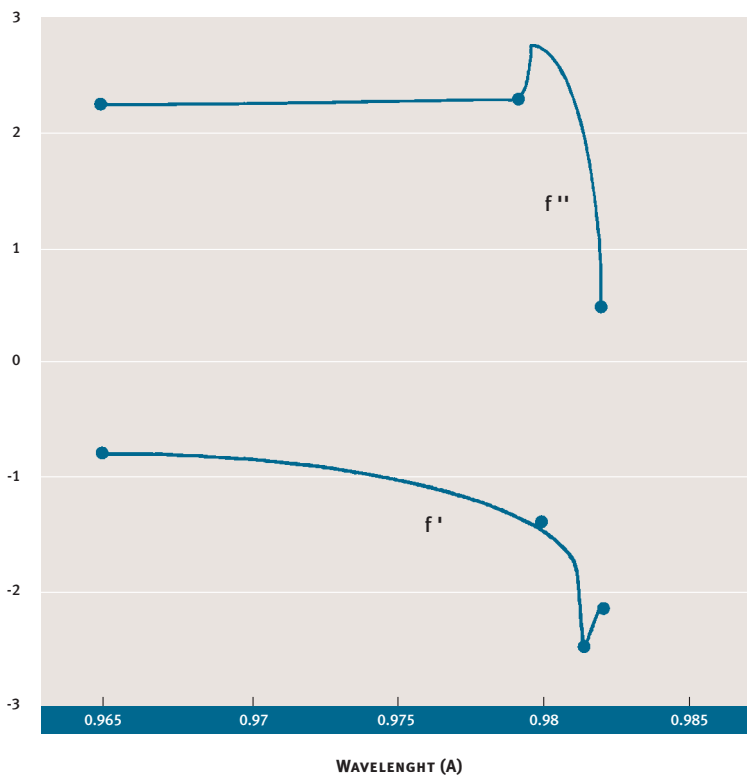
Strands β 1- β 4 make up a twisted beta sheet and the two helix pairs α 1- α 2 and α 3- α 4 are connected by beta strands 5 and 6. It is likely that helices 1 and 2 make key contacts with DNA together with basic residues from the β 5- β 6 loop. The electrostatic potential surface shown in figure 14 shows a shallow basic pocket in this region which constitutes the DNA binding site.

The model will enable us to solve the crystal structure of the mbp DNA binding domain complexed with its cognate DNA by molecular replacement methods thus providing a detailed molecular description of this key regulatory complex.

REFERENCE

JMB, 272, pg 1 (1997).

Fig. 15



SUCCESSFUL DETERMINATION OF THE D[ACGTACG(5BRU)]₂ STRUCTURE USING THE MAD METHOD AT ELETTRA

A few words about MAD.

Determination of the phases of the diffracted beams which are needed to solve complex structures is still a major problem in macromolecular crystallography. A set of initial phases for a protein structure can be extracted using the method of isomorphous replacement with heavy atoms. Differences in diffracted intensities between native and derivative crystals are used to determine the position of the heavy atoms. The calculated contribution from these known centers can be used as reference waves for deducing the correct phases of the native crystal structure from the observed modulations caused by their presence.

A more advanced technique in which the scattering strength at a few special sites is changed physically by change of X-ray wavelength rather than chemically by atomic substitution is called Multiwavelength Anomalous Diffraction (MAD) and is based on the use of anomalous scattering mea-

A. LAUSI, F. ZANINI, A. SAVOIA

(Sincrotrone Trieste, Italy)

✦✦✦ lausi@elettra.trieste.it

✦✦✦ zanini@elettra.trieste.it

✦✦✦ savoia@elettra.trieste.it

surements at appropriate energies, taking into account the strong variations of the scattering factor near an absorption edge.

The anomalous signal depends on the imaginary component f'' of the scattering factor, and thus on the absorption coefficient, and on the wavelength-dependent real component $f'(1)$, which shows a minimum in correspondence with the inflection of f'' at the absorption edge.

The ratio of anomalous signal to total structure may be calculated, and is usually below 10%. Because the MAD signal is so small, it is important to minimize errors in intensity measurements by carefully checking the performance of the beamline during the experiment.

EXPERIMENTAL

No structural information has yet been reported on the binding of acridine-4-car-

boxamide antitumor agents to oligonucleotides. One member of this family, DACA, is currently in phase 3 clinical trials.

The oligonucleotide d(ACGTACGT)2 is known to intercalate the DACA. Having successfully used the MAD methodology on the derivative d(ACGTACG(5-BrU))2, the same technique is being applied to the complex of the drug with this DNA at the ELETTRA diffraction beamline by C.J. Cardin, A. Adams, A. Todd and H.R. Powell (Universities of Reading, Dublin and Cambridge) using the bromine edge around 0.92.

The f'' scattering coefficient has been monitored by recording the fluorescence spectrum on a sample of 5-bromouridine immediately before the experiment to determine the point of inflection.

The experiment was carried out using four wavelengths, of energies 13.268, 13.453, 13.464 and 13.772 KeV. Data were processed to give merging R factors of

Fig. 16: a) fluorescence yield measured from 5-BrU sample. The different markers indicate checks of monochromator stability during the experiment. b) Numerical derivative of the fluorescence yield: the maximum of this curve corresponds to the minimum of f'' .

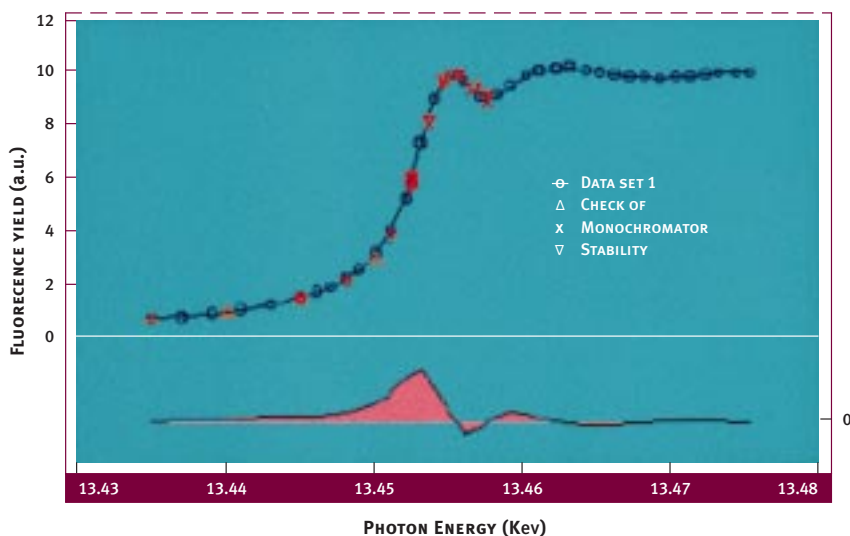
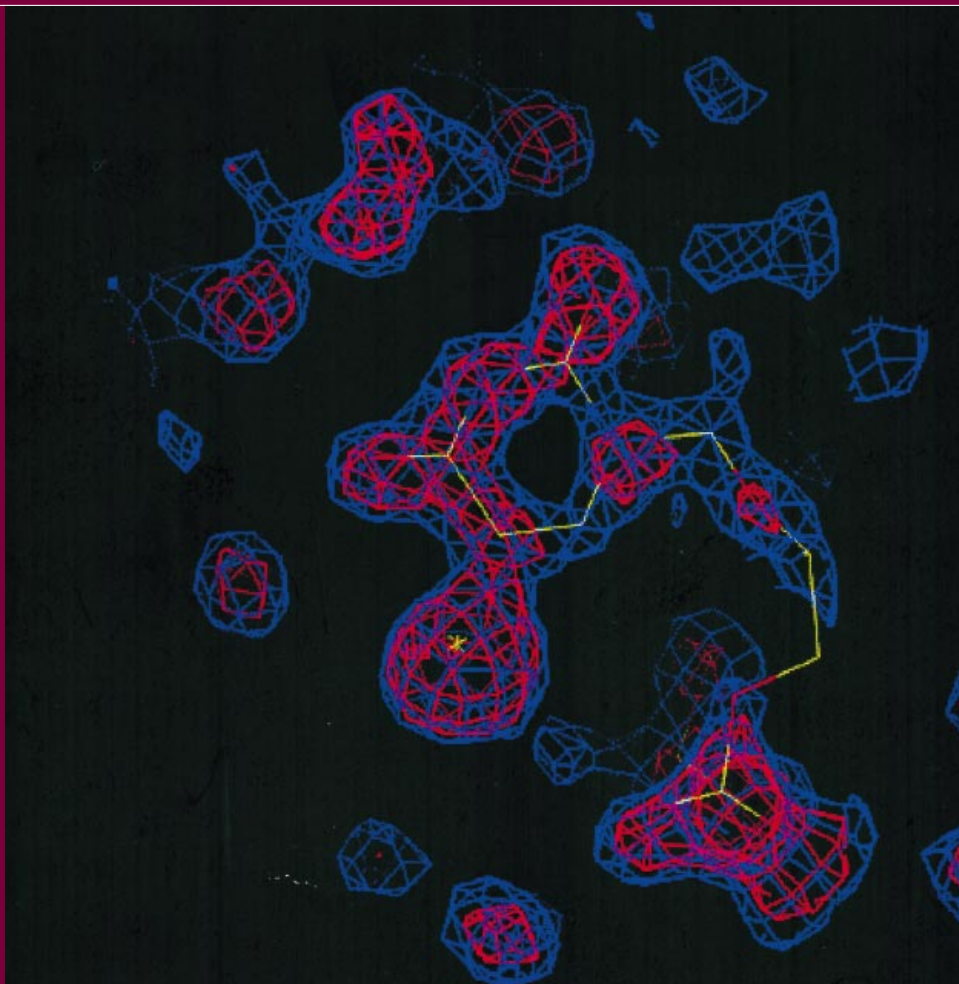


Fig. 17: Electron density at 5-BrU position after MAD phasing and density modification.

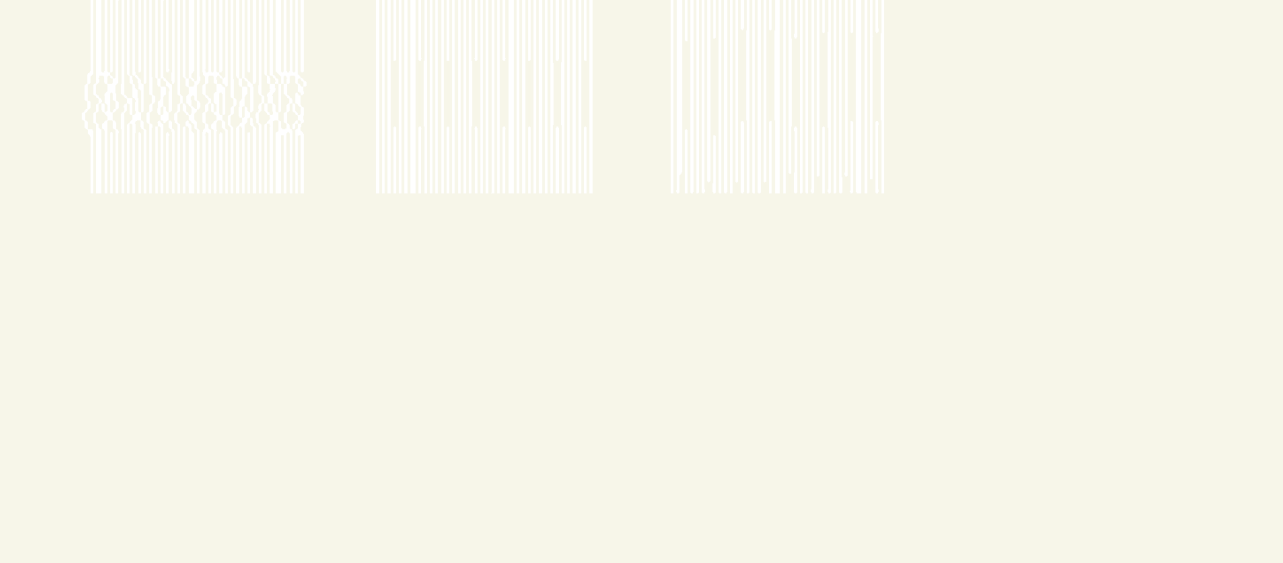


0.051, 0.071, 0.058 and 0.061 for the four wavelengths using the data to 1.6 (The data has actually been measured to 1.45* at these settings).

The Bromine atom was located from the anomalous difference direct method and his position was then refined and the phases further improved to give an interpretable map. The command procedures used were kindly provided by Dr Eleanor Dodson (University of York).

REFERENCE

"Determination by MAD-DM of the structure of the DNA duplex d(ACGTACG(5-BrU))₂ at 1.46 Å and 100 K", A.K. Todd, A. Adams, H.R. Powell, D.J. Wilcock, J.H. Thorpe, A. Lausi, F. Zanini, L.P.G. Wakelin and C.J. Cardin, Acta Cryst. (D), submitted.



IN-SITU SYNCHROTRON X-RAY SCATTERING

STUDY OF THE TENSILE PROPERTIES

OF COLLAGEN

P. FRATZL, K. MISOF, I. ZIZAK

*(Materials Physics Inst. and
Ludwig-Boltzmann Inst. of
Osteology, Univ. Wien, Austria)*

G. RAPP

*(European Molecular Biology Lab.
Outstation, Hamburg, Germany)*

H. AMENITTSCH

*(Inst. of Biophysics and X-ray
Structure Research, Austrian
Academy of Sciences, Graz, Austria)*

S. BERNSTORFF

(Sincrotrone Trieste, Italy)

The outstanding mechanical properties of collagen are due to its structure at various levels of hierarchical organisation. To study the relation between tensile properties and structure at the fibrillar level, we have developed a device for in-situ synchrotron X-ray scattering investigations under mechanical tension [1]. Tendons from the rat tail were kept in a humid atmosphere and tension was applied by increasing the length continuously. Both the force and the elongation of the tendons were measured at the same time as the equatorial and the meridional X-ray scattering. Figure 18 shows the meridional peaks as a function of stress on the tendon measured at the SAXS beamline [2] of ELETTRA.

At lower strains, we had previously found that the intensity of the diffuse equatorial scattering increases linearly with the strain, corresponding to an increase in the degree of lateral ordering in the fibrils. This could be reproduced quantitatively by a

model [1] where kinks of the molecules (occurring mostly in the gap-region of the fibrils, case A in figure 18) are straightened out due to stretching (case B). This also explains the upwards curvature of the stress-strain curve (dark part in figure 18) by an entropic mechanism [1].

At larger strains, the force increases linearly with the elongation of the tendon (grey part in the right of figure 18) and further

elongation leads to a dramatic change in the relative intensities of the meridional diffraction orders (see figure 19). In particular, the intensity ratio of second to third order increased, which can be interpreted [3,4] as a parallel gliding of the molecules (case C in figure 18). In addition, we found that all higher diffraction orders vanished gradually with increasing stress, which may be explained by an increasing fuzziness of the

Fig. 18: Model for the stress induced changes in the fibrils at the molecular level (from [4]). At small strains, molecules are kinked inside the gap-region of the fibril structure. At intermediate strains, molecular kinks are straightened out, leading to entropic elasticity [1]. At large strains, molecules glide parallel to each other [3] and the interface between gap and overlap regions is getting increasingly fuzzy [4].

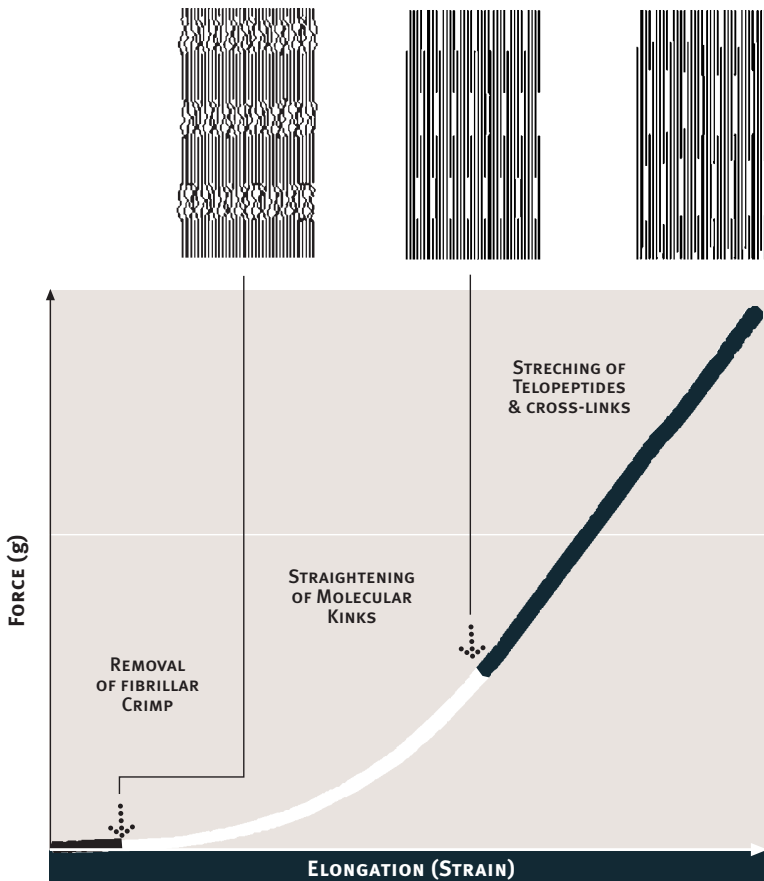
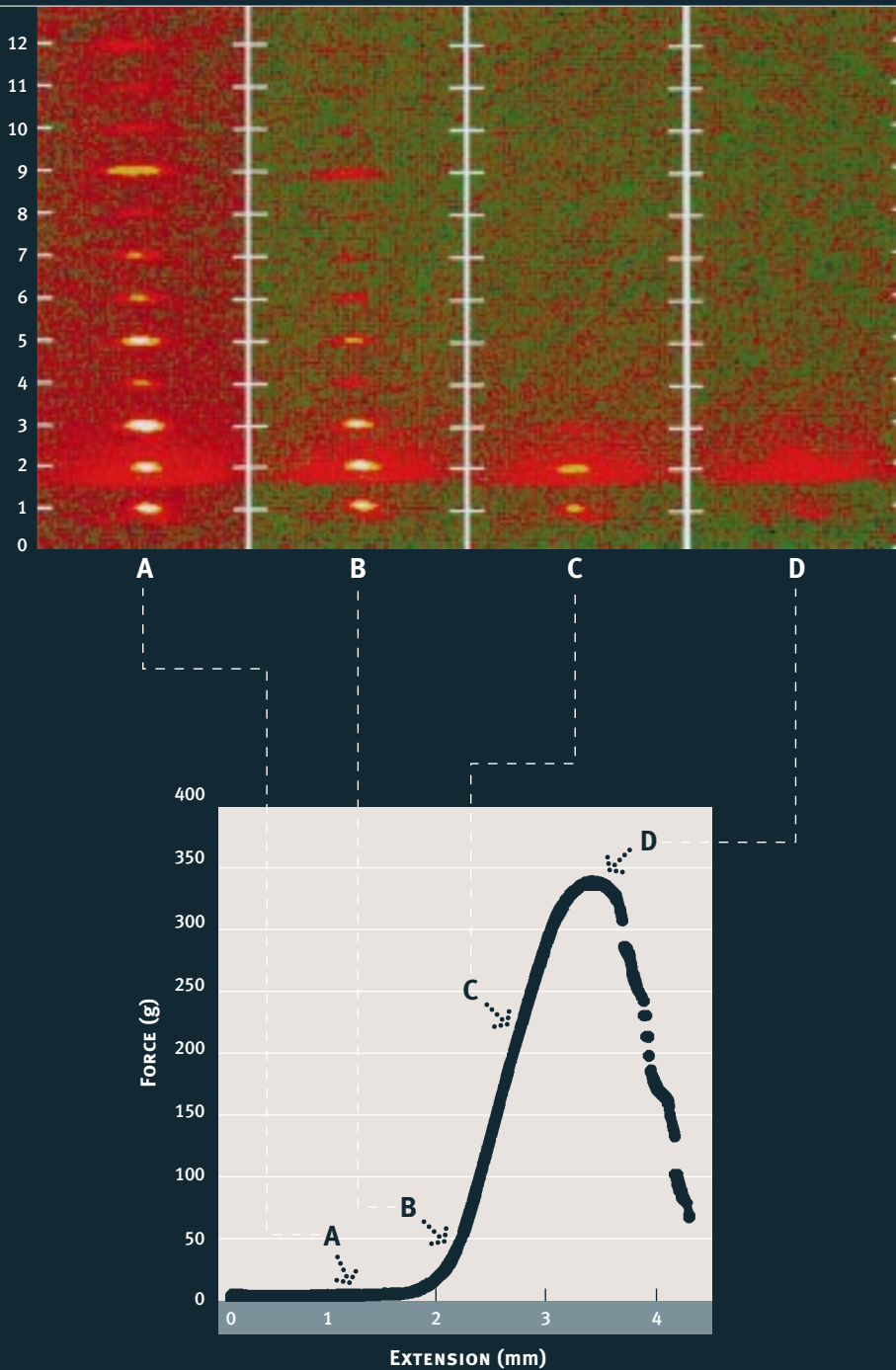


Fig. 19: Meridional reflections of collagen from stretched rat tail tendon measured with a CCD camera as area detector (AXS, Karlsruhe) at the SAXS beamline [2] at ELETTRA. Each of the four spectra were collected during a constant strain rate experiment at different moments during the extension of the fibre.



interface between gap and overlap region. As shown in the figure 18 (C), this would occur when neighbouring molecules glide randomly by slightly different amounts [4].

Finally, it was found that the axial periodicity (defined by the peak spacing in figure 19) changes less than the total length of the tendon under stress. This points towards some mechanism of interfibrillar gliding which is still very poorly understood [4].

Work supported by the Fonds zur Förderung der Wissenschaftlichen Forschung (P11762-PHY).

REFERENCE

- [1] K. Misof, G. Rapp, P. Fratzl (1996) *Biophys. J.* 72:1367-1381.
- [2] H. Amenitsch, S. Bernstorff, P. Laggner (1995) *Rev. Sci. Instr.* 66:1624-1626.
- [3] W. Folkhard et al. (1986) *Int. J. Biol. Macromol.* 9:169-175.
- [4] P. Fratzl, K. Misof, I. Zizak, G. Rapp, H. Amenitsch, S. Bernstorff (1998) *J. Struct. Biol.* (in press).

LOW DOSE PHASE CONTRAST X-RAY

MEDICAL IMAGING AT ELETTRA

F. ARFELLI, G. TROMBA

(Sincrotrone Trieste, Italy)

V. BONVICINI, A. BRAVIN,

G. CANTATORE, E. CASTELLI,

M. DI MICHIEL, R. LONGO,

A. OLIVO, S. PANI, D. PONTONI,

P. POROPAT, M. PREST,

A. RASHEVSKY, A. VACCHI,

E. VALLAZZA

(Dip. di Fisica - Univ. di Trieste

and INFN - Sez. di Trieste, Italy)

L. DALLA PALMA

(Istit. di Radiologia - Univ. di Trieste)

✉ tromba@elettra.trieste.it

Conventional radiology is based on the detection of differences in X-ray absorption of the sample. Image contrast is originated by any density, composition or thickness variation of the sample and of the details inside it.

This technique encounters severe difficulties in detecting low contrast details in soft tissues and mammography is a typical field where these kind of limitations are particularly relevant.

An X-ray source with appropriate spatial coherence, like synchrotron radiation, makes possible to investigate a novel imaging approach, the "phase contrast technique".

The method is based on the detection of the phase perturbations produced by the sample. Any spatial variation of the real part of the refractive index produces interference patterns with the undiffracted wave, that can be detected by a suitable experimental set-up. This means that the contrast is related not only to the absorption but also to the diffraction properties of the sample. The technique enhances image contrast even

if sample absorption is very weak or if absorption differences between details and background are negligible. The effect is greatly amplified by the presence of edges, where a sharp refractive index gradient occurs.

Phase contrast imaging is related to in-line holography [1] or phase contrast microscopy [2,3] but generally its implementation is simpler because it does not require any image manipulation or wave splitting. First tests have been carried out by A. Snigirev et al. [4,5] and by J.T. Davis and S.W. Wilkins et al. [6,7], who obtained high contrast and high spatial resolution images of different organic samples. Their experimental set-up, however, required high radiation doses preventing any application to medical radiology.

Low dose phase contrast X-ray images have been obtained with the SYRMEP beamline at ELETTRA using medical X-ray films. High contrast resolution images of biological samples and of human breast tissue specimens have been acquired at doses comparable to conventional mammographies using a standard screen-film system [8].

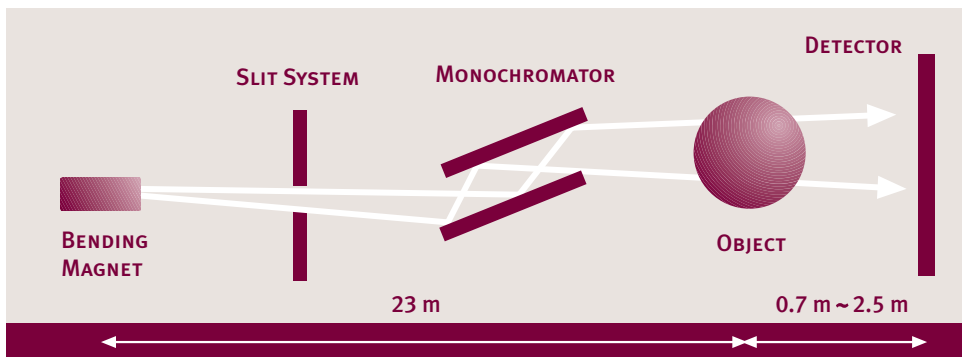
Another method to produce high quality diffraction enhanced images with the same medical purposes has been investigated by W. Thomlinson's group at BNL [9].

An analyser crystal was introduced between the sample and the detector to produce two diffracted images at two different crystal angular positions. The technique, called "diffraction enhanced imaging", allows to obtain, after image processing, two images, the "apparent absorption image", containing information about the absorption and extinction processes, and the "refraction image" including diffraction effects produced by the sample.

At the SYRMEP beamline the beam delivered by the bending magnet is monochromatized by a monolithic channel-cut Si(1,1,1) crystal and impinges on the sample placed at a distance of 23 m from the source. A slit system defines the beam cross section in the experimental area (about 100 x 1 mm²). The interference pattern, produced by the sample, can be detected if the distance between the sample and the detector is large enough to convert the small diffraction angles into a length compatible with the detector spatial resolution. In the phase contrast set-up the sample-to-detector distance varies from 0.7 m to 2.5 m and in the conventional absorption geometry the detector is placed immediately behind the sample.

Images are taken by moving the object and the film through the beam at slightly

Fig. 20: the SYRMEP experimental set-up.



different speeds to simultaneously cover the same solid angle with respect to the source.

Theoretical simulations have been carried out to calculate the interference pattern produced by simple test objects, in order to optimise the sample-to-detector distance and to evaluate the effect of the intensifier screen.

Preliminary experimental tests confirm theoretical expectations and show that phase contrast imaging can be achieved also at low doses, with a relevant improvement in image quality compared to conventional absorption radiography.

Figures 21a, 21b show two images of a mimosa flower recorded at 10 keV on a high resolution Kodak X-ray film with the two techniques. The higher quality of the phase contrast image is evident. Note that the dose delivered for both these images is very high, 50 times larger than a conventional mammography. To reduce the dose, an intensifier screen was introduced behind the film. In figures 22a and 22b two images of the head of a bee, taken at 17 keV, are shown. Compared to the previous high resolution image, the intensifier screen causes a loss in the spatial resolution but the phase contrast image still presents a good contrast enhancement due to the high intensity of the interference peaks.

REFERENCE

- [1] C. Jacobsen *et al.*, *J. Opt. Soc. Am. A* 7, 1847, (1990).
- [2] G. Schmahl *et al.*, *X-ray Microscopy IY, Bogoro-dski Pechatnik, Chernogolovka, Moscow region*, (1994).
- [3] D. Rudolph *et al.*, *Modern Microscopes*, Plenum, New York, (1990).
- [4] A. Snigirev *et al.*, *Rev. Sci. Instrum.* 66 (12), (1995).
- [5] A. Snigirev *et al.*, *E.S.R.F Newsletter reports.* 22, 20 (1994).
- [6] T.J. Davis *et al.*, *Nature* 373, (16 February 1995).
- [7] S.W. Wilkinset *et al.*, *Nature* 384, (28 Nov. 1996).
- [8] M. di Michiel *et al.*, *Proceed. Haga Conference 1997 (in press)*.
- [9] D. Chapman *et al.*, *Phys. Med. Biol.* 42 (1997).

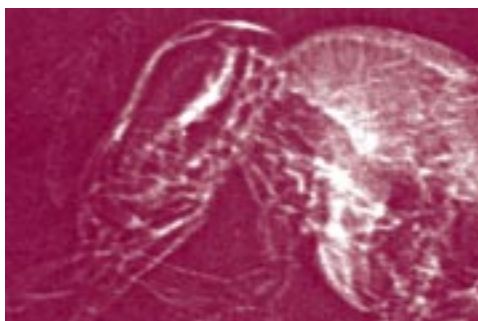
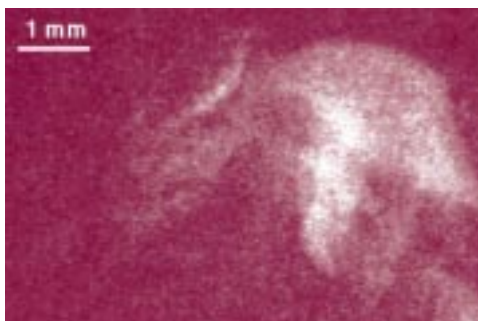
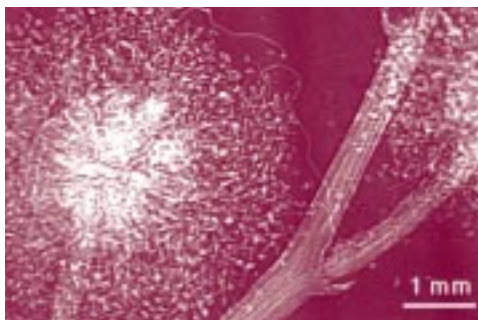
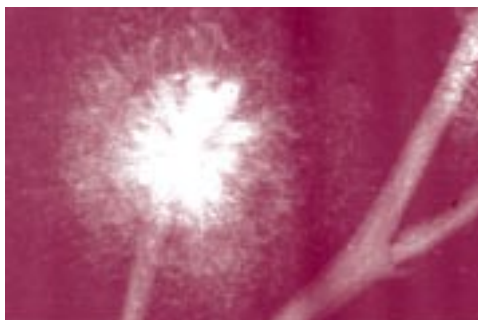


Fig. 21a, 21b: Images of a mimosa flower taken with the conventional absorption technique (a) and with the phase contrast method (b).

Fig. 22a, 22b: Images of the head of a bee recorded at low dose on a standard screen-film system with the conventional absorption technique (a) and with the phase contrast method (b).

TECHNICAL ACHIEVEMENTS



FIRST IMAGE FROM THE SPECTROMICROSCOPE SUPERMAXIMUM

M. BERTOLO, F. BARBO,

A. BIANCO, S. FONTANA,

K. KAZNACHEYEV, S. LA ROSA

(Sincrotrone Trieste, Italy)

✉ bertolo@elettra.trieste.it

On September 18, 1997, the spectromicroscope SuperMAXIMUM achieved an important result in the course of its commissioning phase, namely the acquisition of its very first image which is displayed in figure 1.

SuperMAXIMUM is a spectromicroscope designed to perform photoemission experiments with a high spatial resolution, which is obtained by focusing the radiation on a small spot at the sample (smallest aimed spot size = 50 nm) by means of a multilayer-coated Schwarzschild Objective. Photoemission spectra are recorded by detecting with an electrostatic energy analyzer the electrons emitted from the small radiation spot at the sample. Images of the sample are taken by scanning it perpendicular to the radiation beam.

The image displayed in figure 1 shows a portion of a copper mesh and was acquired by measuring the photon flux downstream of the mesh by means of a photodiode. The estimated spatial resolution is better than 2 microns.

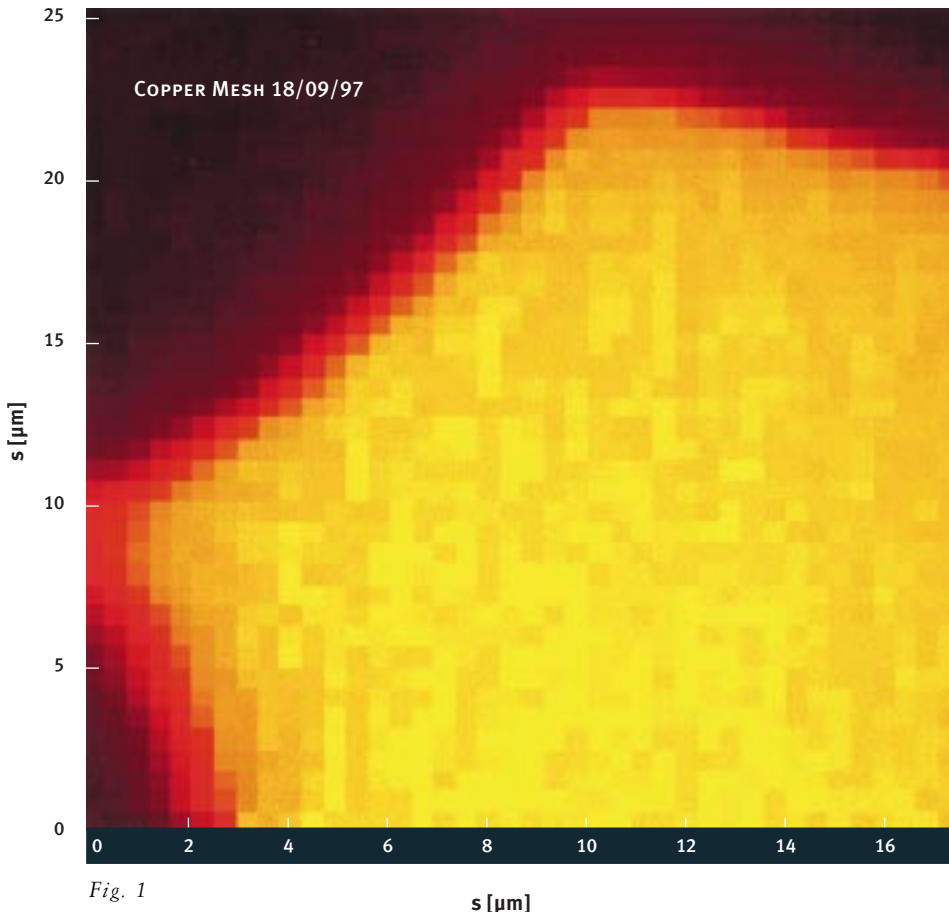


Fig. 1

The following months have been dedicated to improving the spatial resolution, which reached 0.5 microns in December '97.

One of the tests which are used to align the objective is the Foucault test, in which a knife edge is moved across the beam, while its shadow is observed on an MCP placed downstream of it. In the course of such tests we observed interference fringes due to Fresnel diffraction of the X-rays at the knife edge. Figure 2 shows an example recorded at a photon energy of 95 eV. This demonstrates that the beamline preserves up to the sample position the source coherence to an extent which is sufficient to observe interference phenomena.

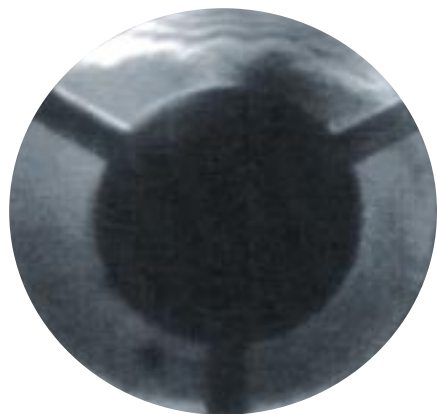


Fig. 2

THE SPELEEM MICROSCOPE

TH. SCHMIDT, J. SLEZAK,

S. HEUN, J. DIAZ,

K.C. PRINCE, E. BAUER

The Spectroscopic PhotoEmission and Low Energy Electron Microscope has been installed at ELETTRA and currently produces the highest spatial resolution of any photoelectron microscope in the world. It is a unique instrument with the possibility of switching from photoemission to LEEM microscopy on the same sample to provide additional structural information.

The picture (figure 3) shows a triangular lead island on a silicon wafer, imaged using photoemission at a photon energy of 91.2 eV. The light is incident from the right hand side and casts a shadow. Parallel to the shadow is a series of diffraction fringes. These are created when the light passes the top edge of the island, as in conventional macroscopic Fresnel diffraction with visible light. In this case the island is flat on the scale of the wavelength of the light (13.6 nm) and so functions as a sharp knife edge. Many fringes are visible because the light is monochromatic and parallel, i.e. partly coherent.



Fig. 3



PROGRESS ON THE GAS PHASE PHOTOEMISSION BEAMLINE

Significant breakthroughs were made both with the monochromator resolution and with the Spectroscopic PEEM-LEEM (SPELEEM) microscope which is attached to a branch-line. The resolving power of the monochromator has been pushed above 16,000 at 65 eV, figure 4.

The SPELEEM microscope developed by Professor E. Bauer and his team at the University of Clausthal has achieved a spatial resolution of 22 nm in an acquisition time of 10 sec, figure 5. The overall energy resolution (photons+analyser) was 1 eV, and will be improved as testing and commissioning proceeds. A resolution better than 0.5 eV has also been achieved in other measurements at slightly reduced spatial resolution.

These achievements have been made possible by the contributions of many people, in particular those who worked directly on the beamline at ELETTRA, the Optics and Electronic Technology groups and many others.

R. CAMILLONI

(I.M.A.I., CNR, Italy)

K.C. PRINCE

(Sincrotrone Trieste, Italy)

✦ prince@elettra.trieste.it

Fig. 4: Resolving power of the Gas Phase Photoemission beamline monochromator, as demonstrated by the absorption spectrum of He near 65 eV. The peaks are due to the N=2 series of the autoionization double excitation states of He. The line shape is a Fano profile and the energy scale has not been converted to eV.

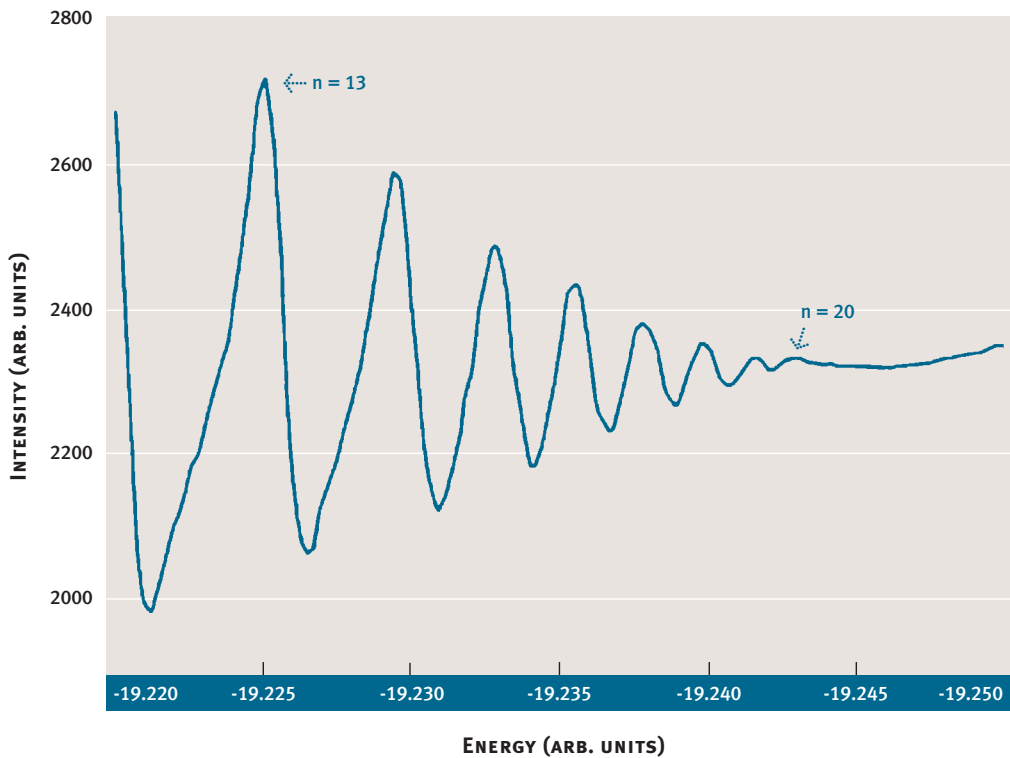
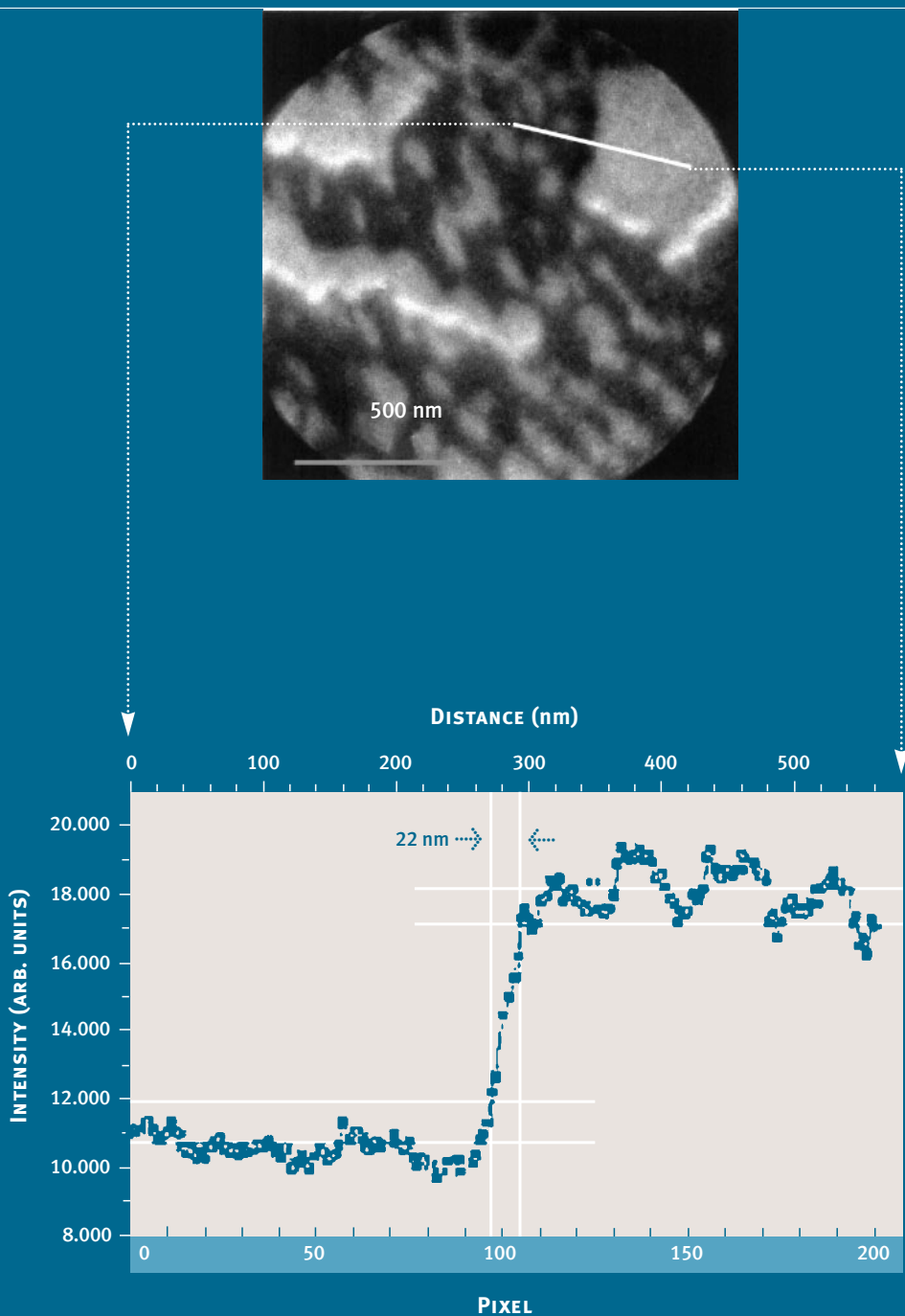
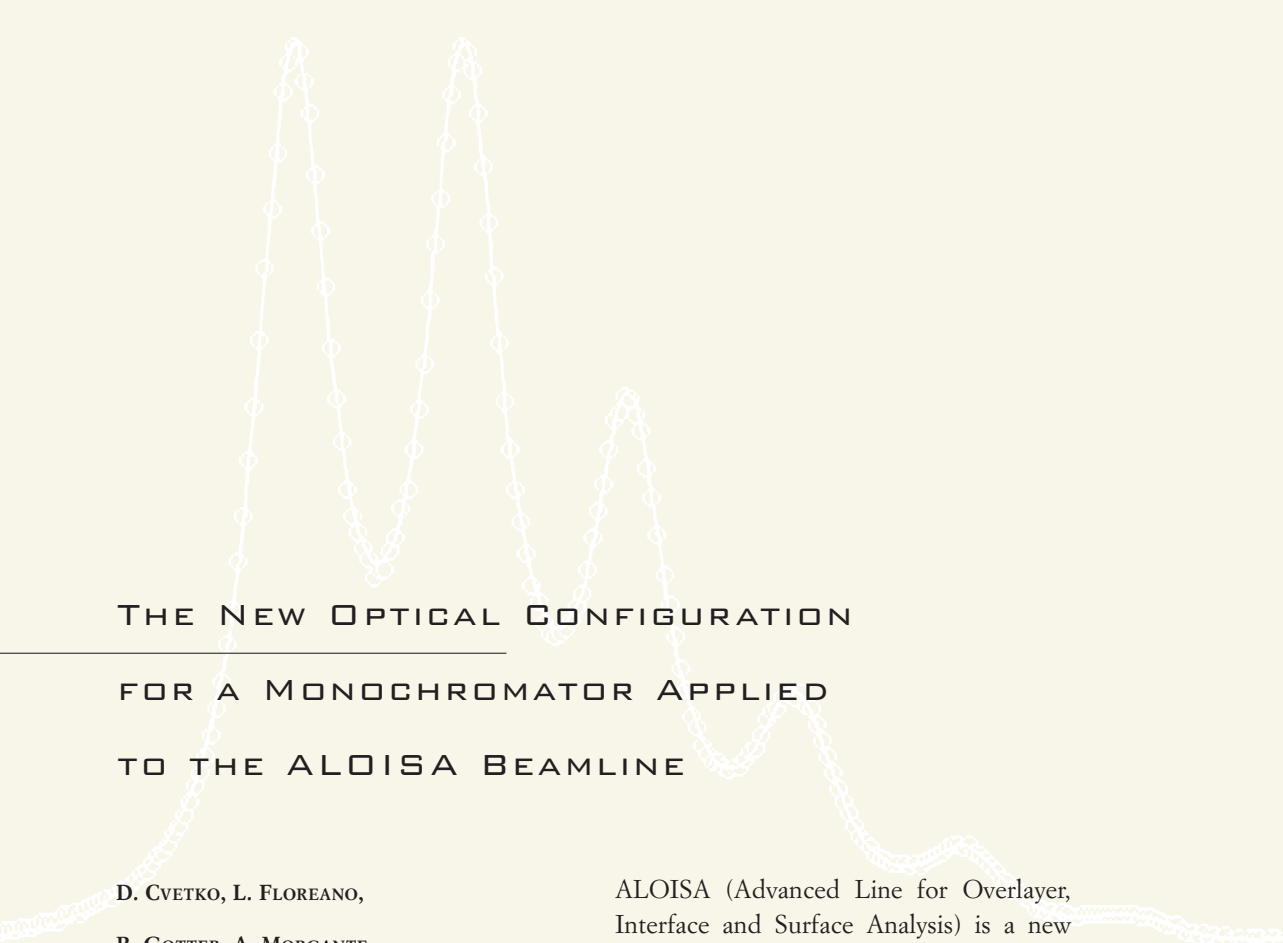


Fig. 5: Silver islands grown in the Stranski-Krastanov mode on W(110). Deposition was done in two steps: the larger islands were evaporated with the substrate at about 600 K, while at lower deposition temperature (400 K) the smaller islands formed. The smaller islands have nucleated at edges of steps of the tungsten substrate. The lower panel shows the line scan (upper panel) across the edge of an island. The resolution is 22 nm or better.





THE NEW OPTICAL CONFIGURATION
FOR A MONOCHROMATOR APPLIED
TO THE ALOISA BEAMLINE

D. CVETKO, L. FLOREANO,

R. GOTTER, A. MORGANTE,

F. TOMMASINI, A. VERDINI

(Laboratorio TASC-INFM, Trieste, Italy)

M. MALVEZZI

(Università di Pavia, Italy)

L. MARASSI

(Università di Modena, Italy)

G. NALETTO, G. TONDELLO

(Università di Padova, Italy)

A. SANTANIELLO

(Sincrotrone Trieste, Italy)

G. STEFANI

(Università di Roma III, Italy)

ALOISA (Advanced Line for Overlayer, Interface and Surface Analysis) is a new multipurpose beamline for surface science experiments, including photoemission, photoelectron diffraction, X-ray diffraction and electron momentum-resolved coincidence experiments. In order to meet the scientific objectives a resolving power of 5000 must be obtained over the full 200-8000 eV energy range while maintaining a high throughput. Also, a good high order rejection is required for a number of experiments. In order to fulfill these requirements, a new monochromator configuration was designed using two separate dispersive systems, one with reflection gratings for energies below 2 keV and another with crystals for energies above 3 keV. The grating-crystal monochromator (GCM) is a four optical elements monochromator (figure 6).

The optical configuration is essentially a slitless Hunter monochromator (HM) in which the dispersive system for the low

energies is a “variable deviation” configuration obtained as a modification of the Zeiss SX-700 one and for the high energies is a channel-cut single crystal. In order to minimise the slope error aberrations in the dispersive plane, the paraboloidal mirrors of the HM are used in the sagittal focusing. The plane optical elements of the dispersive systems work in parallel light, so no aberrations are introduced. The “variable deviation” configuration of the dispersive elements is to fulfill the requirement of a good high order rejection. The possibility of working in parallel light, in the dispersive system, facilitates the exchange between the low and high energy sections. The two sections lay side by side and they can be inserted onto the optical path by means of a slide mechanism. Two independent rotations are used for the low energy scan. The high energy scan mechanism is obtained by coupling the channel-cut crystal to one of these rota-

tions. Two plane gratings (with 1200 and 1600 lines/mm) are used to optimise the monochromator performances in the low energy range and the mechanism for selecting the grating is the same which shifts the two dispersive systems. The channel-cut crystal allows to tune the energy between 3 and 8 keV. The choice of not covering the whole 2-8 keV energy range is dictated by the necessity to limit the vertical shift of the beam coming from the crystal, but it is not a restricting constraint for the present experiments. Moreover, it is already foreseen to install also a larger lattice spacing crystal, beside the Si(111) one, to cover the gap.

The energy resolution of the GCM monochromator has been tested in the low energy range (from about 200 eV up to about 900 eV), which can be covered by the 1200 lines/mm grating. Absorption spectra for few gases (Ar, N₂, Ne, CO) have been taken in a ionisation chamber equipped

Fig. 6: A paraboloidal mirror P_1 collects the radiation from the wiggler-undulator insertion device and collimates the beam on the dispersive system. The energy dispersed beam is collected by a second paraboloidal mirror P_2 and focused on the fixed exit slit. A toroidal mirror T refocuses the monochromatic beam onto the sample in the experimental chamber. This mirror is also used in sagittal focusing, to have similarity with the paraboloidal mirror mounting brackets. The beam deviation angle on P_1 , P_2 and T is 1° . The slope error values are the smallest presently achievable.

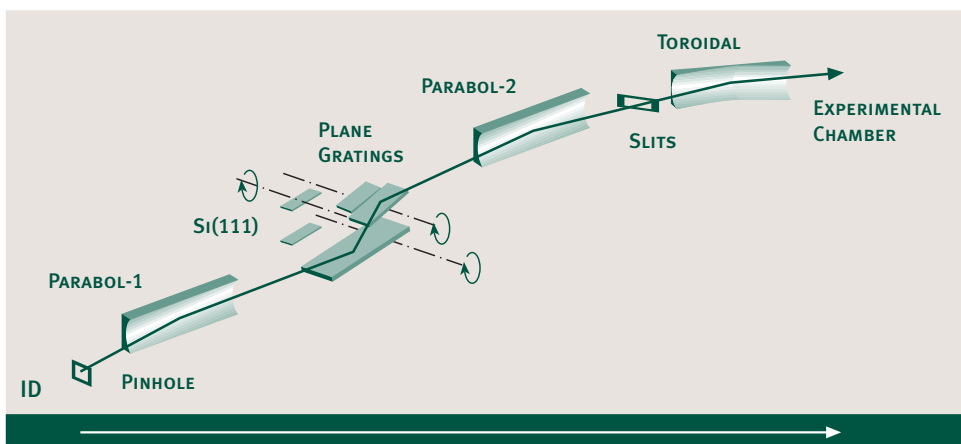
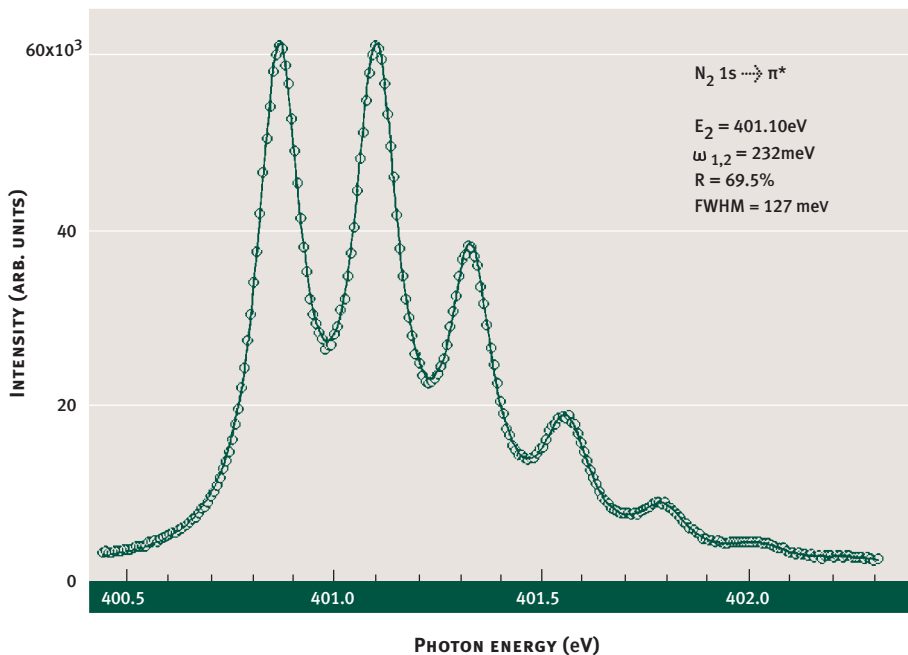


Fig. 7: K-shell excitation spectrum of N_2 . The full line is a fit of seven lorentzian curves to the experimental data. Seven vibrational levels have been acquired. The total width of the lowest energy level is 127 meV.



with a channeltron. This solution allows to operate at very low gas pressures (ranging from 10^{-7} to 10^{-5} mbar) with respect to plate-based acquisition systems. No window is necessary to separate the ionisation region from the beamline, and a small hole (1.5 mm at the entrance, 2.5 mm at the exit) is sufficient to have high vacuum outside the ionisation chamber. In the photoabsorption spectrum of figure 7 the raw data before deconvolution already display a linewidth as narrow as the natural one obtained from the literature (electron energy loss measurements). The preliminary tests have revealed that the GCM at the ALOISA beamline provides a realistic resolving power usually higher than 5000 with top performances close to 10000 in the 400-500 eV range (figure 7). This has been obtained in high

flux conditions, reaching a few 10^{10} photons/s, without shadowing the mirrors and the grating.

The top performances achieved by the GCM have to be attributed to the choice of the optical lay-out with paraboloidal mirrors in sagittal focusing and partly to the high brilliance obtained at ELETTRA, beyond the specifications of the project that were used to design the GCM and calculate its resolving power. As compared to the other monochromators presently working at ELETTRA, the GCM received a larger benefit from this positive result owing to the absence of the entrance slits, so that only the photon source size determines its image size at the exit slits.



THE MULTILAYER TECHNOLOGY LABORATORY
AT ELETTRA PRODUCES STATE-OF-THE-ART
MULTILAYER COATINGS

Within the project of the European Community for the development of an insertion device for circularly polarized light (collaboration of ELETTRA, BESSY and MAX-Lab: ERBFMGECT950007) the Multilayer Technology Laboratory is involved in the part related to a polarimeter (see ELETTRA Newsletter 10-11, July-August 1996). This instrument composed of a polarizer and an analyser is needed for a precise characterisation of the polarization of a photon beam. This is done by deriving the Stokes parameters of a beam, which requires for a beam of unknown polarization characteristics the utilisation of phase retarders (in the ideal case a quarter wave-plate). In the soft X-ray range with photon energies above 100 eV such objects can only be constructed around transmission multilayers [1-3]. These multilayers are prepared on thin (0.1 μm) self standing membranes. Analysers are instead multilayers deposited onto Si wafers.

S. DI FONZO, G. SOULLIE,
W. JARK

(Sincrotrone Trieste, Italy)

✉ difonzo@elettra.trieste.it

✉ soullieg@elettra.trieste.it

✉ jark@elettra.trieste.it

Table 1

PERIOD	NUMBER OF PERIODS	PHOTON ENERGY	(WAVELENGTH)	GRAZING ANGLE	MEASURED REFLECTIVITY	DERIVED INTERFACE ROUGHNESS
4.45 nm	50	146 eV	(8.5 nm)	76.3	0.11	0.5 nm rms
3.18 nm	50	193 eV	(6.4 nm)	85	0.06	0.4 nm rms
3.22 nm	100	202 eV	(6.1 nm)	74.6	0.10	0.5 nm rms

In our attempt to reproduce an already successfully tested Cr/C multilayer [4-7], we produced a number of test objects with varying parameters for the period (between 3.2 nm and 4.5 nm) and the number of periods (between 34 and 100). The reflectivity performance, which is closely related to the transmission performance [6-8], was tested at the BESSY laboratory at a reflectometer beamline receiving the monochromatic light from an SX700 type monochromator.

The best performance for phase-shift with respect to transmission is obtained for angles of incidence close to 45%. Consequently the analysis concentrated onto this range of angles. However, all objects were also measured at almost normal incidence (75 - 85%).

The coatings were put onto substrates with about 0.5 - 0.6 nm rms roughness as measured by optical profilometry. The same value of 0.5 nm rms interface roughness provides also the best agreement between calculated and experimental results for the reflectivity (see figure 8).

Consequently during growth to more than 300 nm total film thickness the interface micro-roughness did not degrade appreciably. Indeed the performance was not limited anymore by the characteristics of the sputter materials but by the quality of the membranes.

The observed interface roughness of only about 0.5 nm rms is a very encouraging result. Indeed our results present the best entries for the combination Cr/C in the compilation of the Center for X-ray Optics (at the Ernest Orlando Lawrence Berkeley National Laboratory, Berkeley, CA, USA) for the best normal incidence reflectivities measured for this combination for photon energies around 200 eV (further information at the web at <http://www-cxro.lbl.gov/multilayer/survey.html>):

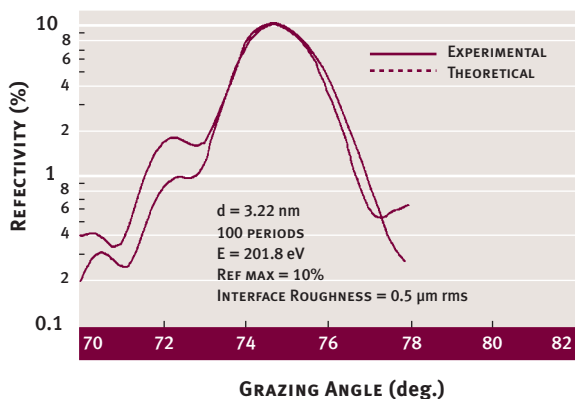
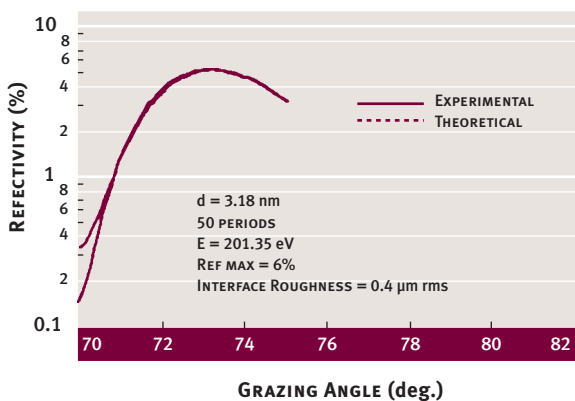
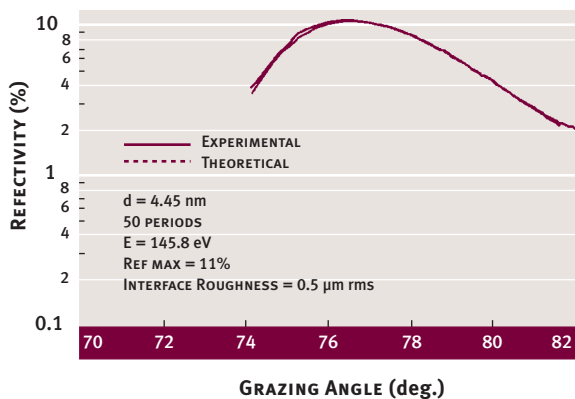
In order to produce phase-shifters for higher energies in the water-window [8] we already produced first multilayers based on Ni/Sc and Cr/Sc structures.

We gratefully acknowledge the help of our colleagues F. Schäfers and H.C. Mertins during the measurements at the BESSY laboratory.

REFERENCE

- [1] J.B. Kortright, J. H. Underwood, *Multilayer optical elements for generation and analysis of circularly polarized X-rays*, Nucl. Instrum. Meth. A291, 272-277 (1990).
- [2] J.B. Kortright, H. Kimura, V. Nikitin, K. Mayama, M. Yamamoto and M. Yanagihara, *Soft X-ray (97 eV) phase retardation using transmission multilayers*, Appl. Phys. Lett. 60, 2963-2965 (1992).
- [3] S. Di Fonzo and W. Jark, *A Quarter Waveplate for the Polarization Analysis close to the Carbon K-edge*, Rev. Sci. Instrum. 63, 1375 (1992).

Fig. 8: Reflectivity curves measured near normal incidence for three Cr/C multilayers.



[4] S. Di Fonzo, W. Jark, F. Schäfers, H. Petersen, A. Gaupp and J.H. Underwood, *First Direct Measurement of the Circular Polarization of Synchrotron Radiation close to the Carbon K-edge*, *Synchrotron Radiation News* Vol. 6, No. 2, 16 (1993).

[5] F. Schäfers, H. Petersen, A. Gaupp, S. Di Fonzo, W. Jark and J.H. Underwood, *Measurement of circular polarization close to the carbon K-edge*, *Proc. of SPIE* 2010, 157 (1993).

[6] S. Di Fonzo, W. Jark, F. Schäfers, H. Petersen, A. Gaupp and J.H. Underwood, *Phase Retardation and Full Polarization Analysis of Soft X-ray Synchrotron Radiation close to the Carbon K-edge using a Multilayer Transmission Filter*, *Appl. Opt.* 33, 2624 (1994).

[7] F. Schäfers, A. Furuzawa, K. Yamashta, M. Watanabe, J.H. Underwood, in *Physics of Multilayer Structures, 1994 Technical Digest Series, Vol. 6* (Opt. Soc. of America, Washington DC, 1994).

[8] S. Di Fonzo, B.R. Müller, W. Jark, A. Gaupp, F. Schäfers and J.H. Underwood, *Multilayer Transmission Phase-shifters for the Carbon K-edge and the Water Window*, *Rev. Sci. Instrum.* 66, 1513 (1995).

A COMPLETE DATA ACQUISITION SYSTEM FOR VERY LOW CURRENT MEASUREMENTS

A. GALIMBERTI, D. GIURESSI,

R. SERGO

(Sincrotrone Trieste, Italy)

✦✦✦ galimberti@elettra.trieste.it

✦✦✦ giuressi@elettra.trieste.it

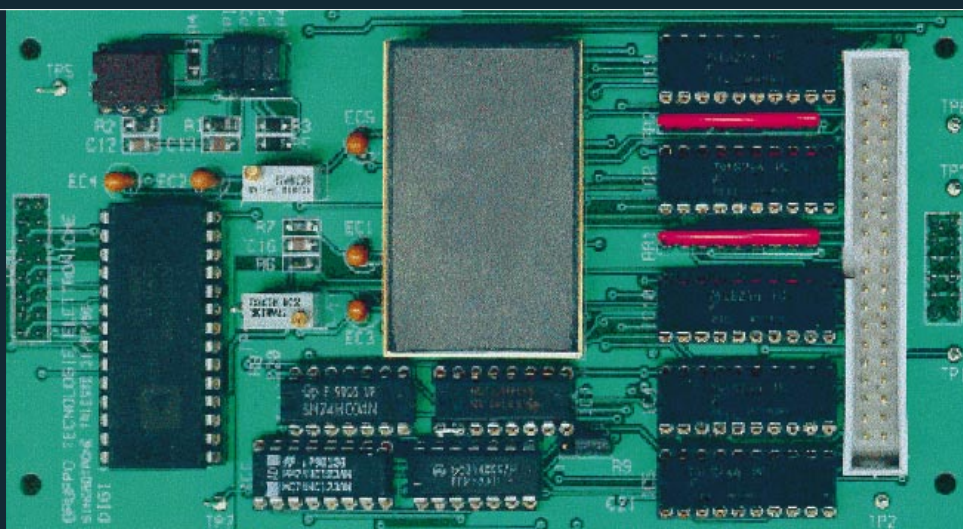
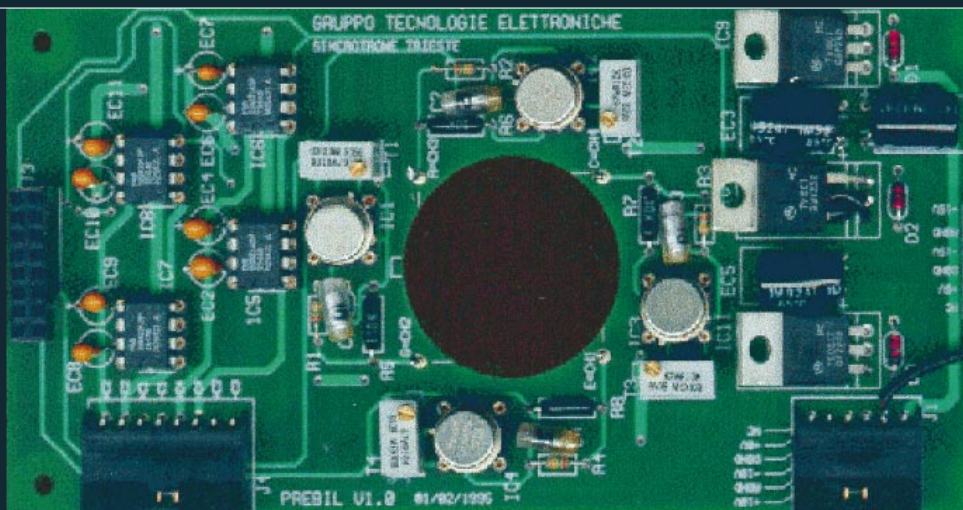
✦✦✦ sergo@elettra.trieste.it

It is very common, within the experimental users equipment, to acquire data of low current values. A complete data acquisition system for very low current measurement has been designed and implemented at ELETTRA.

Photodiodes, wire detectors, photon flux detectors, entrance and exit slits of the monochromators, grids and gratings are only some of the potential low current sources in an experimental environment.

Typically the bandwidth requested for these signals is very low (few Hz), but the current range is wide and cover values from 1mA down until 1pA. Due to the various operation modes of the synchrotron radiation storage ring, these current values have a wide dynamic range and in some acquisition points need very high precision. Usually there are complex commercial instruments that are used for this purpose, but their cost is not negligible, in particular when a single experimental user needs many low current detections at various different locations along his beamline and experimental chamber.

Fig. 9 (above) and fig. 10 (below).



The Beamline Control Group of the Sincrotrone Trieste has developed a versatile instrumentation for this kind of applications. High precision, very low noise, various programmable gain settings, analog and 16bit digital outputs are the main features of this electronics. Moreover the global cost of this system has been considerably lower than commercial ones.

High precision component, small length wire connections, low noise power supply, power supply filtering, accurate grounding design and shielding are some of the highlights of this instrument. We take care, in fact, of a whole data acquisition system design, not only of a single instrument design. So the entire signal path, from the sensor until the host computer, has been taken in account for the design.

No cable connections divided the analog signal treatment from the current source. The preamplification is performed, within a shielded box, immediately outside the vacuum chamber and the air side plug of the vacuum feedthrough is mounted directly on the instrumentation chassis. High insulation materials, like teflon, are used for separating the low impedance input points from the rest of the circuits, avoiding any parasitic current coupling with the signal.

Low input bias components allow a sensitivity down to 1pA and together with low offset devices assure high DC precision in the amplification and current to voltage conversion of the signal. An amplified 10V signal is the analog output of the system.

Each single data acquisition system may be configured up to eight low current measurement points. An optional analog to digital conversion board is available.

A 16bits A/D converter allows a parallel interface with any host computer, in order to acquire the data and control the programmable settings of the instrumentation.

For an ELETTRA experimental user a software package, developed by the Beamline Control Group, allows an immediate interfacing of this electronic device with the Beamline Control System.

The first prototype of this system has been used in 1994 for the commissioning of the SuperESCA, the first operational beamline of the ELETTRA laboratory. Placed on the entrance slit chamber of the monochromator, played a key role in the effort to get the first photon beam in an experimental chamber at ELETTRA.

Another interesting application for the SuperESCA beamline is a first attempt to obtain an automatic alignment control system. A photodiode current is acquired by this electronic device and, due to the good bandwidth performance, a sophisticated fuzzy control system, implemented in a real time environment, acts on the beamline optics performing the alignment. Right now tens of these electronic instruments are installed or being installed in the beamlines, in operation or under construction, of ELETTRA.

HIGHLY RESOLVING (< 10 MILLIK)
TEMPERATURE-GRADIENT-CELL FOR X-RAY
SCATTERING STUDIES ON SOLUTIONS

A temperature gradient cell for X-ray scattering investigations on the thermal behaviour of soft matter manybody-systems, such as in gels, dispersions and solutions, has been developed. Depending on the adjustment of the temperature gradient in the sample, on the focus size of the X-ray beam and on the translational scanning precision an averaged thermal resolution of a few thousands of a degree can be achieved. This is at least one order of magnitude better than what can be reached in commonly carried out temperature scan experiments using either a thermostated water-circuit or electrical devices such as, e.g., a Peltier element. Moreover, the method guarantees best equilibrium conditions in the sample.

The resolving power has been demonstrated in first pilot experiments on the main transition of lecithin. In the figures 11A and 11B the contour plots of this transition display the first two order peaks of the liquid crystalline phase (in each case

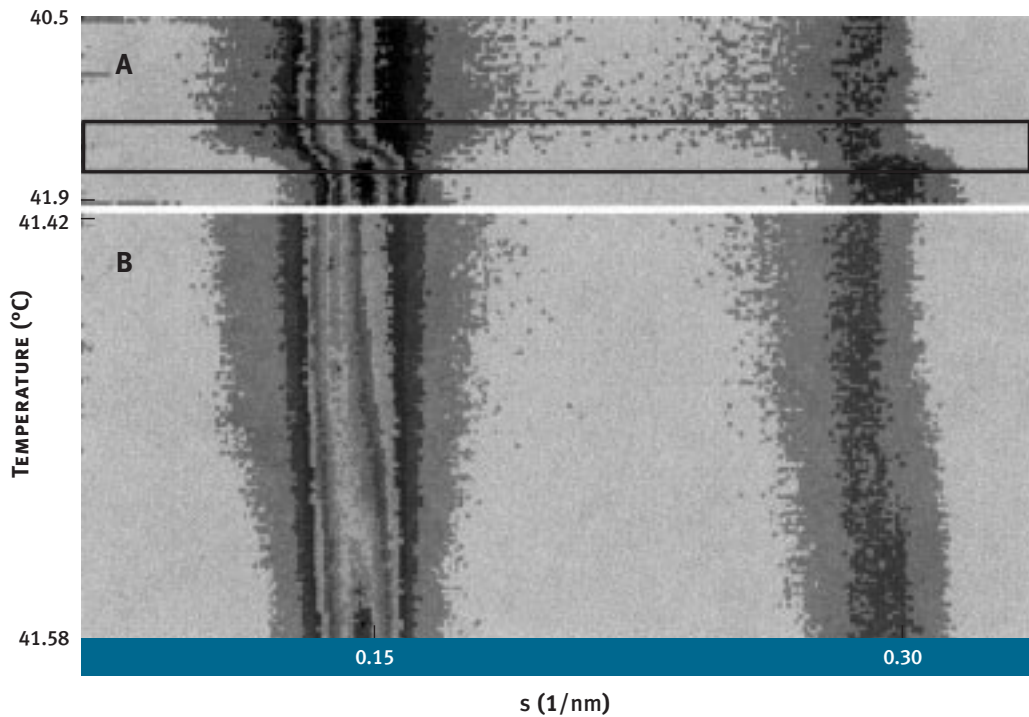
**M. RAPPOLT, H. AMENITSCH,
P. LAGGNER**

*(Institute of Biophysics and X-ray
Structure Research, Austrian
Academy of Science, Graz, Austria)*

S. BERNSTORFF

(Sincrotrone Trieste, Italy)

Fig. 11

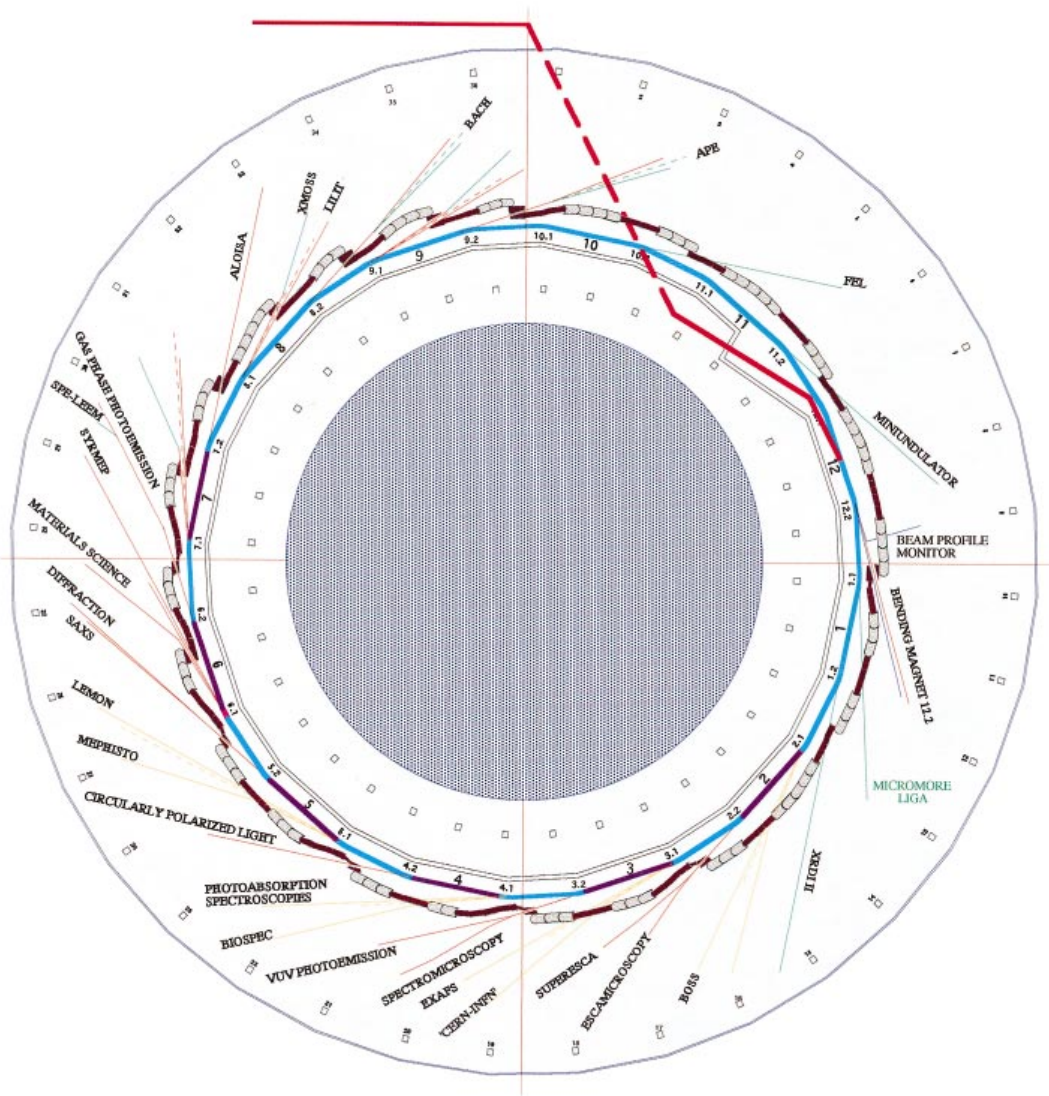


lower half) and the ripple phase (in each case upper half), respectively. In this experiment the temperature gradient was set to 0.28 °C/cm, the FW of the beam at the sample was 0.2 mm and the translational scanning was carried out in steps of 1 mm over a range of 1.40 °C (A) and in steps of 50 μm over a range of 0.16 °C (B), thus achieving nominal thermal resolutions of 0.028 °C (A) and 0.0014 °C (B), respectively. Simply spoken, figure 11B shows a zoomed part of 11A (rectangular box).



ELETTRA BEAMLINE STATUS

(DECEMBER 1997)



Status: Operational

#	BEAMLINE OR FACILITY	RT'S INSTITUTION	USER OPER	PHOTON SOURCE
1	SuperESCA	Sincrotrone TS	Mar 1995	U 5.6 Undulator
2	VUV Photoemission	CNR-ISM	Jun 1995	U 12.5 Undulator
3	ESCAMicroscopy	Sincrotrone TS	Jun 1995	Branch Line of N° 1
4	X-ray Diffraction	CNR	Jun 1995	W 14.0 Wiggler
5	Small-Angle Scattering	Austrian Academy of Sciences	Sep 1996	Branch Line of N° 4

Status: Under Commissioning

#	BEAMLINE OR FACILITY	RT'S INSTITUTION	PHOTON SOURCE	USER OPER
6	Mammography (SYRMEP)	Univ. of Trieste-INFN	Jan 1998	Bending Magnet
7	Gas-Phase Photoemission	CNR-IMAI-Univ. of Rome-INFN	Jan 1998	U 12.5 Undulator
8	SPE-LEEM	Univ. of Clausthal	Jan 1998	Branch Line of N° 7
9	Spectro-Microscopy	Sincrotrone TS-EPFL-CXRL	Jan 1998	Branch Line of N° 2
10	Surface Diffraction (ALOISA)	CNR-INFN	Jan 1998	U 8.0 Undulator/Wiggler

Status: Approved by PAC and CdA - Under Construction or Advanced Design

#	BEAMLINE OR FACILITY	RT'S INSTITUTION	PHOTON SOURCE
11	Circularly Polarized Light	CNR-ISM-Univ. of Rome I-CNR-ICMAT	Cross-Field Undulator/Wiggler
12	EXAFS	Univ. of Trieste - Sincrotrone TS	Bending Magnet
13	LIGA	Micromore	Bending Magnet
14	Materials Science	Czech Academy of Sciences	Bending Magnet
15	A Multipurpose X-ray Beamline (BOSS)	J. Stefan Institute Ljubljana	Bending Magnet
16	Beamline for Advanced Dichroism (BACH)	INFN	Cross-Field Undulator
17	Dichroic Photoemission (APE)	INFN	Cross-Field Undulator
18	Soft X-ray Optical Spectroscopy (X-MOSS)	INFN	Bending Magnet
19	Proximity Photolithography (LILIT)	INFN	Bending Magnet

Status: Approved by PAC - Under Consideration for Funding

#	BEAMLINE OR FACILITY	RT'S INSTITUTION	PHOTON SOURCE
20	Miniundulator	CNR	Undulator
21	BIOSPEC	CNR	Bending Magnet
22	MEPHISTO	CNR	Bending Magnet
23	Photoabsorbion Spectroscopies	CNR	Bending Magnet
24	High Resolution Photoemission (LEMON)	CNR	Bending Magnet
25	XRD II	Sincrotrone TS	Wiggler

Status: To Be Reviewed by SAC

#	BEAMLINE OR FACILITY	RT'S INSTITUTION	PHOTON SOURCE
26	Nanospectroscopy	Sincrotrone TS	FEL Undulator
27	Fluorescence Microanalysis	Sincrotrone TS	Bending Magnet

Status: Under Final Consideration

#	BEAMLINE OR FACILITY	RT'S INSTITUTION	PHOTON SOURCE
28	Soft X-ray Test BL	Sincrotrone TS	Bending Magnet
29	Hard X-ray Test BL	Sincrotrone TS	Bending Magnet
30	TEST	INFN-CERN	Bending Magnet



THE MACHINE



THE ACCELERATORS

The third generation light source ELETTRA is optimised for the VUV/Soft X-ray photon range. The storage ring is a twelve fold symmetric Double Bend Achromat structure with one straight section used for injection and eleven straight sections available for insertion devices. The main parameters with the lattice functions are shown in table 1 and figure 1.

The layout of the accelerator complex in figure 2 shows the storage ring in the centre, with a service gallery located internally and the experimental hall of 20 m radial width on the outer side. A linear accelerator outside the experimental hall is used for the pre-acceleration of the electrons up to the injection energy. The linac is made up of a 100 MeV low energy part (which has also been designed to drive a possible Free Electron Laser) and seven six metre long sections equipped with SLED type energy compression cavities. From the end of the linac the particles traverse an underground transfer line to the inner side of the storage ring, where they are deflected upwards and then injected into ELETTRA.

Tab. 1: ELETTRA ring parameters.

PARTICLES	ELECTRONS
Storage ring lattice type	DBA
Circumference [m]	259.2
Number of achromats	12
Beam energy range [GeV]	0.7 to 2.35
Beam height in experimental area [m]	1.3
Length of Insertion Device (ID) straight sections [m]	6 (4.8 useful for ID's)
Number of straight sections of use for ID's	11
Number of bending magnet source points	12
Beam revolution frequency [MHz]	1.157
Number of circulating electron bunches	1 to 432
Time between bunches [ns]	864 to 2
Energy lost per turn without ID's [keV]	255.7
Energy lost per turn with ID's [keV] at 2.0 GeV*	290.2
Critical energy [keV]	3.2
Bending magnet field [T]	1.2
Tunes: horizontal/vertical	14.3/8.2
Natural emittance at 2.0 GeV [nm-rad]	7.0
Geometrical emittance coupling %	< 1
Spurious dispersion**: horizontal (rms max/min) [cm]	6/2
Spurious dispersion**: vertical (rms max/min) [cm]	1.5/0.5

* U_{5,6}, U₈, two U_{12,5} and W₁₄ at minimum gap.

** At the centre of insertion straights

Fig. 1: The lattice functions.

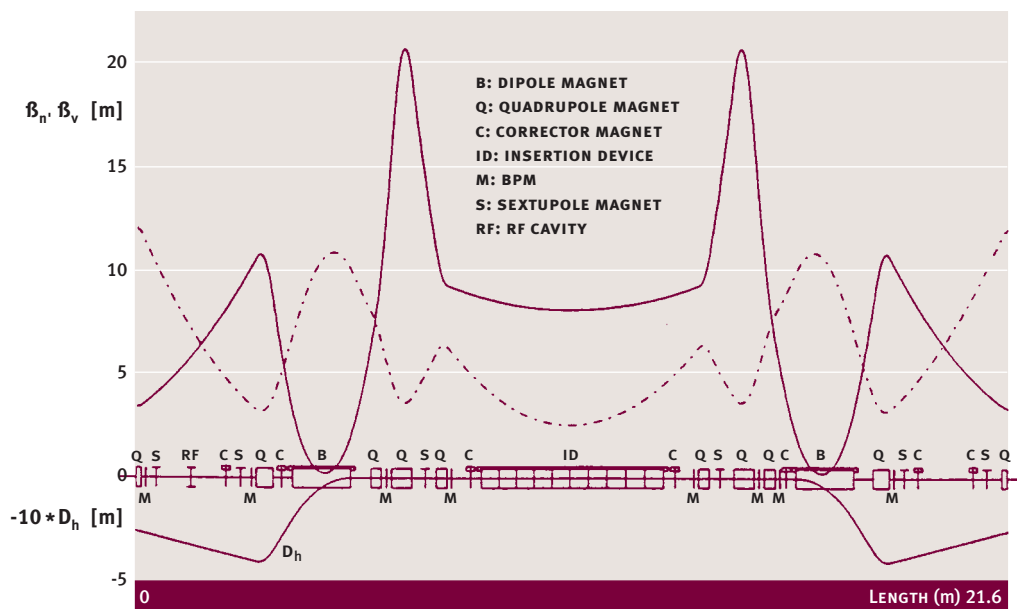


Fig. 2: Layout of the accelerator complex.

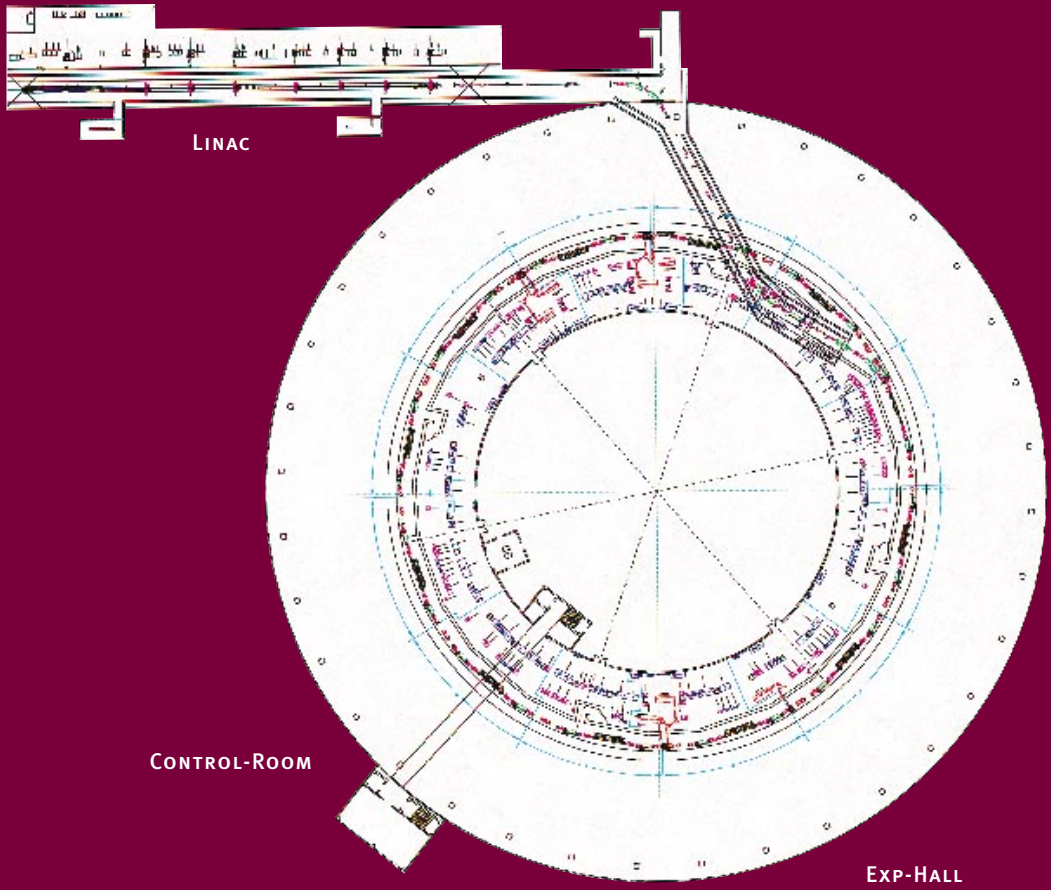


Fig. 3: The injection system in one straight section.

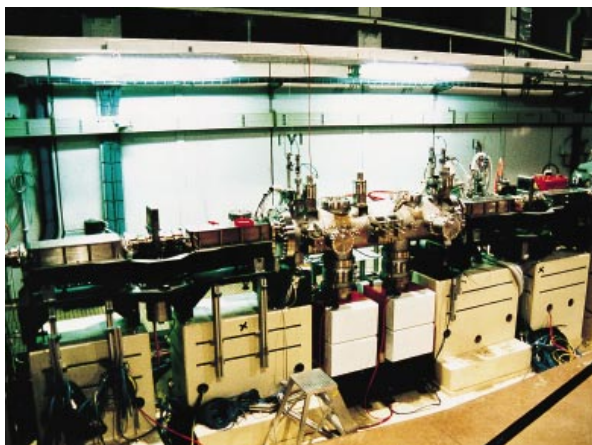
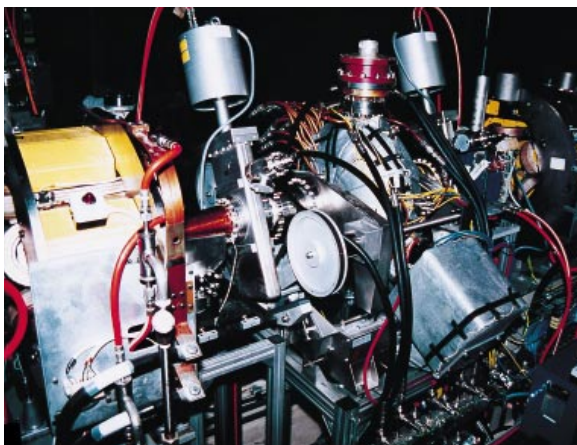


Fig. 4: A radio frequency cavity with the mechanical tuning system.



The injection system in the storage ring is composed of two septa, housed in a common vacuum tank and two pairs of kickers placed symmetrically around the straight section centre. Figure 3 shows the injection system occupying one straight section of the achromat structure.

There are four independent 60 kW RF-stations with single cell cavities used for acceleration. Each cavity is equipped with a mechanical tuning system that acts on the length of the cavity and a precise cooling/heating system that allows high precision cavity temperature selection in the range 35 to 70 °C. The cavity, with its tuning system, vacuum pump and vacuum valves is shown in figure 4.

For diagnostics there are six fluorescent screens distributed around the ring, 96 Beam Position Monitors (BPM's), 12 single button electrodes, three pairs of scrapers, two striplines, a synchrotron light monitor, one current measurement device and one tune measurement system. The BPM system is an essential feature of the machine by which we provide the Users a reproducible orbit and has a resolution of 2 μ m. The con-

trol system uses a distributed architecture with 3 computer layers and 2 networks. On the highest level there are powerful UNIX workstations providing graphical user interfaces to facilitate operation which are connected by Ethernet to the process level that uses VME standards. Figure 5 shows a part of the storage ring synoptic as seen by the operator on the computer screen with some application windows opened.

There are at present five permanent magnet insertion devices installed, four undulators and a wiggler, with characteristics

Fig. 5: A typical screen view in the control room whilst operating the machine.

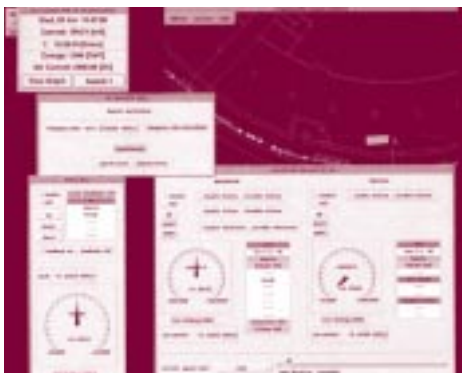
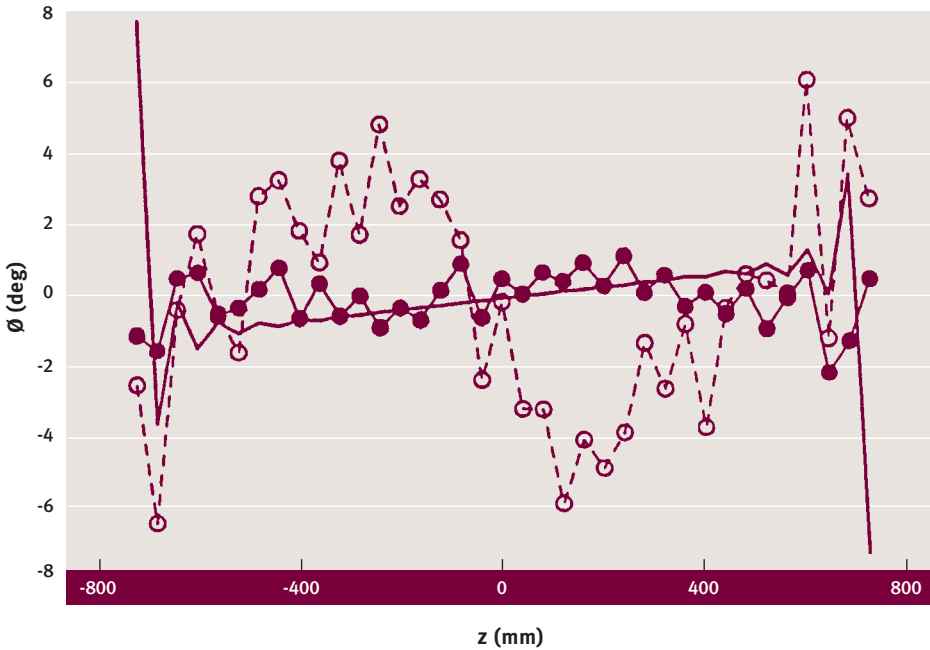


Fig. 6: Radiation phase errors at minimum gap, before (dashed) and after (solid).*
 * Phase shimming for U8.0



given in table 2. A full insertion device is split in three identical units (1.5 m long) and there are a total of 13 individually controlled modules. The individual units make handling very easy and one full device and the low gap vacuum chamber (including bake out) can be installed during a one week shut down. The five insertion devices feed nine beamlines.

Great progress has been made in the shimming of insertion devices, leading to rms phase errors as small as 1°. Figure 6 shows the measured phase errors of an ELETTRA insertion device before and after shimming. The light spectrum calculated from the field measurements for zero emittance is shown in figure 7 and makes evident that even the 45th harmonic has still 70% of its full intensity, however, a realistic beam with final emittance and

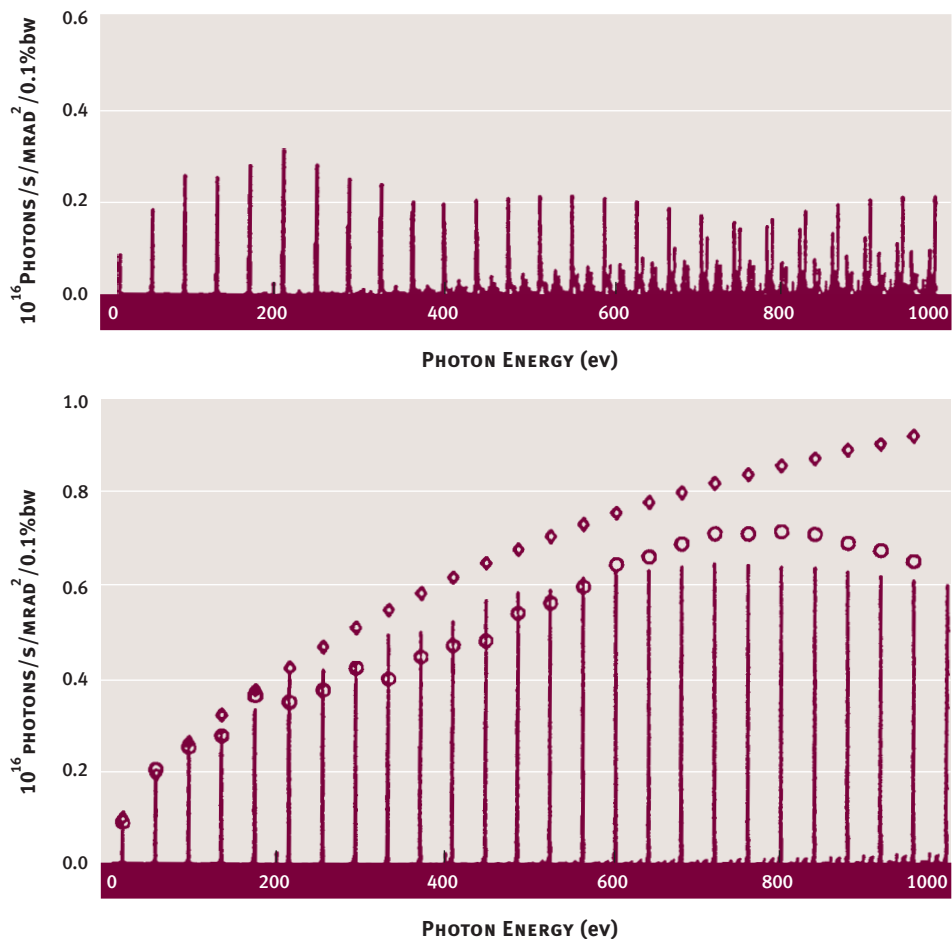
energy spread of the present generation of light sources cannot really make use of this excellence. In addition to the above mentioned insertion devices an electromagnetic elliptical wiggler has recently been installed (see figure 5).

Tab. 2: Initial Insertion Devices installed in ELETTRA.

BEAMLINE	ID#	TYPE	N	GAP (mm)	Bo (T)	K
SuperESCA ESCA microscopy	2	U5.6	81	27.0	0.44	2.3
VUV photoemission Spectromicroscopy	3	U12.5	36	28.0	0.51	5.9
X-ray diffraction Small angle scattering	5	W14.0	30	22.0	1.50	19.6
Gas phase photoemission SPE-LEEM	6	U12.5	26	26.0	0.55	6.4
Surface diffraction	7	U8.0	19	26.0	0.71	5.3

+ one bending magnet source (SYRMEP)

Fig. 7: Calculated on-axis spectrum at minimum gap, before (upper) and after (lower) phase shimming for U8.0. The intensities of an ideal undulator are as indicated.



MACHINE OPERATION

The commissioning of ELETTRA started in October 1993 and right from the beginning a fraction of the operations time was dedicated to users, which in the following years has been steadily increasing to a level of 5064 hours in 1997, corresponding to 81% of the total available up-time (see figure 8). The efficiency in delivery of the scheduled time for 1997 is shown in figure 9. For 1998 a total of 6528 hours up-time is foreseen of which 5256 are scheduled for user experiments. The amount of beamtime scheduled for machine studies and unscheduled maintenance has remained constant at around 18% for the last three years.

In 1997 the machine operated 24 hours per day, 7 days per week during 10 runs of 3 to 5 weeks for scientific experiments, followed by periods of shut down of 1 to 2 weeks (3 weeks for the summer shutdown). All major maintenance and installation work were carried out during these periods. To accommodate the increased number of operating hours in 1998 six operating periods have been planned having a duration of 6 to 8 weeks interrupted by 3 short (1 week) and 2 long (4 weeks) shutdown periods.

Fig. 8: Operating hours since the start of commissioning.

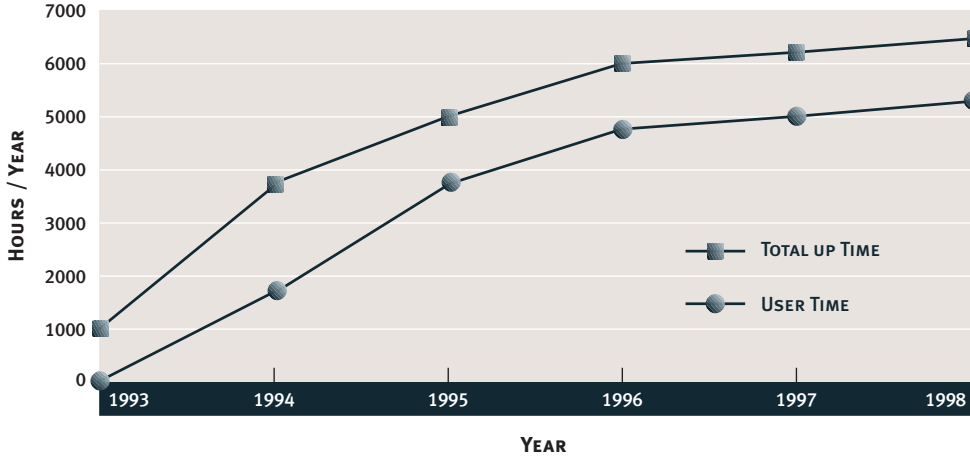
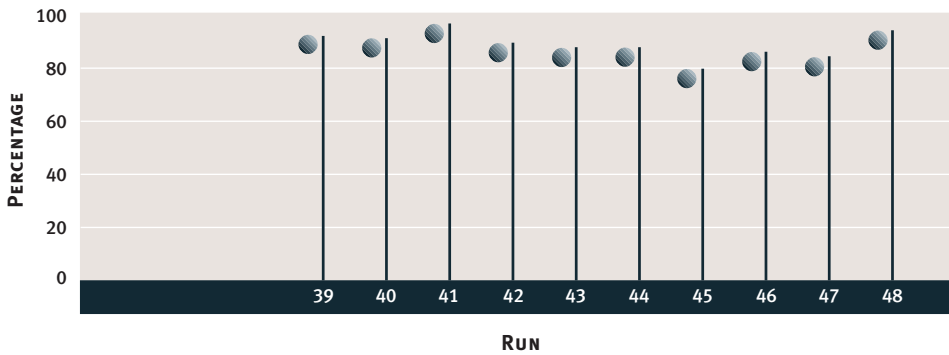


Fig. 9: Run uptime during 1997 which gave an overall yearly uptime of more than 91%.



The longer runs are more advantageous permitting a more efficient operation of the machine.

Normal operation during 1997 foresaw one refill per day, except when operating in the higher brightness mode when two refills per day were performed because high brightness entails a reduction of lifetime (see above). Table 5 shows machine parameters under various modes of operation.

The linac provides beam at 1.0 GeV which then has to be ramped to the final operating energy of 2.0 GeV. The procedure was fine-tuned over the years to reduce the amount of time spent for a refill which during the latter part of last year has been reduced to little less than fifteen minutes.

A high degree of machine automation has been achieved by the installation of a program task manager called the One Button Machine or “1bm” which allows normal operation to be run by a single operator thereby freeing human resources. The program performs all processes required for a refill, from the closing of machine shutters and beam dump to energy ramping. Improvements are continuing to be made to this program which will be extended to intelligently start machine systems from both normal and fault states and to perform shutdowns.

The operations efficiency during experimental runs, as shown in figure 9, is on the average since the beginning of 1997 above 91%. The distribution of down time caused

Tab. 5: Machine Operating Conditions.

Operation mode	multibunch
Duration of a refill (incl. ramping etc.) [min]	~15
Injection energy [GeV]	1.0
Beam energy for Users [GeV]	2.0
Injected current [mA]	300
HIGH BRIGHTNESS MODE (lifetime dominated by the Touschek effect)	
Energy spread (rms) ‰	0.8
Lifetime (250 mA) [hours]	11
Bunch length (1 σ) [mm]	5.4
BEAM DIMENSIONS (1 σ)*	
ID source point - horizontal/vertical [μ m]	241/15
Bending magnet source point - horizontal/vertical [μ m]	139/28
BEAM DIVERGENCE (1 σ)*	
ID source point - horizontal/vertical [μ rad]	29/6
Bending magnet source point - horizontal/vertical [μ rad]	263/9
NORMAL MODE (relaxed Touschek effect)	
Energy spread (rms) ‰	2.8
Lifetime (250 mA) [hours]	26
Bunch length (1 σ) [mm]	11
BEAM DIMENSIONS (1 σ)*	
ID source point - horizontal/vertical [μ m]	255/23
Bending magnet source point - horizontal/vertical [μ m]	371/43
BEAM DIVERGENCE (1 σ)*	
ID source point - horizontal/vertical [μ rad]	31/9
Bending magnet source point - horizontal/vertical [μ rad]	698/14

* The values shown (taking into account the rms energy spread) are averages, obtained from a consideration of different angle and position values of the spurious dispersion, and can vary by $\pm 10\%$.

by various systems for the period is shown in figure 10. Thunderstorms and external electrical disturbances accounted for 15% while water cooling service accounted for 10% of all down time. Taking into account pure machine failures and operator handling gives an uptime of 93% for 1997. The largest source of downtime was due to power supply failures. The time lost during a refill (arising from the difference between practical and theoretical refill time and miss-handling) has dropped to 8% in 1997 compared to 14% in 1996 because of the improvements to the '1bm' code.

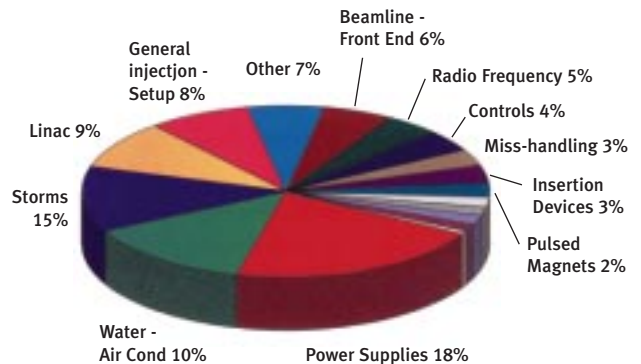


Fig. 10: Statistics of system faults over the year.

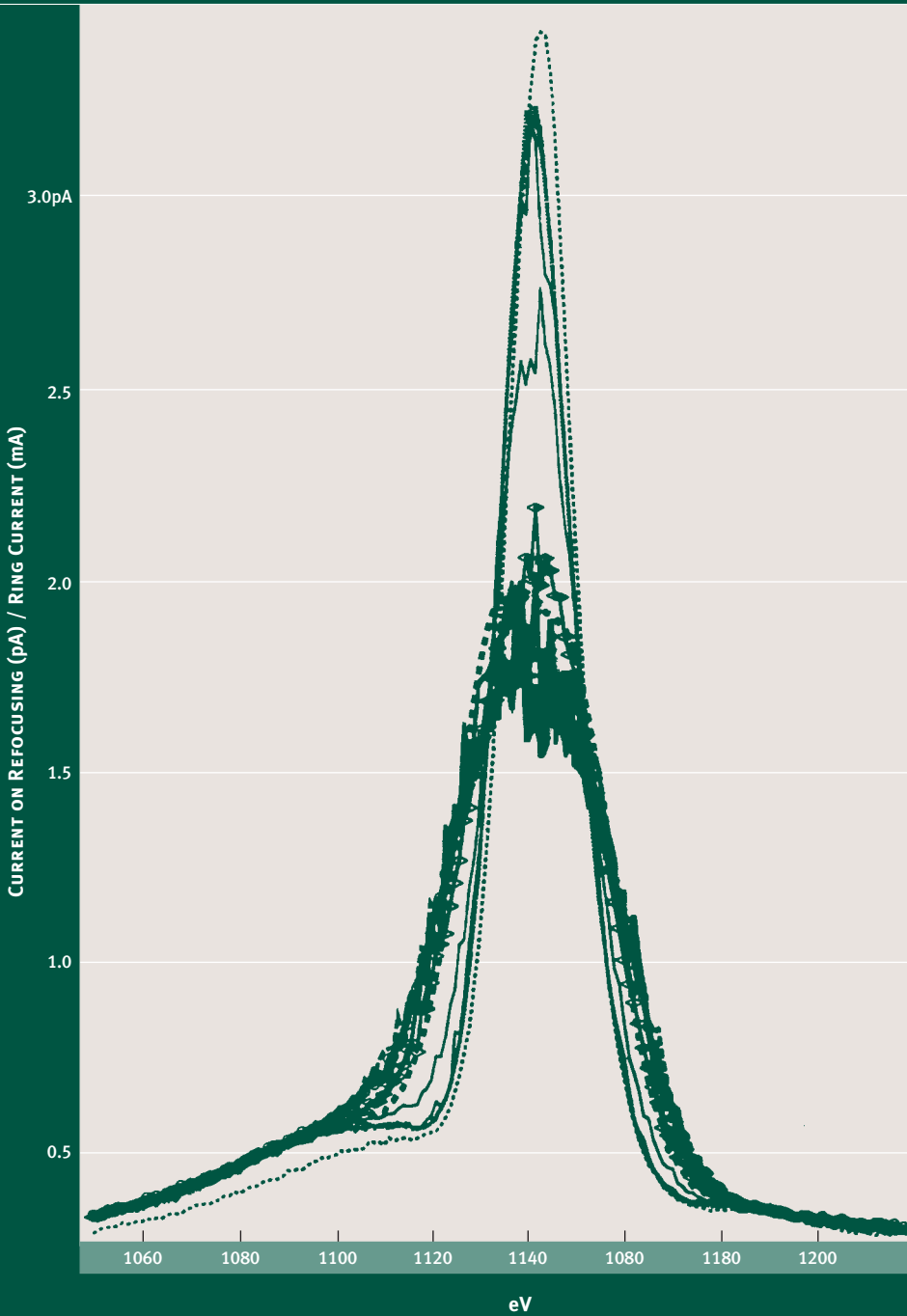
MACHINE PERFORMANCE ISSUES

At the ELETTRA nominal energy of 2 GeV no effect of insertion devices on beam dynamics has so far been observed, in agreement with calculations. Only at lower energies, 1.0 GeV, is a slight reduction in dynamic aperture observed.

Ground vibrations are also not an issue, demonstrating the high quality of the selected site. No harmful vibrations are observed in the frequency range from 2-10 Hz and the short term beam stability is better than $\pm 2 \mu\text{m}$. Slow thermal effects are compensated by an orbit feedback system implemented at the highest control level.

Ground setting effects, which would require frequent re-alignments are also not harmful. The machine has been surveyed 7 times since 1993, but only re-aligned once and is today still within an accuracy of 0.1 mm for one standard deviation. A large reduction of the setting effects was observed between the first and second measurements. A difference in circumference length of 1.2 mm has been measured between summer and winter. During summer time a daily cycle of the orbit change is occasionally observed. The largest orbit

Fig. 11: The effect of longitudinal multibunch instabilities on the 5th harmonic of ID spectra, as a function of cavity temperature. The dotted line corresponds to a good control of instabilities.



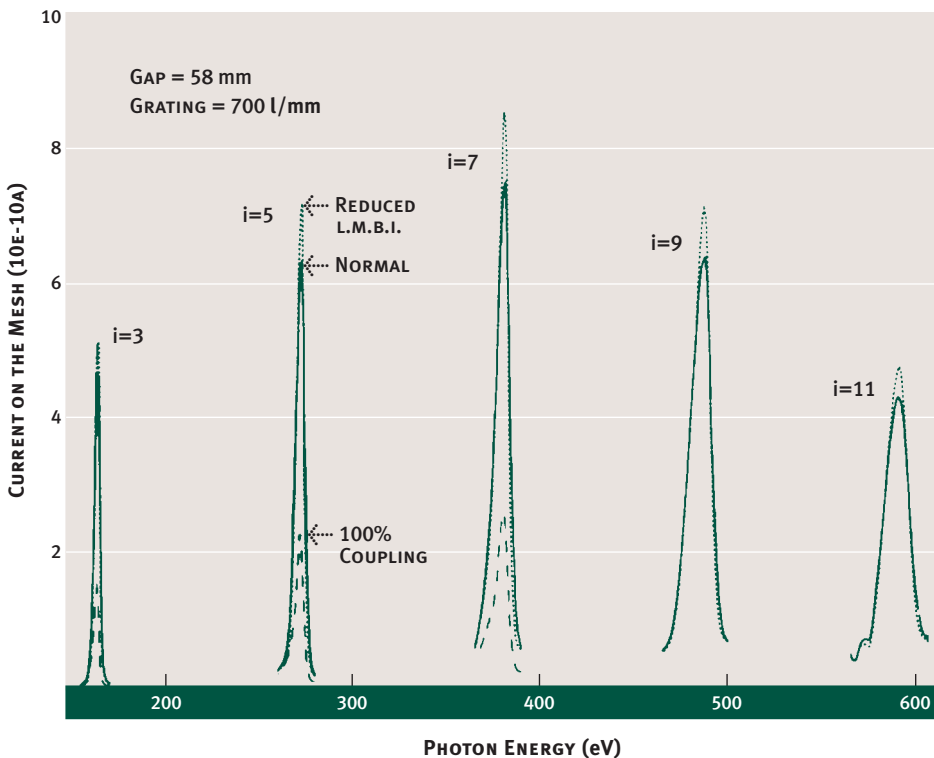
variation occurs during the injection procedure, when a strong change in the thermal load takes place because of ramping.

Coupled bunch instabilities caused by higher order modes in the r.f. accelerating cavities are successfully cured by mode shifting, performed by a change in cavity temperature. Each cavity can be adjusted to a different temperature level with an accuracy of 0.1°C. A figure of merit for the compensation is the quality of the insertion device radiation spectra. Figure 11 shows the dramatic effect of the cavity temperature [i.e. the energy widening due to longitudinal coupled bunch instabilities (LMBI's)] on the fifth harmonic of the SuperESCA spectrum. Between 54-59° the parasitic cavity modes are coupled strongly to the oscillation modes

of the multi-bunch filling. Since beamline spectra are not always available for the optimisation, a procedure has been developed which continuously measures the amplitudes of all coupled bunch modes and displays them. The system is being further improved by the implementation of adjustable mechanical higher order mode shifters in the single cell cavities allowing one to find temperature ranges which are free of multi-bunch instabilities.

The lifetime at ELETTRA is dominated by the Touschek effect - intra-beam electron-electron collisions - reflecting the high quality of the electron beam. The Touschek effect is the main loss mechanism for storage rings in the ELETTRA energy range that have low emittances and therefore

Fig. 12: Changes in the quality of ID spectra taken on the VUV beamline under various operating conditions.



dense bunches. Increasing the lifetime by reducing the bunch density is detrimental to beam quality in one way or another.

Lifetime can be improved by increasing the bunch dimension in the transverse plane by increasing the emittance coupling or by manipulating the dispersion and/or longitudinally lengthening the bunch. Measurements on the machine show that lengthening the bunch - through a residual excitation of longitudinal coupled bunch mode instabilities (LMBI) - is preferable to increasing the vertical emittance and also helps combating transverse multi-bunch instabilities. At 250 mA and 2.0 GeV a factor of 5 increase in the lifetime can be obtained. Figure 12 shows the effect on the insertion device spectra for various operating conditions.

The effects of a longitudinal multibunch instability depend on the strength of the excitation. For a strong excitation we observe a relaxation oscillation whereby the oscillation amplitude rapidly increases until the beam motion decoheres via Landau damping; consequently the excitation stops until radiation damping has restored the particle density to its initial value and the process starts anew. For a medium excitation a persistent coherent dipole oscillation can instead be established.

The stronger excitation results in a lower average bunch density and therefore longer lifetime, but is also associated with a larger effective energy spread. This energy widening is detrimental to the higher harmonics of the undulator spectra.

The situation is further compounded by the spurious horizontal and vertical dispersion. This contributes to an increase in the vertical emittance and increases the beam dimensions in both planes in association with the energy spread. The spurious dispersion is regularly globally corrected, however, there is a practical limit to the correc-

tion and at the insertion device symmetry point is in the range 2 to 6 cm horizontally and 0.5 to 1.5 cm vertically. The maximum effort is made to maintain the dispersion throughout a run but observations show that there may occur a slow degradation towards the upper limit. This is reflected in table 5 which gives the beam sizes and divergences for the machine source points.

A third harmonic cavity is being developed, as part of the machine upgrade programme, to control the bunch length independently of the energy spread (see previous page).

MACHINE DEVELOPMENTS IN 1997

FAST LOCAL ORBIT FEEDBACK

The last year saw the implementation of digital signal processing to the local feedback programme in association with sophisticated mathematical packages with the goal of closing the loop on the photon beam position monitors (pBPM's) housed in the front end. Two systems are installed in sections 2 (Super ESCA) and 6 (Gas-phase) in the vertical plane only. A third system is being set up in section 3 (VUV). The method uses a Proportional-Integral-Derivative (PID) regulator with an attenuation bandwidth of 150 Hz.

To correct a spurious 50 Hz (plus harmonics) signal seen in the beam a newly developed multiple Harmonic Suppression technique was developed which showed extremely good results on the pBPM signals, in good agreement with the developed system model. However, the results were not as satisfactory beyond the pBPM's. A program has been initiated to improve the dynamic signal to noise ratio of the system, to implement concurrent two plane correc-

tion along with the evaluation of cross-talk at the pBPM's and within the machine. In addition a more in depth analysis of the effect of the bending magnet radiation on the pBPM's is being performed.

In the meanwhile to provide more flexibility to the users improvements were performed in the compensation of orbit changes due to insertion device gap changes. This permitted partial control of the ID's to be given to the users. For the moment the gap can be changed at will within a range of ± 10 mm from a nominal value.

IMPROVEMENTS TO INSERTION DEVICE ORBIT COMPENSATION

Each undulator is equipped with four sets of correction coils, two each for both horizontal and vertical magnetic fields, thus allowing complete correction of first and second field integrals in both planes. A program in each ID VME crate has been installed that automatically sets the 4 coil currents as a function of gap and minimises the effect of closed orbit (or BPM reading) drift.

The results are five times better than previously obtained: the correction of the difference orbit is at the level of $\leq 2 \mu\text{m}$ rms horizontally (x) and $\leq 1 \mu\text{m}$ rms vertically (y), which translates to maximum changes at any ID centre of 1% and 7% of the nominal size/divergence in the horizontal and vertical planes respectively for a 1% coupled beam. Furthermore developments are being planned for 1998 which will further minimise the effects of orbit drift.

ELECTROMAGNETIC ELLIPTICAL WIGGLER

The EC funded collaboration between ELETTRA, BESSY and MAX-lab involving

the construction of an electromagnetic elliptical wiggler and soft X-ray polarimeter was brought closer to completion with the start of installation of the wiggler in the ring at the end of December (see figures 13 and 14). The device, whose parameters are given in table 6, arrived from it's constructors Danfysik at the end of November and underwent a series of tests and magnetic measurements in the laboratory before the two day ring installation. The single module device allows flexible operation in either wiggler and undulator mode, with helicity switching at up to 100 Hz. The beamline has been designed to provide circularly (or linearly) polarized photons covering the range 5-1500 eV and operates in undulator mode for photons in the energy range 5-200 eV (1st and 3rd harmonics) and wiggler mode for 80-1200 eV photons. It provides high flux $5 \cdot 10^{13}$ to 10^{14} phot./s/0.1% on the sample with a high polarization rate of 0.5 to 0.9 and high resolving power (5000 to 10000). The helicity switching is performed in a trapezoidal manner in the range 0.1 to 1 Hz and sinusoidally from 10 to 100 Hz. The front end and vacuum chamber were installed in the autumn shutdowns. The elliptical cross-sectioned vacuum chamber is pump free along it's length and required a brief conditioning of a few days before life-time returned to normal values.

Table 6: Main characteristics of the electromagnetic elliptical wiggler.

Period	212 mm
gap	18 mm
No. vertical poles	32
No. horizontal poles	31
Length (iron)	3.322 m
Max. vert. field	0.5 T
Max. horiz. field	0.1 T

Fig. 13: The latest addition to ELETTRA's insertion devices: the electromagnetic elliptical wiggler.



HIGHER CURRENT

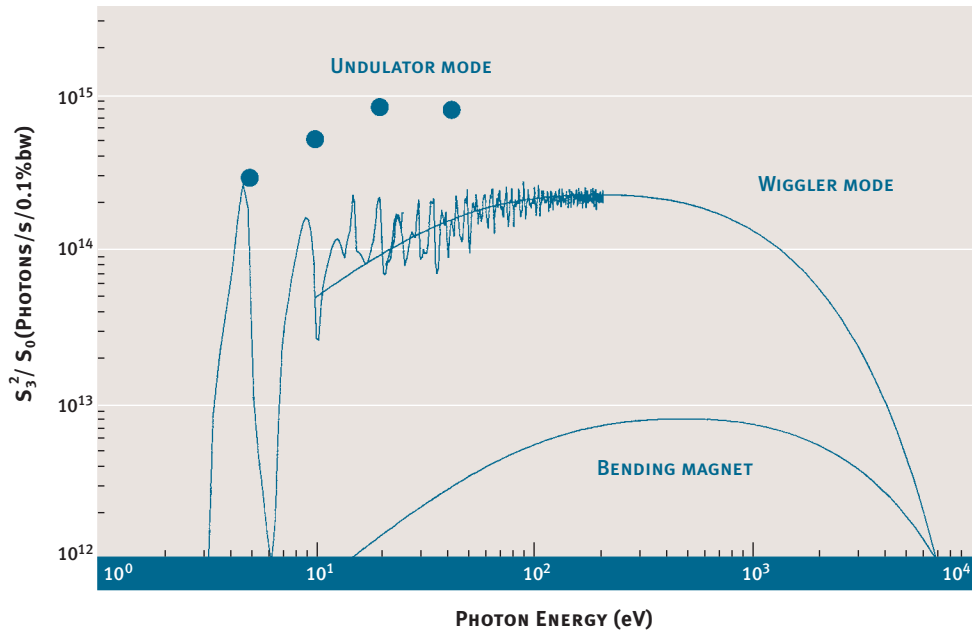
The current is limited by the thermal load on the vacuum chamber, which stresses the gaskets on the BPM's about the bending magnets. A simple solution has been found using gaskets of composite materials - steel and copper. An upgrade to these gaskets was started in the Summer of 1996 and terminated in the Summer 1997. The first tests allowed a current increase to 340 mA with no vacuum problems. Furthermore the upgrade permitted the ramping of 150 mA of beam to 2.35 GeV. The machine is now routinely operated with a starting current of 300 mA and future tests will be performed to allow even higher starting currents of 330 mA. The increased thermal load, however, causes significant movement of the BPM downstream of the bending magnet. Horizontal movements of up to 80 microns are observed,

whilst the vertical movement is significantly less. Solutions to the consequences of the movement will be sought in 1998.

CONTROLLING MULTIBUNCH INSTABILITIES

In 1997 adjustable higher order mode frequency shifters (HOMFS's) were installed on two cavities thereby eliminating troublesome transverse higher order modes. The other two cavities will be provided with frequency shifters in 1998. With the present current of 300 mA at 2.0 GeV the temperature tuning of the cavities is sufficient for the control of both longitudinal and transverse multibunch instabilities to satisfactory levels. Higher currents render the technique more laborious for routine operation. To better deal with this problem a transverse

Fig. 14: Performance curves of the electromagnet elliptical wiggler in undulator and wiggler modes of operation.



multibunch feedback system is being developed in addition to the above mentioned installation of adjustable HOMFS's.

A collaboration for such a development is in progress with DAΦNE and SLAC and first tests are planned for the end of 1998. Studies were initiated in 1997 and have highest priority for the development and installation of a digital processing system. The system, based on one or two pickups, digital processing and fast transverse kickers will be a broadband bunch-by-bunch feedback allowing improved operation efficiency, digital delay, flexibility and beam and system diagnostics.

With full control of all multibunch instabilities machine performance will be maximised giving higher brightness, better orbit control but with lower lifetime. To overcome the limitation on lifetime a passive higher harmonic cavity, mentioned earlier, is planned to lengthen the bunch by up

to a factor of three giving more than twice the lifetime. First studies on the cavity geometry have been performed and the system will be further developed in 1998.

FEW BUNCH MODE OF OPERATION

During the later months of the year time resolved experiments were performed on the ALOISA beamline. To enable this the machine had to work in a few bunch mode i.e. injecting 6, 12, 18 etc. equidistant bunches. Few bunch mode spectra were also obtained on the GAS PHASE beamline. The results of both lines are very promising and further experiments are scheduled for the first quarter of 1998.

ELETTRA SR PARAMETERS (1997)



ELETTRA SR PARAMETERS (1997)

Table 1

Beam energy [GeV]	2.0
Storage ring circumference [m]	259.2
Beam height in experimental area [m]	1.3
Number of achromats	12
Length of Insertion Device (ID) straight sections [m]	6 (4.8 useful for ID's)
Number of straight sections of use for ID's	11
Number of bending magnet source points	12
Beam revolution frequency [MHz]	1.157
Number of circulating electron bunches	1 to 432
Time between bunches [ns]	864 to 2
Tunes: horizontal/vertical	14.3/8.2
Natural emittance [nm-rad]	7.0
Energy lost per turn without ID's [keV]	255.7
Energy lost per turn with ID's [keV] [¶]	290.2
Critical energy [keV]	3.2
Bending magnet field [T]	1.2
Geometrical emittance coupling %	1
Spurious dispersion [¶] : horizontal (rms max/min) [cm]	6/2
Spurious dispersion [¶] : vertical (rms max/min) [cm]	1.5/0.5
Operation mode	multibunch
One refill per day (09:30) of duration (incl. ramping etc.) [min]	~15
Injection energy [GeV]	1.0
Injected current [mA]	300

Machine Dominated by the Touschek Effect

Energy spread (rms) ‰	0.8
Lifetime (250 mA) [hours]	11
Bunch length (1 σ) [mm]	5.4
BEAM DIMENSIONS (1 σ)*	
ID source point - horizontal/vertical [μ m]	241/15
Bending magnet source point - horizontal/vertical [μ m]	139/28
BEAM DIVERGENCE (1 σ)*	
ID source point - horizontal/vertical [μ rad]	29/6
Bending magnet source point - horizontal/vertical [μ rad]	263/9

Machine with Relaxed Touschek Effect (Usual Operating Condition)

Energy spread (rms) ‰	2.8
Lifetime (250 mA) [hours]	26
Bunch length (1 σ) [mm]	11
BEAM DIMENSIONS (1 σ)*	
ID source point - horizontal/vertical [μ m]	255/23
Bending magnet source point - horizontal/vertical [μ m]	371/43
BEAM DIVERGENCE (1 σ)*	
ID source point - horizontal/vertical [μ rad]	31/9
Bending magnet source point - horizontal/vertical [μ rad]	698/14

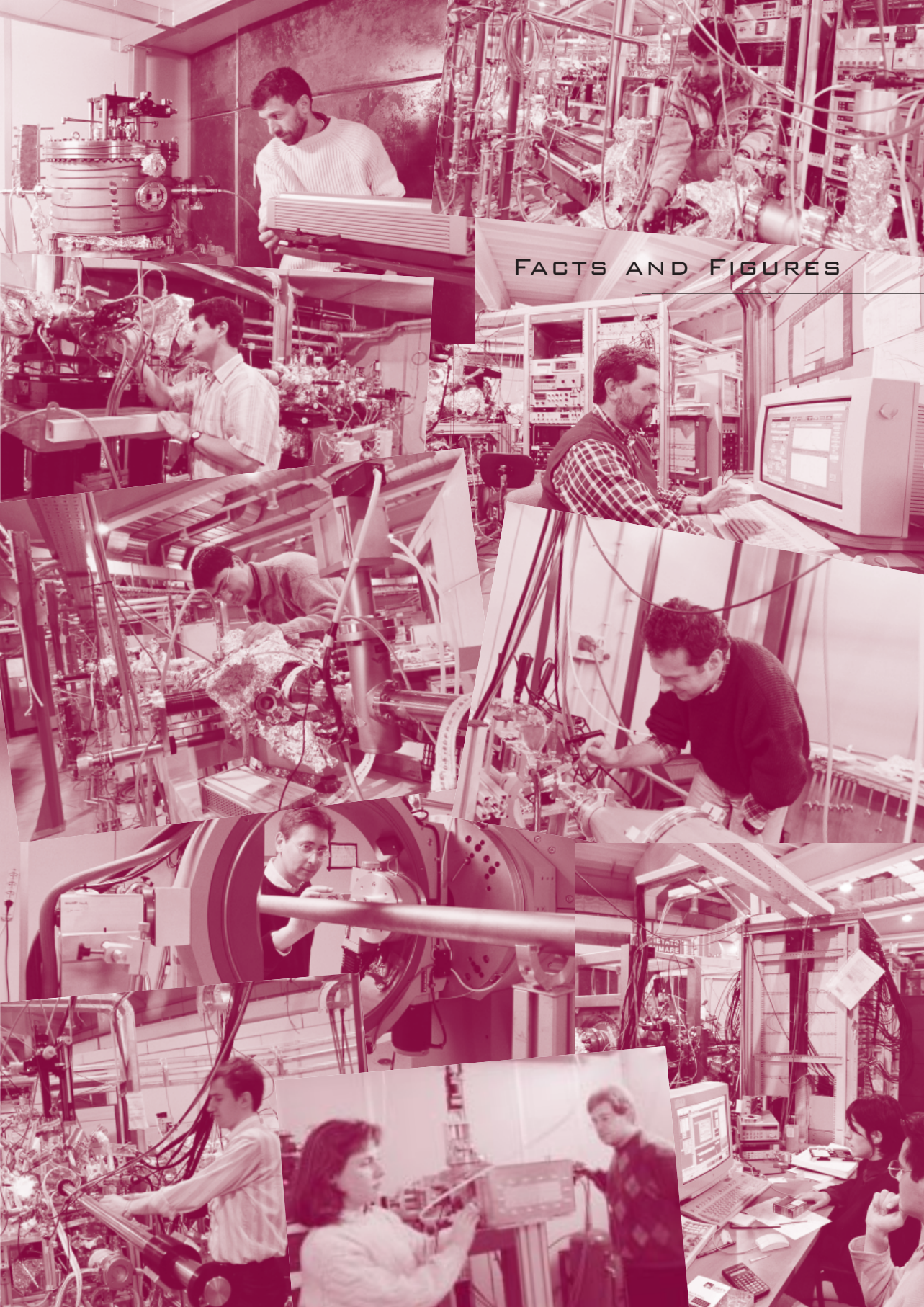
Table 2: Wiggler and Undulator Specifications (ID)

STRAIGHT SECTION NUMBER	DEVICE TYPE	PERIOD LENGTH [cm]	NUMBER OF PERIODS	MINIMUM GAP [mm]	B ₀ [T]	K
2	Undulator	5.6	81	27.0	0.44	2.3
3	Undulator	12.5	36	28.0	0.51	5.9
5	Wiggler	14.0	30	22.0	1.50	19.6
6	Undulator	12.5	36	26.0	0.55	6.4
7	Undulator	8.0	19	26.0	0.55	6.4

¶: U5.6, U8, 2 x u12.5 W14 at minimum gap.

∗: At the centre of ID's.

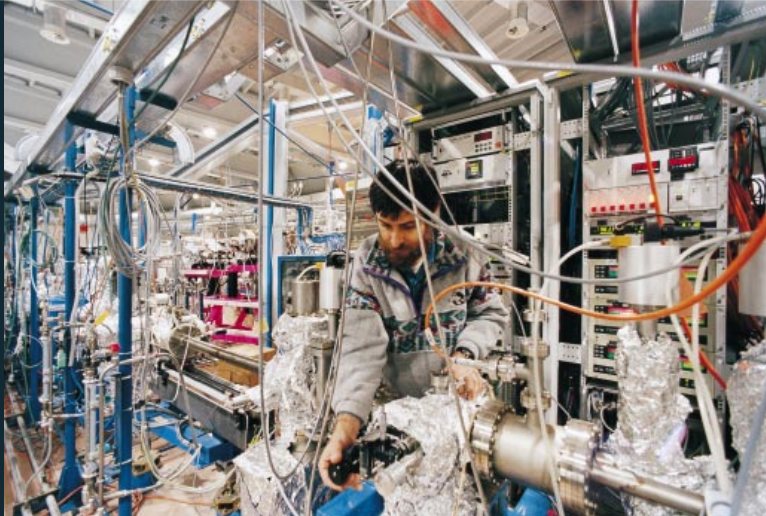
*: The values shown (taking into account the rms energy spread) are averages, obtained from a consideration of different angle and position values of the spurious dispersion, and can vary by ±10%.



FACTS AND FIGURES

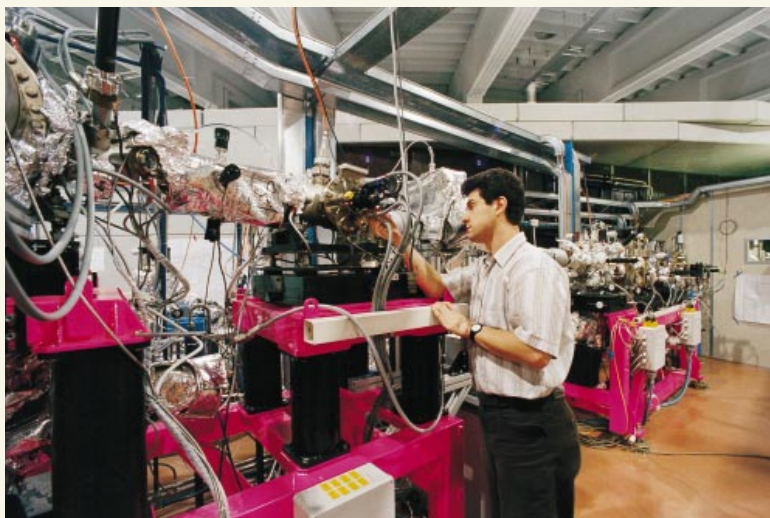


Circular Polarization



VUV Photoemission

Spectromicroscopy

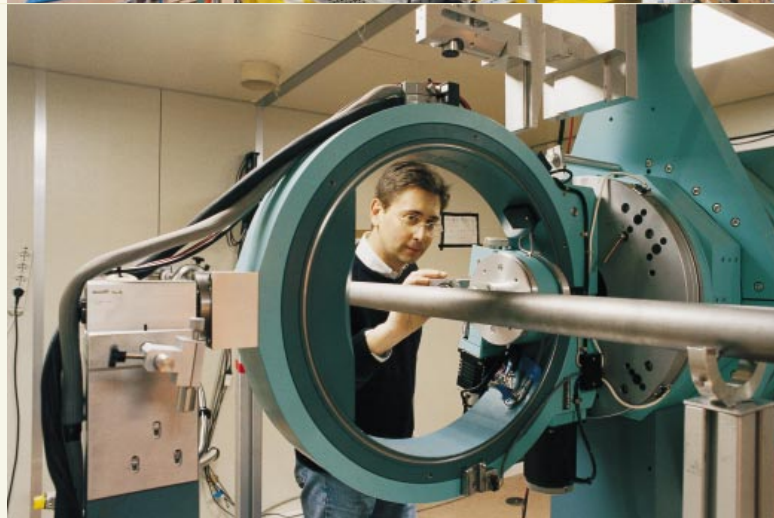


SuperESCA



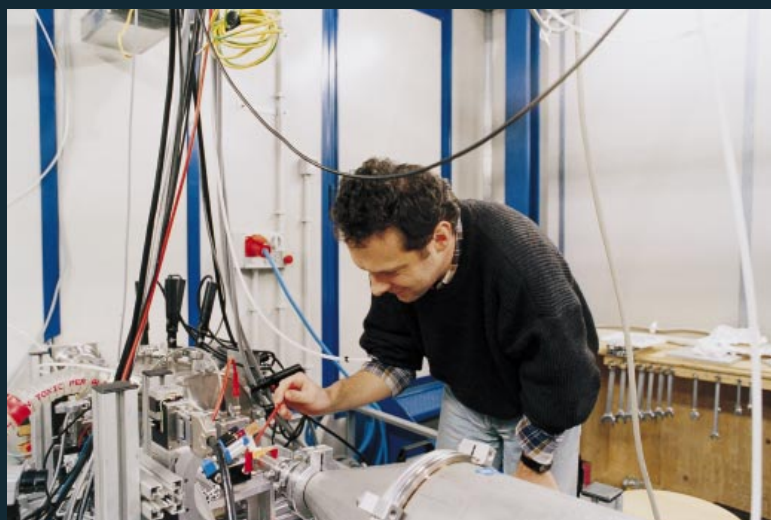


ESCAmicroscopy

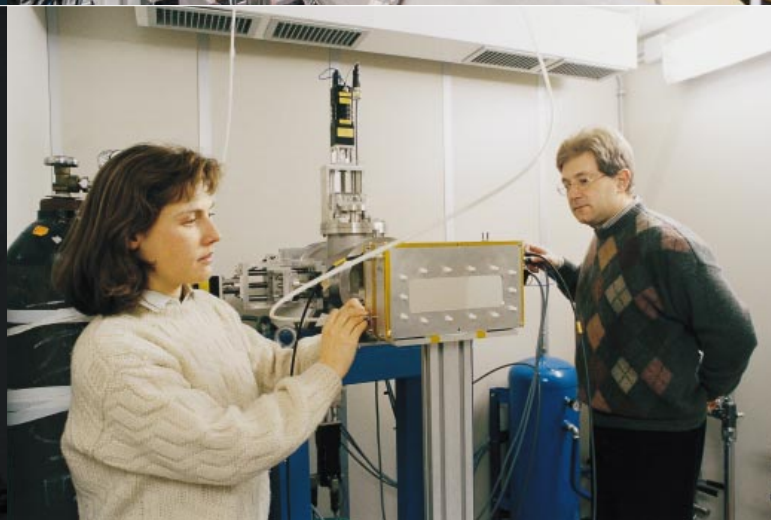


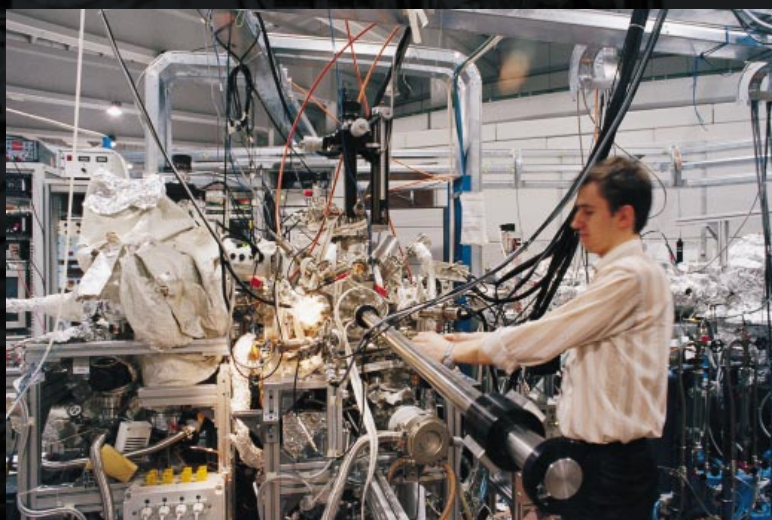
X-ray Diffraction

SAXS



SYRMEP





Gas Phase Photoemission



ALOISA



Open House (June 8, 1997)



Open House (June 8, 1997)



“Antimicrobial Peptides and their interaction with membranes: towards a structure - Based Design Strategy” Workshop (December 5-6, 1997)



5th ELETTRA Users' Meeting (December 1-2, 1997)



5th ELETTRA Users' Meeting (December 1-2, 1997)

Organizational Structure of ELETTRA

The ELETTRA Laboratory has been built and is managed by a Share Consortium (Società Consortile per Azioni) whose ownership is as follow:

AREA Science Park	51.0171%
Friulia S.p.A.	39.8100%
SPI	4.0439%
EniRicerche S.p.A.	5.1241%
INFM	0.0049%

The Consortium has an Administration Council which appoints a Chief Executive Officer and the Laboratory Directors.

Directorate (end of 1997)

Icilio Agostini
Carlo J. Bocchetta
Fabio Cargnello
Giorgio Margaritondo
Carlo Rizzuto
Adolfo Savoia
Sergio Tazzari
Richard P. Walker

SAC - Scientific Advisory Committee

Renzo Rosei	<i>Chair</i>
-------------	--------------

Lucio Braicovich
Ingolf Lindau
Dietrich Menzel
Calogero Natoli
Neville Smith
J. Friso Van Der Veen
M. Van Der Wiel
Keith S. Wilson

Users' Delegates

Giovanni Stefani	<i>Chair</i>
------------------	--------------

Sandro Carrara
Doriano Lamba
Tommaso Prospero

Administration Council (1997)

Paolo Maria Fasella	<i>President</i>
Luciano Fonda	<i>Vice President</i>
Carlo Rizzuto	<i>Chief Executive Officer</i>

Massimo Altarelli
Edoardo Castelli
Franco Forlani
Marcello Fontanesi
Claudio Furlani
Giorgio Frassini
Mario Gregori
Franco Quadrifoglio
Domenico Romeo
Carlo Rubbia

Board of Auditors

Ugo Braico	<i>Chair</i>
------------	--------------

Pompeo Boscolo
Enrico Leoncini
Fabio Matarazzo
Antonio Meucci

Review Committee

David W. Lynch	<i>Chair</i>
----------------	--------------

Carl-Ivar Branden
Denise Caldwell
Mark Chance
Fabio Comin
John R. Helliwell
Massimo Marezio
George Sawatzky
D. Philip Woodruff

Personnel

	EXPERIMENTAL DIVISION	ACCELERATORS AND TECHNICAL SERVICES SECTOR	ADMINISTRATIVE AND GENERAL SERVICES SECTOR	TOTAL
Employees	46	76	60	182
Full-time Collaborators	1	1	1	3
SUBTOTAL PERMANENT STAFF	47	77	61	185
Post Doctoral Fellows and Collaborators	25	1	4	29
TOTAL PERSONNEL	72	78	65	215

DEGREES OF STAFF PERSONNEL

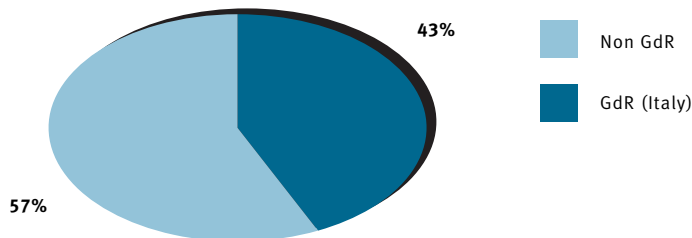
University Level	35%
High School	51%
Vocational School	14%

The Elettra Annual Budget - Planned Allocations for 1998 in Billion Italian Liras

INCOME	1998
Italian Government Support	43.200
Grants from the Local Government	2.950
EC Grants	0.535
Other Grants	0.150
External Contracts	1.445
Total Yearly Income	48.280
EXPENDITURES	
Personnel	16.700
Utilities	3.900
General Management Costs	0.490
Accelerator Operation and Maintenance	3.080
Beamlines Operation and Maintenance	3.643
Service and Administration Sector	3.660
Development Project and Contracts	8.960
Taxes	2.250
Debt Service	4.400
Operation and Other Expenditures	1.197
Total Expenditures	48.280

Allocated Shifts: Percentage of GdR and non GdR Beamtime*

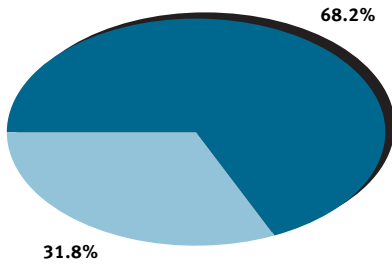
GdR (Italy)	43%
Non GdR	57%



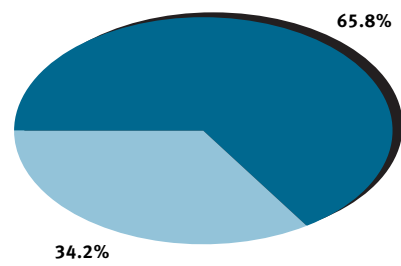
*Total Experiments from September 1996 to December 1997 (non GdR)**

	# EXPERIMENTS	%	# SHIFTS	%
Italy	49	31.8*	604	34.2
Other Countries	105	68.2	1162	65.8
Belgium	1	0.6	6	0.3
Denmark	3	1.9	16	0.9
Deutschland	19	12.3	278	15.7
France	4	2.6	84	4.8
Greece	5	3.2	33	1.9
Österreich	19	12.3	199	11.3
Suomi/Finland	1	0.6	21	1.2
Sverige	1	0.6	22	1.2
The Netherlands	4	2.6	69	3.9
United Kingdom	35	22.7	324	18.3
Croatia	1	0.6	9	0.5
Czech Republic	6	3.9	30	1.7
Switzerland	2	1.3	23	1.3
Hungary	1	0.6	9	0.5
India	1	0.6	9	0.5
U.S.A.	2	1.3	30	1.7
Total	154		1766	
	# EXPERIMENTS	%	# SHIFTS	%
UE	141	91.6	1656	93.8
Europe Non UE	10	6.5	71	4.0
Non Europe	13	1.9	39	2.2
Total	154		1766	

TOTAL EXPERIMENTS (NON GdR)*



TOTAL SHIFTS (NON GdR)*



* GdR: Gruppi di Ricerca - Research Groups.

ELETTRA is a public facility open to all national and international users, who meet high level standards as required by the international Program and Scientific Advisory Committees. The mission of ELETTRA is to be an institution where researchers of Italy and other Countries work together at the highest quality level.

Access to ELETTRA is granted either by submitting experimental proposals (calls are published and selections are made twice annually) or by collaborating in the construction and daily operation of beam-lines and/or experimental stations. Proposals which meet the standards and the international selection, are accepted on the basis of their merit, without "entry fees". Collaborating Research Groups are accepted following specific rules and on the basis of proposals submitted to the Scientific Advisory Committee.

Further information on rules and procedures for the submission of proposals are available both on the WEB (<http://WWW.elettra.trieste.it>) and/or by writing to the Direction of the Experimental Division.

Agreements Concerning Research Groups

	BEAMLINE/LABORATORY	GROUP	INSTITUTION **
1	VUV Photoemission Beamline	GdR-VUV	CNR
2	Hard X-ray Diffraction Beamline	GdR-XRD	CNR
3	Circular Polarization Beamline	GdR-POLAR	CNR
4	Gas Phase Photoemission Beamline	GdR-Gas Phase	CNR-INFM
5	Surface Diffraction (ALOISA) Beamline	GdR-ALOISA	INFM
6	TASC Laboratory	GdR-TASC	INFM
7	Litography Beamline	GdR-LILIT	INFM
8	X-ray Magneto Optics and Surface Science Beamline (X-MOSS)	GdR-X-MOSS	INFM
9	Beamline for Advanced Dichroic Experiments (BACH)	GdR-BACH	INFM-ETH
10	Advanced Photoelectric Effects Experiments Beamline (APE)	GdR-APE	INFM
11	Synchrotron Light Applications	GdR-ICTP/INFM	ICTP-INFM
12	Small Angle X-ray Scattering Beamline SAXS	GdR-SAXS	AAS
13	SYRMEP Beamline	GdR-SYRMEP	Univ. TS
14	LFO Laboratory	GdR-LFO	ITI

** CNR: Consiglio Nazionale delle Ricerche; INFN: Istituto Nazionale di Fisica della Materia; ETH: Eidgenössische Technische Hochschule; ICTP: International Center for Theoretical Physics; AAS: Austrian Academy of Sciences; ITI: Istituto Tecnologie Innovative.



1997

ELETTRA HIGHLIGHTS 1997
97 ELETTRA HIGHLIGHTS
HIGHLIGHTS

SINCROTRONE TRIESTE SCPA
S.S. 14, KM 163,5
IN AREA SCIENCE PARK
34012 BASOVIZZA (TRIESTE), ITALY